A NOVEL NUMERICAL METHOD TO ANALYZE LAMINAR FLOW IN SERRATED PLATE-FIN HEAT EXCHANGER DESIGNS

by

Nabila Rubaiya

A Thesis Submitted in

Partial Fulfillment of the

Requirements for the Degree of

Master of Science

in Engineering

at

The University of Wisconsin-Milwaukee

December 2018

ABSTRACT

A NOVEL NUMERICAL METHOD TO ANALYZE LAMINAR FLOW IN SERRATED PLATE FIN HEAT EXCHANGER DESIGNS

by

Nabila Rubaiya

The University of Wisconsin-Milwaukee, 2018
Under the Supervision of Professor Kevin Renken

In the present research work, a simple numerical method has been explored to calculate the performance of serrated plate-fins. The numerical data of heat transfer and pressure drop performances have been compared with the available literature [6, 21], by means of calculating Chilton-Colburn j Factor and Fanning Friction Factor f, respectively. The numerical findings show good agreement with the experimental results from literature. Hence, the numerical analysis procedure proposed in this paper can be used to predict the performance of new designs of plate fins including different types of notched serrated fins. A detailed calculation and analysis of results have been carried out to compare the performance of three different patterns of serrated fins. The numerical setup has been kept constant to perform the tests for different laminar flow intensities. Finally, a design for an experimental setup has been proposed for future experimental data collection of temperature and pressure for various plate fin assemblies.

To the strongest and most sacrificing woman, who taught me how to be strong in hard times, My Lovely Mother,

Mahmuda Begum

To the most emotional and hardworking man, whom I am proud to be his daughter, My Dear Father,

Mahmud Hasan

And

To my caring husband and life partner, whose support made me stand in the place where I am today,

Golam Mushih Tanimul Ahsan

TABLE OF CONTENTS

LIST OF FIGURES

LIST OF TABLES

LIST OF NOMENCLATURE

Q	heat transfer rate, [W]
q_w''	heat flux, [W/m^2]
h	convection heat transfer coefficient, [$W/m^2 \cdot K$]
A_S	heat transfer surface area, [m^2]
A_c	mass flow area/ cross section, [m^2]
ΔT	temperature difference, [K]
Δp	pressure drop, [Pa]
C_p	specific heat, [$J/kg \cdot K$]
k	thermal conductivity, [$W/m \cdot K$]
v	inlet velocity, [m/s]
D_h	hydraulic diameter, [m]
h_f	fin height, [m]
S_f	fin pitch, [m]
L_f	fin length, [m]
L	effective length of test piece, [m]
$\dot{m}$	mass flow rate, [kg/s]
$\dot{v}$	volume flow rate, [m^3/s]
G	mass flux, [$kg/m^2 \cdot s$]
R_e	Reynolds number
St	Stanton number
Pr	Prandtl number
j	Chilton Colburn j factor

f	Fanning friction factor
T_i	inlet temperature, [K]
T_o	outlet temperature, [K]
T_w	wall temperature, [K]
T_m	mean temperature, [K]

Greek Symbols

ρ	density, [kg/m^3]
μ	dynamic viscosity, [kg/m·s]
δ_f	fin thickness, [m]

Subscripts

f	fin
w	wall
s	surface
i	inlet
i	outlet
m	mean value

Abbreviations

CO_2	carbon dioxide
CHE	compact heat exchanger
PFHE	plate fin heat exchanger
CFD	computational fluid dynamics
CAD	computer aided design
AC	alternate current

DC	direct current
DAQ	data acquisition software

ACKNOWLEDGEMENTS

I owe my gratitude to my God who has always granted me invaluable blessings. I thank You for Your will to let me do my masters and finish writing up my thesis. You have always showed me the right path to make my goals achieved.

At first, I want to express my deepest gratitude and appreciations to my teaching as well as research advisor, Dr. Kevin Renken. I have been amazingly privileged to work with such a brilliant mind like him for the last two years who made me passionate about heat transfer. He always believed in my capability and wanted me to learn more and more. Thank you for your support and encouragement with everything.

Next, I would like to thank my thesis committee members, Dr. John Reisel and Dr. Benjamin Church for serving on my thesis committee. Because of both of your cooperation, I have been able to find a defense date with such a short notice.

I want to further extend my gratitude to all academic staff at UW-Milwaukee who helped me a lot throughout these two years of my study. I am especially thankful to Ms. Betty Warras, Ms. Gerri Meloy and Mr. Avie Judes for always being there for me whenever I needed their support.

Furthermore, I am very much thankful to all my undergrad students, colleagues and friends. Teaching and doing research wouldn't be so much enjoyable without your immense encouragement to build up my confidence and strategy. I would like to thank Ali Bakshinejad, Mohammad Amin, Mandana Saravani, Sridhar Lanka, Oluwatosin Samuel for all your support and direction on every part of my study here at UWM.

I am extremely grateful to all the hard-working employees of EMS machine shop. Michael Powley, whom I consider as my undergrad student and friend, not only helped me building my experimental setup, but also taught me how to be dedicated and respectful to the work you love.

Last but not the least, I cannot express my deepest respect in words to Dr. Robert Balmer. He continuously gave me his valuable time to solve all my concerns. He worked with me in the lab to set up the experiment, advised me on my numerical analysis and writeup of the thesis paper. I would ever cherish those learning moments and I would never forget his kind favor to me for the rest of my life.

1 INTRODUCTION

1.1 Introduction

Global warming is a major concern in today's world. Because of population growth and industrial development, the demand for energy has risen steadily in the last few decades, thus contributing to environmental pollution. There is increasing pressure on industry to save energy and reduce the associated CO_2 emissions during their production. An important and profitable strategy that industry can take is heat transfer enhancement by recovering some additional process energy as efficiently and economically as possible. Recovering process energy not only reduces the use of primary energy supply but also contributes to environmental protection due to reduced emissions. It also reduces process heat rejection which contributes to long term operation of associated equipment and saves on operating costs [1, 2].

A significant number of thermal engineering researches have been carried out to find new heat transfer enhancement methods. Thermal reuse requires efficient and economical design of heat exchangers. Compact heat exchangers (CHEs) are one of them which considerably increases the efficiency of the systems by reducing heat loss and other process energy [1, 3].

1.2 Basic Theory of Heat Exchangers

Heat Exchangers are thermal devices which are basically used to transfer heat from one fluid to another fluid. This rate of heat energy transfer is a direct function of the temperature difference between the hot and cold fluids, the area where heat is transferred, and the conductive/convective properties of the fluid and the solid materials.

In the 1700s, Sir Isaac Newton formulated a physical relationship based on this heat transfer theory which is called Newton's Law of Cooling. It states:

$$Q = h\, A_S\, \Delta T \tag{1.1}$$

where, h is called the convection heat transfer coefficient ($W/m^2 \cdot K$), A_S is the heat transfer area (m^2), and ΔT is the temperature difference (K) [4].

Figure 1.1 shows basic design of a heat exchanger. Here, two fluids having two different temperatures are flowing inside of a chamber and their flows have been separated by a flat metal surface. By the help of this common surface, two fluids will exchange heat. At the exit, cold fluid's temperature will get increased and the hot fluid's temperature will get decreased indicating heat exchange between two fluids. They will exchange this heat from the common metal surface. This flat metal surface area has been indicated by a dotted line in Figure 1.1.

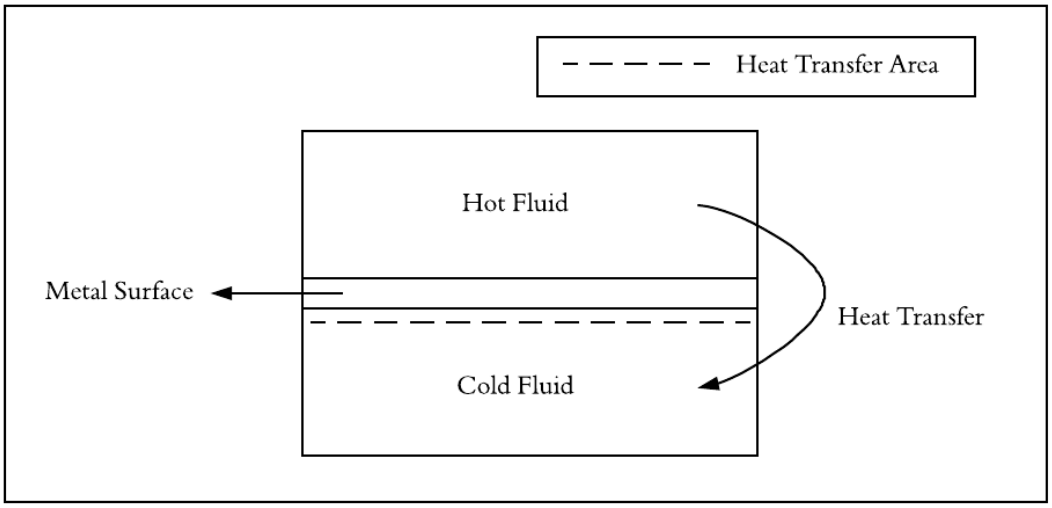

Figure 1.1 Basic heat exchanger design.

From Equation 1.1 we can see that heat transfer rate is directly proportional to the total heat transfer surface area. That means if we can increase the surface area we can increase the system's total heat transfer rate. Heat transfer rate can also be increased by increasing the coefficient of heat transfer or increasing the temperature difference between the hot and cold fluids.

The convection heat transfer coefficient depends on fluid properties as well as fluid velocity and the surface interaction with the fluid. On the other hand, increasing the temperature difference between the hot and cold fluids of the system can create unwanted thermal stresses on the metal surfaces. This situation usually results in deformation and decrease of life span of a heat exchanger body. As a result, the best solution is to increase the heat transfer surface area. Various methods have been evolved over the years to minimize the manufacturing difficulties and to increase the surface area of a heat exchanger [3].

In Figure 1.2, the surface area between the hot and cold fluids has been increased to increase the rate of heat transfer. Instead of having a flat surface like Figure 1.1, the metal plates are made with some irregular shapes. Hence, it can sufficiently increase the total surface area from where the heat will get transfer from one fluid to another. In Figure 1.2, the increased irregular surface has been shown with the dotted line. There are many ways of increasing the surface area which has common contact with the fluids. One of the most widely used methods is to employ different uneven shaped metal interface on the path of fluid flow to extend the heat transfer surface area. These extended metal surfaces are called “fins”. Using plate or tube fins are the most commonly employed methods in heat exchangers. These types of exchangers are called as “Extended Surface Heat Exchangers” or “Compact Heat Exchangers.” In Figure 1.2, square plate fins have been used to increase the total heat transfer surface area.

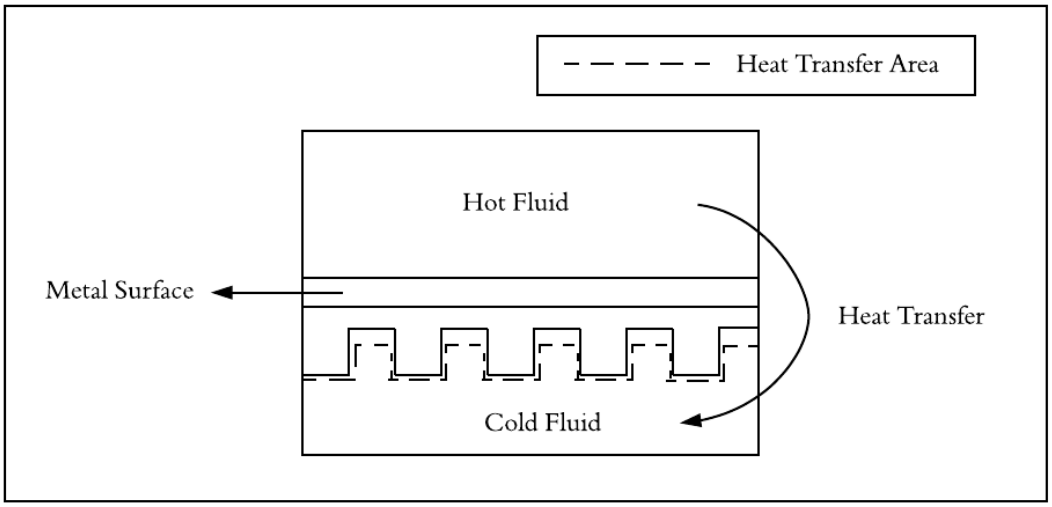

Figure 1.2 Basic heat exchanger design with fins.

1.3 Compact Heat Exchangers

Compact heat exchangers are a class of heat exchangers incorporating a high ratio of heat transfer surface area to heat exchanger volume. Hence, the overall surface area is much higher than the total volume of the heat exchanger which makes it possible to provide high heat transfer coefficients compared to other types of exchangers. The heat transfer surface area is increased by introducing multiple uneven shaped fins which is shown in Figure 1.3. There are many variations of fin designs available. The inserted fins have a very small hydraulic diameter which enlarges the fluid turbulence and enhances the local convective heat transfer coefficient. It can also handle several streams in one unit which reduces the number of heat exchanger rows and thus reduces the capital cost of heat exchangers. A typical design of a plate-fin heat exchanger assembly has been shown in Figure 1.3 where the fins are arranged inside of a heat exchanger one after one. Each fin row is separated from one another by means of a parting sheet. Headers and nozzles are placed to

get the fluid in and out easily by maintaining a desired flow rate and pressure. Figure 1.3 also depicts cap sheets and side bars which are very important parts of plate-fin heat exchangers that make the design more rigid and compact.

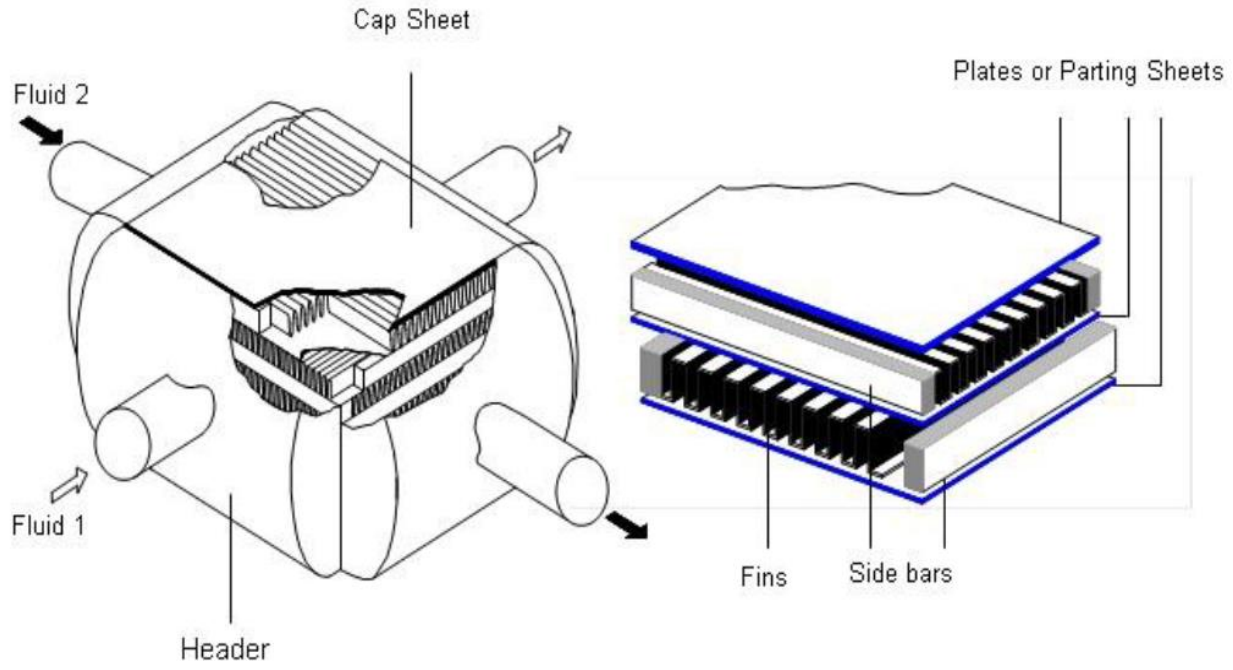

Figure 1.3 Details of plate-fin heat exchanger assembly [1].

Compact heat exchangers are not a new technology. There is a continuous need to produce innovative designs to suit market requirements. Such designs are motivated to focus on lower pressure drop and higher amount of heat transfer rate so that the heat exchangers can be more efficient and suitable for different kinds of applications.

Based on distinguished advantages, compact heat exchangers are widely used in various energy-intensive process industries. Compact heat exchangers are mostly used in cryogenic applications for refrigeration, petrochemical plants, natural gas processing, refineries, condensers, etc. Their versatile area of use has also been reached towards automotive radiators, air conditioning systems, electronic cooling devices, regenerators, air compressors and so on [3, 5].

1.4 Plate Fin Heat Exchangers

There are various fin designs used in compact heat exchangers to increase the heat transfer rate. Among those, plate fins are known to be attractive for their manufacturing easiness and balanced thermal-hydraulic performance. As shown in Figure 1.4, there are various plate-fin designs that have been developed over these years.

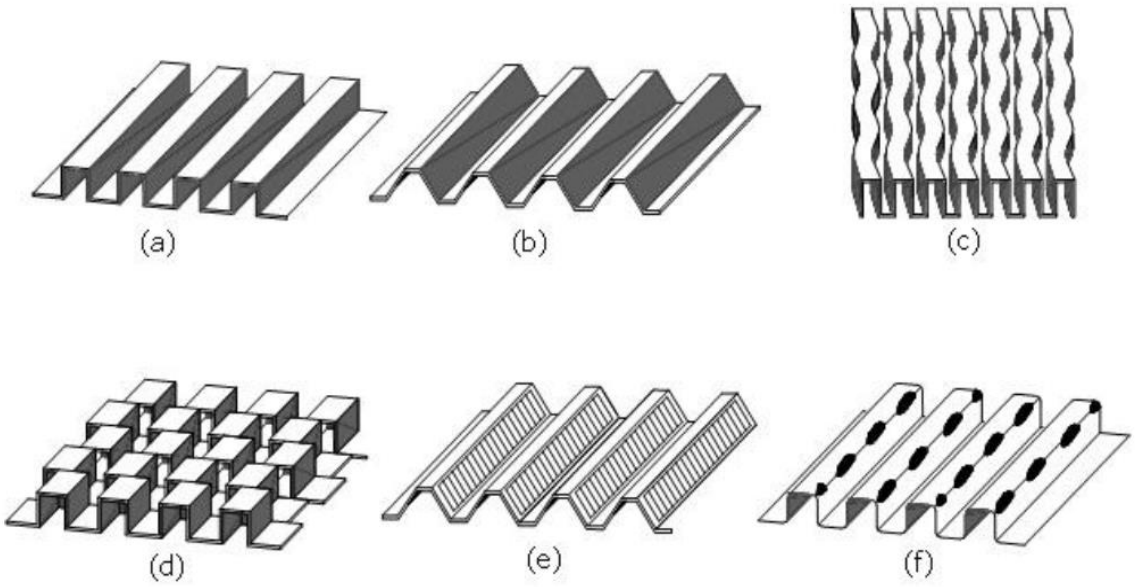

Figure 1.4 Types of plate fin surfaces: (a) plain rectangular, (b) plain trapezoidal, (c) wavy, (d) serrated, (e) louvered, and (f) perforated [1].

Extended surfaces or fin designs for plate fin heat exchangers have been continuously changed and improved over the years. By using specially configured surface geometries, heat transfer coefficients can be enhanced as compared to plain extended surfaces. Consequently, the pressure drop penalties also become higher, but may not be severe enough to negate the thermal benefits. Although, a major challenge is designing an optimal multi-stream plate fin heat exchanger by selecting the perfect fin geometry which would have the best balance of thermal and hydraulic performances [3]. In Figure 1.4, different fin geometries have been shown such as plain

rectangular, plain trapezoidal, wavy, serrated, louvered, and perforated. All these geometries are commonly used in industry to make heat exchangers.

1.4.1 Components of Plate-Fin Heat Exchangers

Plate-fin heat exchanger (PFHE) is a type of compact heat exchanger where the heat transfer surface area is enhanced by providing extended metal plate which is called the fins. A series of these plate-fin surfaces are sandwiched between parting sheets and stacked together by brazing (i.e., a method of joining two parts of metals or alloys at high temperature). The parting sheets are called primary surface of heat transfer and the interior stack of fins work as a secondary heat transfer surface. Both primary and secondary surfaces are intimately bonded together so that it can act like a solid block. In between the parting sheets, streams flow along the passages made by these plate fins and thus exchange heat among themselves. Fins not only form the extended heat transfer surfaces, but also work as a structural support against internal pressure difference between the fluid inlet and outlet. Fin enlarges turbulence by flowing the fluid through narrow passages and corrugated surfaces. This increased fluid turbulence enhances the local convective heat transfer coefficient which contributes to maximize the efficiency of heat exchanger. The side bars prevent the fluid from leaking outside or mixing with the fluid of another section. The fins and side bars are brazed with the parting sheets to ensure good thermal link and to provide mechanical stability [4, 6, 7].

1.4.2 Advantages of Plate Fin Heat Exchangers

There are several unique features of plate-fin heat exchanger which make it competitive in the market. Compactness and high thermal efficiency are the most demanding advantage of PFHE. It can avoid local overheating on the joints which makes it possible to control the overall temperature along the whole volume. Its superior construction makes it possible to maintain lower weight with moderate manufacturing cost. It can operate multiple streams at the same time of operation. PFHE are very much flexible for modification and custom design according to the specific use of customers [3, 5, 8, 9].

1.4.3 Applications of Plate Fin Heat Exchangers

The plate-fin heat exchanger is suitable for use over a wide range of temperatures and pressures for gas-gas, gas-liquid and multi-phase duties. They are mainly employed in the field of cryogenics. Separation and liquefaction of air, processing and liquefaction of natural gas, production of petrochemicals and large refrigeration systems utilize large PFHE designs [3, 10].

Brazed aluminum plate-fin heat exchangers are widely used in the aerospace industry because of their compactness and low weight to volume ratio. They are mainly used in environment control system of aircraft, avionics cooling, hydraulic oil cooling and fuel heating. Because of their compactness and less space consumption, they are used for making the radiators in the automobile sector as well [6, 10].

The other miscellaneous applications are: (i) fuel cells, (ii) process heat exchangers, (iii) heat recovery plants, (iv) pollution control systems, (v) fuel processing and conditioning plants, and (vi) ethylene and propylene production plants [1, 11].

1.5 Serrated Plate Fins

Serrated fin or offset strip fin is a discontinuous type of fin geometry where boundary layers are interrupted so that it cannot become a continuous type boundary layer just like plain fin. Serrated corrugation is made by cutting the fin at the serration length and placing the second fin to a point which is exact half way between the preceding fin. This gives substantial increment at the heat transfer rate.

Fresh boundary layers are being generated adjacent to the leading edge of each serrated fin layers. Therefore, heat transfer coefficient and friction factor are high near the leading edge of the fins. The offset part interrupts the flow and creates a series of very thin new boundary layers which have lower thermal resistance than the thick boundary layers of plain fins.

On the other hand, pressure drop also increases in a substantial amount at the end of the leading edge of each fin due to increased amount of friction in the interrupted flow field. Not only the frictional drag, but also form drag is created due to the finite thickness of the fins. Friction drag incorporates high heat transfer coefficient, but form drag has no significant contribution for heat transfer enhancement. This form drag can be substantial depending on the quality of the cutting edge of the fins at the serration length. However, machined-formed fins create very small amounts of form drag which can be neglected while taking account of high thermal performance of serrated fins [7, 9].

1.5.1 Geometry of Serrated Fins

Typically, a serrated fin array is arranged perpendicularly in the flow direction. The surface geometry is described by the fin serration length, fin height, transverse spacing between two fins

and thickness. The fin offset is usually uniform and placement is equal to a half-fin spacing. These dimensions can be varied to provide great versatility of the serrated design [12, 13].

A nonuniform and other than half fin spacing offset can be introduced as an additional geometric variable which will also contribute to the change in thermal and hydraulic performance of serrated fins. Furthermore, manufacturing irregularities such as burred edges, bonding imperfections and roughness of fin separating plates in the top and bottom also have a great influence over the flow and heat transfer characteristics in actual heat exchanger cores. Creating notches at the fin leading edge can also contribute to a considerable difference in the performance of serrated fins [13, 14].

Many studies have been performed over years to understand the convection mechanisms in serrated fin cores so that the thermal-hydraulic behavior can be predicted for different types of serrated fins. It is still a matter of great interest. Previous studies include experimental data, empirical correlations, flow visualization, analytical models, and numerical solutions for actual serrated fin cores or scaled-up models of them [12, 13, 14].

1.6 Computational Fluid Dynamics

Computational fluid dynamics (CFD) is a branch of fluid mechanics. CFD is called the "virtual flow laboratory" [3] which analyzes systems involving fluid flow, heat transfer, mass transfer and associated phenomena such as phase change, chemical reactions and multi-phase phenomena. Computers are used to perform these types of complex calculations. Using high-speed supercomputers, scientists and engineers can perform numerical experiments to get better and faster solutions. CFD provides a qualitative and sometimes quantitative prediction of fluid flows by means of mathematical modeling (partial differential equations), numerical methods

(discretization and solution techniques), and software tools (solvers, pre- and postprocessing utilities) [3, 14].

1.6.1 CFD Working Procedure

At first a specific fluid dynamics problem needs to be stated into the software program. By using the software code algorithms, scientific details can be easily converted into a mathematical language so that the software program can understand the problem. Later computer hardware performs the actual calculations by using their RAM power. Finally, the user inspects and interprets the CFD simulation results. These results are used for highly interdisciplinary research, comprised of physics, applied mathematics and computer science. The major steps of CFD analysis are problem information to state the fluid flow, conversion into the mathematical model, mesh generation to create nodes or cells or time instants, space and time discretization, iterative solver selection, simulation run parameters, stopping and converging criteria, postprocessing visualization and analysis, verification of results, model adjustment and optimization for improved results [11, 15].

1.6.2 Advantages of CFD Software

These steps of numerical simulations reduce lead times and costs of new designs. It creates the ability to study systems where controlled experiments are difficult or impossible to perform (enormous systems). CFD also helps to explore systems under hazardous conditions at and beyond their normal performance limits (safety studies and accident scenarios). Practically unlimited level of detail of results can be achieved by computational fluid dynamics [11].

1.6.3 Applications of CFD

Computational fluid dynamics has a broad range of applications over different fields of studies. It helps architects to design comfortable and safe living environments. Designers of vehicles can improve the aerodynamic characteristics by taking help of CFD. Chemical engineers also use CFD software to maximize the yield from their equipment. Petroleum engineers can devise optimal oil recovery strategies. In the field of medical science, surgeons take help from CFD to cure arterial diseases (computational hemodynamics). Meteorologists simulate to forecast the weather and warn of natural disasters. Safety experts use CFD to reduce health risks from radiation and other hazards. Military organizations are also dependent on CFD to develop weapons and estimate the damage of an activity [1, 4].

1.7 Objectives

The main objective of this thesis is to develop a novel, simpler, straightforward numerical modeling method to investigate plate-fin heat exchanger performance by using the CFD technique. Basically, pressure drop and heat transfer characteristics are to be analyzed in detail to compare hydraulic and thermal performances, respectively for several different types of serrated fins in PFHE at low Reynolds numbers. Thermal performance can be determined by comparing the Chilton Colburn j Factor and hydraulic performance can be determined by comparing the Fanning Friction Factor f. The accuracy of the new numerical model is verified by comparing results with the available experimental data from the literature [16, 17]. The numerical Chilton Colburn j Factor and the numerical Fanning Friction Factor f both need to be compared with the available literature data to make reliable assumption of performance for various fin designs. If the comparison shows less error and same pattern of data, the numerical model can be proved as

reasonable and appropriate. To explore the performance of notched serrated fin by numerical modeling which should provide the method and theoretical basis for the selection, optimization and analysis of different pattern of notch in the plate-fin heat exchangers for future investigation. Hence, the numerical analysis procedure proposed in this thesis can be used to predict the performance of many types of plate-fin designs. Finally, to develop an experimental setup to experimentally investigate thermal and hydraulic performance of plate-fins by means of measuring temperature and pressure, respectively. To design a successful experimental setup, research is needed on flow separation, flow straightening, hydraulic and thermal entrance length to achieve fully developed flow, experimental apparatus selection, etc.

1.8 Literature Review

Kays and London [16] undertook systemic experiments and obtained Chilton-Colburn Factor j and Fanning Friction Factor f for all different types of fin design such as straight, serrated, and herringbone. Design parameters as well as the manufacturing process of plate-fin heat exchangers have been discussed in detail by Dubrovsky [18]. Patankar and Prakash [19], Suzuki [20], and Manson [21] worked with very thin serrated fins and tried to develop predictive equations for them in the laminar and transition flow region. Wieting [22] worked on adjusting the dimensions for serrated geometries and redefined their hydraulic diameter to find some easy-to-use correlation for heat transfer and pressure drop performance of serrated plate fins. Later, Joshi and Webb [7] reevaluated the empirical correlations of Wieting [22]. Most of the equations which were established later to determine the thermal and hydraulic performance of plate-fin heat exchangers, are a reworking of the Wieting [22] expressions. Mullisen and Loehrke [23] worked to relate their correlation not only with the fin dimensions like length, width and thickness of fin,

but also with fin separation length and fin offset. Over eight decades of work has been associated by Manglik and Bergles [2] for serrated fin heat exchangers. Their extensive work presented a fully analytical model for laminar flow and a semi-empirical approach for the turbulent flow. Later, the design issues were addressed in several reviews by Shah [6]. Foumeny [24] presented rational design equations for j and f in the form of single continuous expression covering the laminar, transition and turbulence flow region. Zhang [25] studied the effect of the staggered strip and provided correlation equations base on experimental data. Dubrovsky and Vasiliev [26], Norris and Spofford [27], and Kelkar and Patankar [28] also provided experimental data to determine thermal and hydraulic performances of plate-fins. Shenone and Tanda [29] worked with forced convection Chilton-Colburn j factor and Friction factor f data for different types of plate-fins and compared the forced convection fin performance data with the free convention fin performance data. A numerical study was done by Feng [8] on constant surface heat flux to find the heat transfer performance of heat sink. Maiti [30] and Ismail and Velraj [31] presented results on the constant surface temperature. Different numerical strategies for simulating multiple streams have been found in some recent papers [9, 10]. For square serrated fins, an empirical correlation has been presented by Peng and Ling [17] for low Reynolds number. A patent [32] on the different patterns of notches for the serrated fins has been presented.

2 NUMERICAL ANALYSIS

2.1 Why Numerical Analysis?

It is hard to investigate the hydraulic and thermal performance of complex fin geometries analytically because there are many geometrical parameters that need to be considered while calculation. Very few systematic experimental studies have been carried in past regarding serrated fins. Such studies [2, 18, 19, 20, 21, 22, 23, 24] have used just the empirical correlations to find the performance of serrated fins. These available studies are inadequate to find the real trends of serrated fins for different patterns, dimensions, and geometries [17]. Experimental models are usually constructed in a large-scale prototype and the arrangements to collect data from model [30].

On the other hand, numerical analysis can be easily adopted to all kinds of arrangement for every possible physical condition. Virtually any realistic problem for all kind of operating conditions can be adopted to perform numerical analysis. It can directly provide reliable results and detailed information on fluid flow and heat transfer for many nodes and elements at a relatively low cost. Multiple types of simulation arrangements can be performed in parallel at the same time which saves time. Moreover, CFD software is portable, and easy to use. Under the above stated circumstances, CFD data collection technique is more convenient than experimental data collection for this study.

2.1.1 Necessity of Numerical Model

Plate-fin heat exchangers are compact in size. The feature size of the fluid flow channel between the fins is usually a millimeter in magnitude, while that of the whole heat exchanger is of a meter in magnitude. Hence, the feature size of the fin is far less than that of overall heat exchanger [15]. It is difficult to run a numerical simulation for the entire heat exchanger model

efficiently when a fine mesh for the fins is required for reliable results. The fins are symmetrical and repeatable in each layer of a plate fin heat exchanger. The fluid channels are also independent in each layer and the flow characteristics are symmetrical because of the plate layout. Exceptions only occur in sections close to the boundary wall, inlet and outlet. A simpler, small and repeatable numerical model is needed to accurately solve the problem [33]. In this study, a representative repeating unit cell (1 inch × 1 inch) of the multi-channeled heat exchanger has been taken as the computational domain to run numerical analysis. This strategy not only reduces the computing requirements, but also reveals a detailed reliable characteristics of fluid flow and heat transfer. The model and method used in this thesis can also be applied for the research and development of plate-fin heat exchangers having structures other than serrated design.

2.1.2 Necessity of One Layer and One Stream

One layer of fins having an upper and a lower separating plate was considered in the current numerical simulations. There have been assumed tight contact between each fin and plate so that effective heat transfer through them can occur by heat conduction. The thermal resistance of the plate and fins were ignored because of high thermal conductivity of aluminum. Single flow of air stream has been considered from inlet through outlet which gained heat from the upper and lower plates of the structure.

This simulation is designed so that it can replicate future experimental tests that can be run easily in a laboratory environment. Normally plate-fin heat exchangers work at cryogenic temperature (-150˚C to -273˚C). It conducts multiple streams at a time having different temperature and flow rate. The flow of multiple streams at different temperature cause heat transfer inside of a heat exchanger [34]. Here, a single layer of fins having a heated upper and

lower plate has been considered to replace the second stream. Instead of a refrigerant at cryogenic temperatures, air at STP has been used for the simulation to compare the overall performance of different serrated fins. Having one layer of heat exchanger fins and single flow of stream simplified the numerical analysis as well as helped to model a realistic experimental setup for future data collection.

2.2 Steps of Numerical Solution

The software ANSYS Workbench is an intuitive up-front finite element analysis tool that is used in conjunction with CAD systems and/or Design Modeler. ANSYS Workbench is a software for performing structural, thermal, and electromagnetic analyses. Here, the user can create geometry and optimize, attach existing geometry, set up the finite element model, solve, review and interpret results. ANSYS Workbench is a platform to deliver unprecedented productivity and enable simulation driven product development [35, 36]. In this numerical analysis, only the thermal and flow characteristics are of interest, thus "Fluid Flow Fluent" was chosen to run the numerical simulations.

2.2.1 Geometry

The first step of simulation using ANSYS Workbench [36] is to upload a fin design or design an innovative one on which thermal and flow analysis will be performed. Three different serrated fin designs have been uploaded into Design Modeler of ANSYS Workbench at the beginning of the numerical analysis. These serrated fin designs were provided by Chart Industries, La Crosse, Wisconsin. The fins, upper plate and lower plate were set altogether as solid zone, and

the passages in between them were set as fluid zone. The accurate geometric set up of identifying the solid zone and fluid zone by the computer program was also done in this step.

Three different serrated fin designs (Design 1, Design 2, and Design 3) have been shown in Figures 2.1-2.3 respectively. All three designs have the same serrated fin pattern: every plate-fin has been placed uniformly in a discontinuous manner where the next row of fin placing is half-way between the two fins of the preceding row. The main difference among them is the number of fins in each row, fin dimension and fin geometry. The fins of Design 3 in Figure 2.3 are also called "notched serrated fins" as there is a small notch in the leading edge of every fin. Design 1 and Design 2 have traditional serrated design but their fin numbers in each row and fin dimension is different. However, all the designs of serrated fins in Figures 2.1-2.3 have identical upper and lower plates.

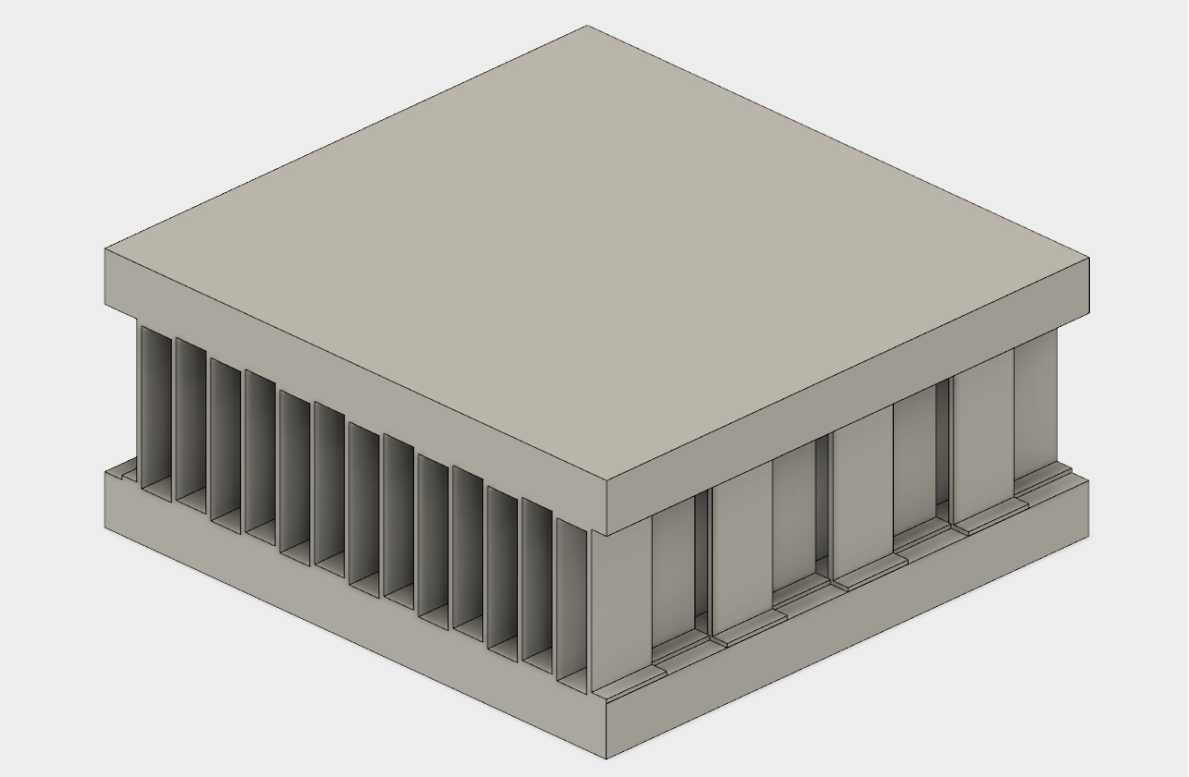

Figure 2.1 Schematic of serrated Fin Design 1.

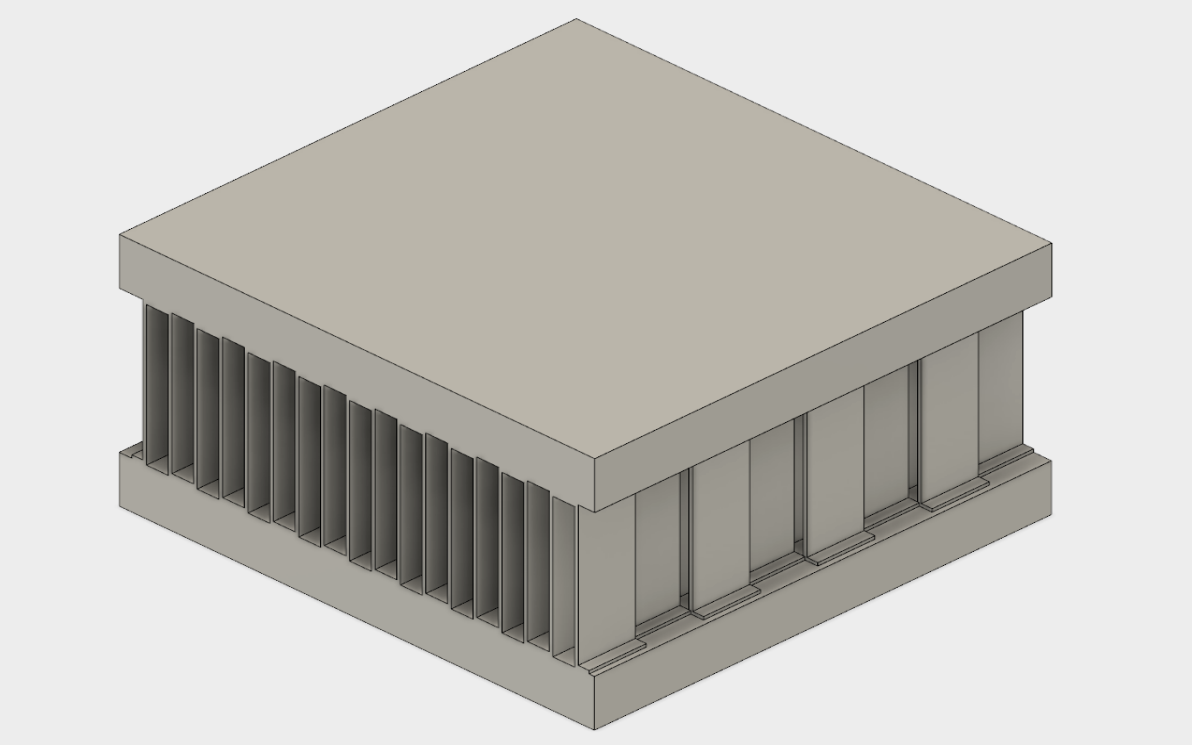

Figure 2.2 Schematic of serrated Fin Design 2.

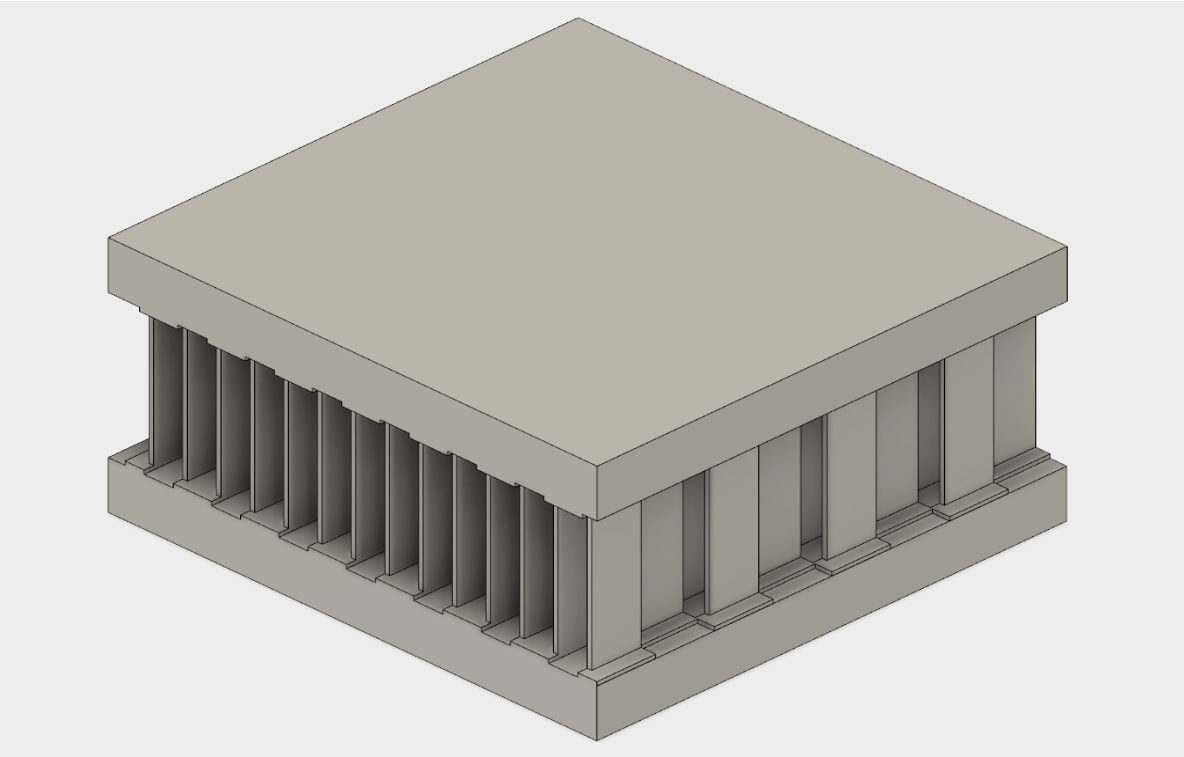

Figure 2.3 Schematic of serrated Fin Design 3.

As per Table 2.1, Designs 1 and 3 have 14 fins in the width-wise direction (perpendicular to the flow) and 8 fins in the length-wise direction (parallel to the flow). The fin dimensions are also same for both Designs 1 and 3 according to Table 2.1. The only difference between both designs is the presence of a notch. Design 1 does not have a notch, while Design 3 has a tiny notch of 0.02 inch on the leading edge of every fin. Design 2 also does not have any notches in its fins, has a higher number of fins in the width-wise direction than Designs 1 and 3. As per Table 2.1, Design 2 has four extra fins in each row as compared to the other two designs. Moreover, the height of the fins is a bit longer in Design 2 at 0.38 inch, whereas the fins of Designs 1 and 3 have heights of 0.375 inch each. The thickness of the fins in Design 2 is 0.008 inch and the thickness of fins in both Designs 1 and 3 is 0.01 inch. Table 2.1 also shows that, the upper plate and lower plate dimensions are all the same for three fin designs. Table 2.2 provides the dimensions of fins and plates in millimeters.

Table 2.1 Dimension of working geometries of serrated fins in inches.

Parameter	**Fin Design 1**	**Fin Design 2**	**Fin Design 3**
Total fins (perpendicular to flow direction)	14	18	14
Total fins (parallel to flow direction)	8	8	8
Fin Geometry			
Height (inch)	0.375	0.38	0.375
Thickness (inch)	0.01	0.008	0.01
Serration length (inch)	0.125	0.125	0.125

Notch depth (inch)	N/A	N/A	0.02
Plate Geometry			
Width perpendicular to flow direction (inch)	1.04	1.04	1.04
Length parallel to flow direction (inch)	1	1	1
Thickness (inch)	0.125	0.125	0.125

Table 2.2 Dimension of working geometries of serrated fins in millimeters.

Parameter	**Fin Design 1**	**Fin Design 2**	**Fin Design 3**
Total fins (perpendicular to flow direction)	14	18	14
Total fins (parallel to flow direction)	8	8	8
Fin Geometry			
Height (mm)	9.525	9.652	9.525
Thickness (mm)	0.254	0.203	0.254
Serration length (mm)	3.175	3.175	3.175
Notch depth (mm)	NA	NA	0.508
Plate Geometry			
Width perpendicular to flow direction (mm)	26.41	26.41	26.41
Length parallel to flow direction (mm)	25.4	25.4	25.4
Thickness (mm)	3.175	3.175	3.175

2.2.2 Mesh

Mesh and grid generations were done using the same tool of ANSYS Workbench Fluid Flow Fluent Meshing. Each connection and contact point were revised between the fluid zone and solid zone before running the mesh. Meshing was also revised and optimized periodically to finally create a fine mesh that would take minimum amount of time to produce a converged solution of the defined numerical problem. Fine mesh option was chosen during the simulation of all three fin designs which is shown in Figure 2.4.

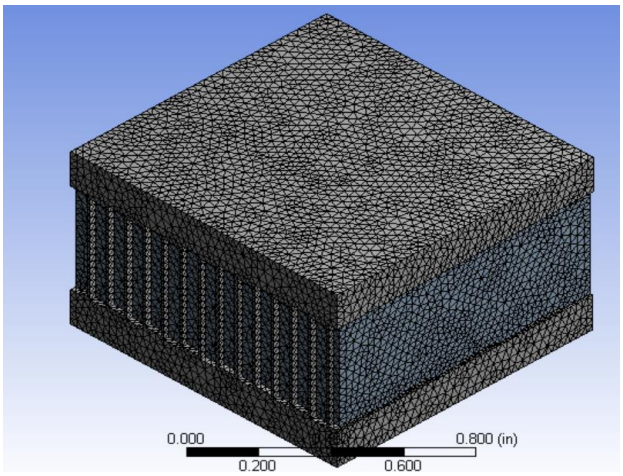

Design 1

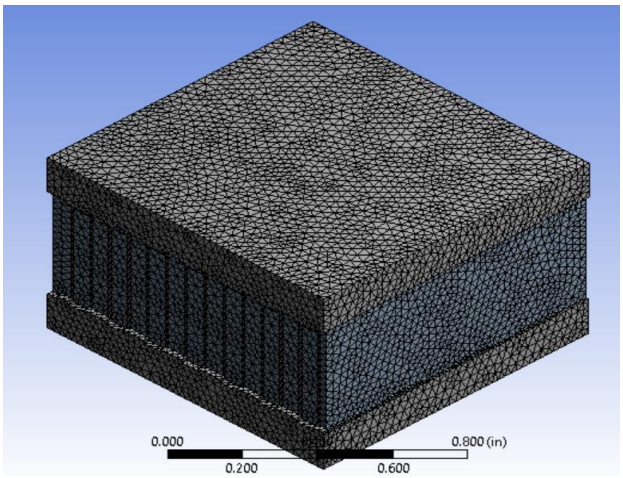

Design 2

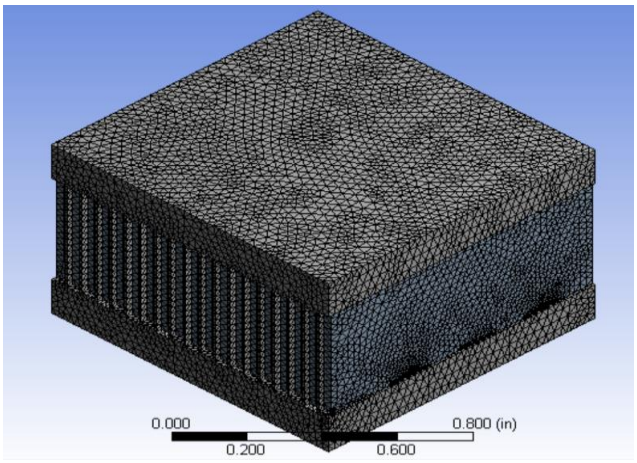

Design 3

Figure 2.4 Mesh quality for three simulations of different fins.

After completing the mesh, the fin designs would get divided into millions of small elements for which the numerical calculation was performed individually. The output of a fine mesh is depicted in Figure 2.4 where the intensity of millions of meshed particles is illustrated. Finally, the air inlet, air outlet and heat flux placement were identified and marked for the software program.

Table 2.3 provides the mesh quantity information. Here the size function had been chosen as adaptive rather than curvature or square to match every small part of the design. In Table 2.3, the minimum edge length from one node to another node, total number of nodes and elements came same for Fin Designs 1 and 3 because they have almost the same type of geometry. Since Fin Design 2 has more fins in the width-wise direction, the total number of nodes and elements were larger and minimum edge length were shorter. As per Table 2.3, for all the fin designs, quality of mesh was fine so that divergence can be avoided during calculation and numerical results could be achieved as much accurate as possible.

Table 2.3 Mesh quality information.

Parameter	**Fin Design 1**	**Fin Design 2**	**Fin Design 3**
Size function	Adaptive	Adaptive	Adaptive
Minimum edge length (inch)	4.2652e-004	2.2222e-004	4.2652e-004
Bounding box diagonal (inch)	1.57230	1.57130	1.57230
Quality of mesh	Fine	Fine	Fine
Total number of nodes	61966	73627	65154
Total number of elements	347254	411824	367333

2.2.3 Setup

The mesh was uploaded in ANSYS Fluent for further setup, processing and analysis of fluid flow and heat transfer equations. The Fluent code is based on the finite volume method where the following assumptions were made before proceeding towards the actual setup:

- Steady-state heat transfer.
- Laminar fluid flow over the serrated fins.
- Incompressible fluid.
- Negligible thermal radiation and natural convection heat transfer.
- Thermal contact resistance is negligible.
- The thermo-physical properties of both materials are temperature independent.

Solid and fluid properties were assumed constant because variations of these properties are small within the temperature range tested [37]. Natural convection of air was also neglected because the fins are covered by rigid aluminum wall and the passages of air in between the fins are very narrow which should suppress natural circulation of the air.

2.2.3.1 Solver Selection

The pressure-based solver was used for calculation of steady state equations and produce absolute results. In the pressure-based solver, physical properties of the fluid such as density, viscosity, specific heat, etc. remained constant throughout the channel flow and the fluid flow has not been influenced by the inlet and outlet conditions for all simulations. To predict the heat transfer and temperature throughout the computational cell, an additional solver was employed to solve the energy equation. In this study, low velocity inlet producing only laminar flow inside of each fluid passage was considered where viscous heating option was also added. Because most of

the data in past studies have used Reynolds numbers greater than 300 for laminar flow, the numerical simulations here used 290 < Re < 2300. When the Reynold number is less than 300, the flow inside the tiny chambers almost becomes stagnant in the barriers of the serrated fin plate pattern [6, 7, 12, 17, 21, 23, 24].

Table 2.4 provides values of the following air properties used in this study like density, specific heat, thermal conductivity, and dynamic viscosity which is assumed in the room temperature. Table 2.4 also provides the following material properties of the pure aluminum like density, specific heat and thermal conductivity which is used for the upper and lower plates as well as the fins.

Table 2.4 Selection of default properties from ANSYS records.

Parameters	**Symbols**	**Values**	**Units**
Fluid (Air)			
Density	ρ	1.225	kg/m^3
Specific Heat	C_p	1006.43	J/kg·K
Thermal Conductivity	k	0.0242	W/m·K
Dynamic Viscosity	μ	1.7894e-05	kg/m·s
Solid (Aluminum)			
Density	ρ	2719	kg/m^3
Specific Heat	C_p	871	J/kg·K
Thermal Conductivity	k	202.4	W/m·K

2.2.3.2 Boundary Conditions

Basically, three boundary conditions have been defined as known input parameters to solve the fluid and heat transfer equations by the Fluent software. These include:

- Air inlet type was selected as velocity inlet. Air Velocity direction was indicated as normal to the boundary and its magnitude was varied between 2-10 m/s. Inlet air thermal condition was kept constant for every simulation by selecting a compressed air temperature of 295 K which is approximately equal to the room temperature.
- Air outlet was selected as pressure outlet where the gauge pressure value was given as 0 Pa. The outlet fluid backflow temperature was assumed at a room temperature of 300 K. Although, no backflow was detected by the solver while solving the equations for 1000 iterations.
- The outside faces of the upper and lower plates were selected as heat flux wall boundary. Its thermal condition had been set as 10 W/in^2 for every simulation of constant surface heat flux condition. The wall temperature was set as 350 K for every simulation of constant surface temperature condition.
- The contact faces between fluid and solid were set as coupled wall heat transfer conditions. The fin walls on the side of the fluid were set as a stationary wall with standard no slip condition.

2.2.3.3 Solution Methods, Initialization and Iteration

A coupled algorithm was used for pressure-velocity coupling. The gradient was selected as least square cell based, standard equations were chosen to solve for pressure and second-order upwind scheme was selected to discretize both the momentum and energy equations.

Monitor Check Convergence Absolute Criteria were selected as 10^{-6} so that the equations for velocity, momentum and energy equation solutions would converge more quickly. Hybrid initialization of 1000 iterations and final calculation run of 1000 iterations were selected at first to inspect solution convergence graph. Up to 100 iterations, the graph was steadily converging and after that it followed a straight line at a specific convergence point in the y- axis. Hence only 100 iterations for initialization and 200 iterations for calculation were used for final data collection [23]. Figures 7.1-7.3 in the Appendix show the convergence of the numerical results of all the fin designs for three different velocities. In these figures, the solutions of the governing equations to calculate pressure and temperature converge within 100 iterations. Figures 7.1-7.3 also show that after 100 iterations the results of the calculations became almost linear which is shown by straight horizontal lines along x-axis. In these figures, three lines represent the convergence of x-momentum, y-momentum, z-momentum equations, one line represents the convergence of the continuity equation and one line represents the convergence of the energy equation.

2.2.3.4 Governing Equations

The program ANSYS Fluent pressure-based solver solves equations for mass, momentum and energy using standard finite volume techniques. The finite volume method was originally developed as a unique finite difference formulation. The numerical algorithm consists of the following steps:

- Formal integration of the governing equations of fluid flow over all the finite control volumes of the solution domain. This step distinguishes the finite volume method from all other finite difference techniques [11].

- Discretization involves the substitution of a variety of finite difference type approximations for the terms in the integrated equation representing flow processes such as convection, diffusion and sources. This process converts the integral equations into a system of algebraic equations [11, 31].
- Solution of algebraic equations by an iterative process [35].

The continuity, momentum and energy equations for the three-dimensional models are as follow [11, 38]:

Continuity Equation

$$\frac{\partial u}{\partial x}+\frac{\partial v}{\partial y}+\frac{\partial w}{\partial z}=0 \tag{2.1}$$

Momentum Equation

$$\rho\left(u\frac{\partial u}{\partial x}+v\frac{\partial u}{\partial y}+w\frac{\partial u}{\partial z}\right)=-\frac{\partial p}{\partial x}+\mu\left(\frac{\partial^2 u}{\partial x^2}+\frac{\partial^2 u}{\partial y^2}+\frac{\partial^2 u}{\partial z^2}\right) \tag{2.2}$$

$$\rho\left(u\frac{\partial v}{\partial x}+v\frac{\partial v}{\partial y}+w\frac{\partial v}{\partial z}\right)=-\frac{\partial p}{\partial y}+\mu\left(\frac{\partial^2 v}{\partial x^2}+\frac{\partial^2 v}{\partial y^2}+\frac{\partial^2 v}{\partial z^2}\right) \tag{2.3}$$

$$\rho\left(u\frac{\partial w}{\partial x}+v\frac{\partial w}{\partial y}+w\frac{\partial w}{\partial z}\right)=-\frac{\partial p}{\partial z}+\mu\left(\frac{\partial^2 w}{\partial x^2}+\frac{\partial^2 w}{\partial y^2}+\frac{\partial^2 w}{\partial z^2}\right) \tag{2.4}$$

Energy Equation

$$\rho c_p\left(u\frac{\partial T}{\partial x}+v\frac{\partial T}{\partial y}+w\frac{\partial T}{\partial z}\right)=\lambda\left(\frac{\partial^2 T}{\partial x^2}+\frac{\partial^2 T}{\partial y^2}+\frac{\partial^2 T}{\partial z^2}\right) \tag{2.5}$$

3 DISCUSSION OF RESULTS

3.1 Data Correlation

3.1.1 Equations for Hydraulic Diameter, Fluid Flow Area and Total Surface Area

The hydraulic diameter is defined as four times the area between two consecutive fins which is also called one free flow area of fluid divided by the total perimeter of that free flow area. The fluid mass flow area is the same as one free flow area taking account only the face area or the area which is perpendicular to the flow direction of fluid into one channel. The surface area of one fin is the surface area of total one channel which is the summation of the surface area of both sides of a fin and corresponding upper and lower plates surface area. This one fin surface area needs to get multiplied by the total number of fins to find the total surface area of the test piece.

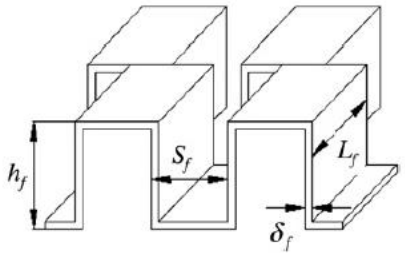

Figure 3.1 Geometrical parameters of serrated fins [19].

Figure 3.1 presents the geometrical parameters of serrated fins used in this study. Here, h_f is the height of the fin, δ_f is the thickness of the fin, L_f is the length of the fin which is also called serration length and $(s_f - \delta_f)$ is the distance between two consecutive fins.

Where,

$$\text{Hydraulic diameter,} \quad D_h = \frac{2\left(h_f - \delta_f\right)\left(s_f - \delta_f\right)}{\left(h_f - \delta_f\right) + \left(s_f - \delta_f\right)} \tag{3.1}$$

Total surface area, $A_s = Total\ fins \times 2 \times L_f \times (h_f + S_f - 2\delta_f)$ (3.2)

Free Flow area, $A_c = (s_f - \delta_f)(h_f - \delta_f)$ (3.3)

Table 3.1 provides the geometrical parameter values of the three serrated fin designs. Fin Design 2 has the maximum height and least thickness in comparison to the serrated Fin Design 1 and serrated Fin Design 3. As per Table 3.1, all the three fin designs have the same serration length. Serrated fins of Designs 1 and 3 have the same dimension of the fins other than the presence of a notch. Hence, the hydraulic diameters and fluid flow areas are the same. Fin Design 3 has the least heat transfer surface area because it has a notch on every leading edge of the fins. Fin Design 2 has the most amount of heat transfer surface area. Because it has more fins than the other two designs.

Table 3.1 Geometrical parameter values of the three serrated fin designs.

Parameters	**Fin Design 1**	**Fin Design 2**	**Fin Design 3**
h_f (mm)	9.525	9.652	9.525
S_f (mm)	1.821	1.412	1.821
δ_f (mm)	0.254	0.203	0.254
L_f (mm)	3.175	3.175	3.175
D_h (mm)	2.681	2.144	2.681
A_c (mm^2)	14.53	11.424	14.53
A_s (mm^2)	7708.114	9745.53	6653.148

3.1.2 Equations Used for Performance Determination

Three equations are used to determine the overall performance of the fin designs the fluid flow, the heat transfer, and the pressure drop equations.

Fluid Flow

The first type has been defined as fluid flow equations. These include the mass flow rate ṁ, the mass velocity G, and the Reynolds number, R_e . The Reynolds number increases when inlet velocity or mass flow rate of the fluid increases. To study laminar flow, velocities which produce a Reynolds number between 300- 2200 are considered.

$$\text{Mass flow rate,} \quad \dot{m} = \rho A_c v = \rho \dot{v} \tag{3.4}$$

$$\text{Mass velocity,} \quad G = \frac{\dot{m}}{A_c} \tag{3.5}$$

$$\text{Reynolds number,} \quad R_e = \frac{\rho v D_h}{\mu} \tag{3.6}$$

Heat Transfer

The Chilton-Colburn j factor has been considered to find the thermal performance of the fins. As the j factor is proportional to the convection heat transfer coefficient, h an increase in the value of j will increase the thermal performance of the fin. Here, the Prandtl number, Pr is constant which is dependent on the inlet condition of fluid which is same for every flow rate of all the fins. The input heat flux has been maintained as a constant value as well. Hence, the Chilton-Colburn j factor is only dependent on Stanton number where Stanton Number is dependent on the wall temperature of the solid and mean temperature of fluid inlet and outlet.

$$\text{Mean temperature,} \quad T_m = \frac{T_i + T_0}{2} \tag{3.7}$$

$$\text{Heat transfer rate,} \quad q = q_{in}{}'' \, A_w \tag{3.8}$$

$$\text{Heat flux,} \quad q_w{}'' = \frac{q}{A_s} \tag{3.9}$$

$$\text{Convection heat transfer coefficient,} \quad h = \frac{q_w{}''}{(T_w - T_m)} \tag{3.10}$$

$$\text{Prandtl number,} \quad Pr = \frac{\mu \, c_p}{k} \tag{3.11}$$

$$\text{Stanton number for constant surface heat flux,} \quad St = \frac{q_w{}''}{c_p \, \rho \, v \, (T_w - T_m)} \tag{3.12}$$

$$\text{Stanton number for constant surface temperature,} \quad St = \frac{D_h}{4L} \ln\left(\frac{T_i - T_w}{T_o - T_w}\right) \tag{3.13}$$

$$\text{Chilton Colburn factor,} \quad j = St \, Pr^{2/3} \tag{3.14}$$

Pressure Drop

The Fanning friction factor f has been considered to find the hydraulic performance of the fins. Pressure drop is proportional to the friction factor. So when the friction factor increases, the pressure drop also increases and thus contributes to less hydraulic performance of the fins.

$$\text{Pressure drop,} \quad \Delta p = \frac{2 \, f \, L \, \dot{m}^2}{D_h \, \rho \, {A_c}^2} \tag{3.15}$$

Dynamic viscosity, specific heat and thermal conductivity have been assumed as constant throughout the flow regime. The Prandtl number is also constant throughout the flow length for every fin design. Table 3.2 lists values of the properties. For the solid part, Table 3.2 details the input heat flux and wall area.

Table 3.2 Fluid and wall property data for all three plate fin designs.

Parameter	**Symbols**	**Values**	**Units**
Fluid (Air)			
Dynamic viscosity	μ	1.789e-05	kg/m.s
Specific heat	C_p	1006.43	J/kg.K
Thermal Conductivity	k	0.024	W/m.K
Prandtl number	Pr	0.744	
Density	ρ	1.225	kg/m^3
Total flow length	L	0.025	m
Solid (Aluminum)			
Input heat flux	q_{in}''	15500	W/m^2
Wall area	A_w	0.002	m^2

Using the above equations and the data, Tables 3.3-3.6 have been created for the three different fin designs. The input or known values in the tables are velocity, inlet temperature, and outlet pressure. From the numerical analysis, the values of outlet temperature, wall temperature and inlet pressure are generated. Finally, using the above equations, the Reynolds number, mass flow rate, Stanton number, Chilton Colburn j factor, and Fanning friction factor f are determined. These variables changes their values for different velocities. All the velocities have been selected corresponding to laminar flow. The individual fin geometrical parameters like hydraulic diameter and total surface area have been taken into account during the j and f value calculations for each fin design. The geometrical parameters of serrated Fin Design 1 has been used to create Tables

3.3 and 3.4. Individual values of j and f for Fin Designs 2 and 3 can be found in Tables 3.5 and 3.6 respectively.

The Chilton Colburn j factor and the Fanning friction factor f values of Tables 3.4-3.6 have been ploted versus the Reynolds number in Figures 3.4 and 3.5, respectively. Figures 3.6 and 3.7 present the heat transfer coefficient h and the pressure drop Δp versus the inlet velocity v, respectively. Constant surface temperature j and f values from Table 3.3 and constant surface heat flux j and f values from Table 3.4 of serrated Fin Design 1 have been compared with previous results [6, 12] to show that the numerical model is in agreement. Figures 3.2 and 3.3 shows these comparisons with the Kays and London [6] data for j and f values, respectively.

Table 3.3 Variable values for serrated Fin Design 1 (constant surface temperature).

Velc v m/s	Mass flow rate M Kg/s	Reynolds Number Re	Inlet Temp Ti K	Outlet Temp To K	Wall Temp Tw K	Stanton No St	Chilton Colburn Factor j	Inlet Pr Pi Pa	Outlet Pr Po Pa	Friction Factor f
2	3.56E-05	3.67E+02	295	341.9996	350	0.050874	0.041778	13.96658	0	0.15044
3	5.34E-05	5.51E+02	295	336.3483	350	0.036772	0.030198	24.78688	0	0.11866
4	7.12E-05	7.34E+02	295	331.6989	350	0.029038	0.023846	37.79893	0	0.10178
5	8.90E-05	9.18E+02	295	327.9339	350	0.024101	0.019792	52.92968	0	0.091218
6	0.000107	1101.3	295	324.8621	350	0.020662	0.016967	70.1853	0	0.083997
7	0.000125	1284.8	295	322.321	350	0.01812	0.014881	89.51691	0	0.07871
8	0.000142	1468.4	295	320.19	350	0.016163	0.013273	110.9475	0	0.074689
9	0.00016	1651.9	295	318.3794	350	0.014607	0.011995	134.4523	0	0.071516
10	0.000178	1835.5	295	316.8217	350	0.013338	0.010953	160.0673	0	0.068964
11	0.000196	2019	295	315.4497	350	0.012269	0.010075	187.6913	0	0.066831
12	0.000214	2202.6	295	315.0705	350	0.011981	0.009839	217.4049	0	0.065047

Table 3.4 Variable values for serrated Fin Design 1 (constant surface heat flux).

	Mass flow rate M Kg/s	Reynolds Number Re	Inlet Temp Ti K	Outlet Temp To K	Wall Temp Tw K	Mean Temp Tm K	HT Coeff h W/m^2K	Stanton No St	Chilton Colburn Factor j	Inlet Pr Pi Pa	Outlet Pr Po Pa	Friction Factor f
2	3.56E-05	367.09	295	364	375.1	329.5	85.926	0.0348	0.0286	13.967	0	0.1504
3	5.34E-05	550.64	295	341.5	356.5	318.2	102.33	0.0277	0.0227	24.787	0	0.1187
4	7.12E-05	734.19	295	330.1	347.5	312.6	112.1	0.0227	0.0187	37.799	0	0.1018
5	8.90E-05	917.74	295	323.3	342.2	309.1	118.6	0.0192	0.0158	52.93	0	0.0912
6	0.00011	1101.3	295	318.7	338.6	306.8	123.27	0.0167	0.0137	70.185	0	0.084
7	0.00012	1284.8	295	315.4	336.1	305.2	126.82	0.0147	0.0121	89.517	0	0.0787
8	0.00014	1468.4	295	312.9	334.2	304	129.63	0.0131	0.0108	110.95	0	0.0747
9	0.00016	1651.9	295	311	332.7	303	131.91	0.0119	0.0098	134.45	0	0.0715
10	0.00018	1835.5	295	309.4	331.5	302.2	133.77	0.0109	0.0089	160.07	0	0.069
11	0.0002	2019	295	308.2	330.6	301.6	135.47	0.01	0.0082	187.69	0	0.0668
12	0.00021	2202.6	295	307.2	329.7	301.1	136.89	0.0093	0.0076	217.4	0	0.065

Table 3.5 Variable values for serrated Fin Design 2.

Velc v m/s	Mass flow rate M Kg/s	Reynolds Number Re	Inlet Temp Ti K	Outlet Temp To K	Wall Temp Tw K	Mean Temp Tm K	H.T Coeff h W/m^2K	Stanton No St	Chilton Colburn Factor j	Inlet Pr Pi Pa	Outlet Pr Pa	Friction Factor f
2	2.80E-05	293.52	295	362.9	368	329	79.96	0.03243	0.0266	17.78	0	0.1532
3	4.20E-05	440.28	295	340.5	349	317.8	100.92	0.02729	0.0224	30.86	0	0.1181
4	5.60E-05	587.04	295	329.3	339	312.2	114.31	0.02318	0.019	46.16	0	0.0994
5	7.00E-05	733.8	295	322.6	334	308.8	123.37	0.02001	0.0164	63.61	0	0.0877
6	8.40E-05	880.56	295	318.1	330	306.5	129.86	0.01756	0.0144	83.19	0	0.0796
7	9.80E-05	1027.3	295	314.8	328	304.9	134.77	0.01562	0.0128	104.9	0	0.0737
8	0.00011	1174.1	295	312.4	326	303.7	138.53	0.01405	0.0115	128.6	0	0.0692
9	0.00013	1320.8	295	310.5	325	302.8	141.58	0.01276	0.0105	154.4	0	0.0657
10	0.00014	1467.6	295	309	324	302	144.06	0.01169	0.0096	182.2	0	0.0628
11	0.00015	1614.4	295	307.8	323	301.4	146.15	0.01078	0.0088	212.1	0	0.0604
12	0.00017	1761.1	295	306.8	322	300.9	147.93	0.01	0.0082	244.1	0	0.0584

Table 3.6 Variable values for serrated Fin Design 3.

Velc v m/s	Mass flowrate M Kg/s	Reynolds Number Re	Inlet Temp Ti K	Outlet Temp To K	Wall Temp Tw K	Mean Temp Tm K	HT Coeff h W/m^2K	Stanton No St	Chilton Colburn Factor j	Inlet Pr Pi Pa	Outlet Pr Po Pa	Friction Factor f
2	3.56E-05	367.09	295	360.5	376	328	95.047	0.0385	0.0317	11	0	0.1176
3	5.34E-05	550.64	295	339.2	358	317	110.56	0.0299	0.0245	19	0	0.0924
4	7.12E-05	734.19	295	328.4	350	312	119.9	0.0243	0.02	29	0	0.0791
5	8.90E-05	917.74	295	321.9	344	308	126.25	0.0205	0.0168	41	0	0.0708
6	1.07E-04	1101.3	295	317.5	341	306	130.89	0.0177	0.0145	54	0	0.0651
7	1.25E-04	1284.8	295	314.4	338	305	134.5	0.0156	0.0128	69	0	0.061
8	0.00014	1468.4	295	312	337	304	137.4	0.0139	0.0114	86	0	0.0579
9	0.00016	1651.9	295	310.2	335	303	139.81	0.0126	0.0103	104	0	0.0554
10	0.00018	1835.5	295	308.7	334	302	141.84	0.0115	0.0094	124	0	0.0534
11	0.0002	2019	295	307.5	333	301	143.55	0.0106	0.0087	145	0	0.0517
12	0.00021	2202.6	295	306.5	332	301	145.08	0.0098	0.0081	168	0	0.0504

3.2 Discussion of Results

Figures 7.4-7.6 in the Appendix show the inlet pressure of fluid for the three fin designs and for velocities of 2, 7 and 12 m/s respectively. A vertical plane perpendicular to the fluid flow direction at the very beginning of the first row of fins where the fluid enters the system, the inlet pressure contour for the respected fins can be determined. These figures show very high pressure for the three fin designs in yellow, orange and red color. If we follow the range of pressure in these figures, we see that with increasing velocity the inlet pressure also increases. Figures 7.4-7.6 show higher pressure near the fin edges for all three fin designs. Near the fin edge, the fluid flow faces barrier because of the resistance of fins. Thus, the fluid flow faces a solid a barrier of fins which creates more pressure near the fin wall. The pressure color contour is much darker on the fluid flow path near the edges of the fins showing this higher fluid pressure.

Figures 7.7-7.9 show the outlet pressure contour of the fluid flow. Again, if we take a vertical plane perpendicular to the fluid flow direction at the end of the last row of fins where fluid flow gets out of the system and mixes up with the outside atmosphere, we see the outlet pressure contour. Since in this analysis we are considering absolute pressure, all the outlet pressure contours will show a pressure of absolute zero which is equal to the atmospheric pressure. When the air exits the system it immediately starts to mix with the surrounding air and drops down to the atmospheric pressure. Hence, therefore the pressure contours of the three fin designs for multiple velocities show the same blue color in Figures 7.7-7.9 indicating zero absolute pressure at the outlet.

Figures 7.10-7.12 present the overall pressure drop from the inlet to the outlet of the system for the three different velocities and for the three fin designs. The pressure drop contour is almost

same for all three figures. In that there is high pressure at the inlet, then gradual pressure drop throughout the fin passages and finally zero pressure at the outlet. Figures 7.10-7.12 show the top view of the fin design. From the shades of different colors, we see that high pressure occurs near the solid fins where fluid flow disturbance occurs, and pressure is relatively low at the hollow space where fluid has less barrier in the flow regime. As expected for high velocity flows the pressure drop is large, while for low velocity flows the pressure drop is smaller.

Figures 7.13-7.15 show the inlet air temperature for the three fin designs at three different velocities. If we take a vertical plane perpendicular to the fluid flow direction at the very beginning of the first row of fins where fluid enters the system, we find the inlet pressure contour for the respected fins. The inlet temperatures are same for all the fin designs for all velocities at 295K. Hence the air inlet temperature shows same color contour. As shown in Figure 7.13-7.15, the temperature is very high in the solid region (upper plate, lower plate and the fins) showing overall red color. In the idle of the hollow fin passages, the fluid inlet temperature is very low showing blue color contour. Near the edges where fluid touches the hot fin plates, the temperature is relatively higher than the middle portion showing different shades of green color.

Figures 7.16-7.18 show the outlet temperature of the fluid for the three velocities tested. Again, if we take a vertical plane perpendicular to the fluid flow direction at the end of the last row of fins where fluid exits the system and mixes up with the outside atmosphere, we find the outlet temperature contour. Accordingly Figures 7.16-7.18 show the outlet temperature is very high for air at every velocity value depicting an orange to yellow color contour. This is a very good indication of effective heat transfer from the solid fins to the fluid flow, since from the inlet to the outlet plane the temperature increase can be visually recognized. The temperature is relatively high near the solid zone where fluid flow touches the hot solid. As expected the outlet

temperature is relatively high when the fluid inlet velocity is low. The outlet temperature gets lower with higher inlet velocities. When the inlet velocity is low, the fluid resonance time increases inside the heated fin passages. The heat transfer from the solid zone to the liquid zone raises the temperature. With increased velocity, the fluid exits more quickly, and there is less resonance time to heat.

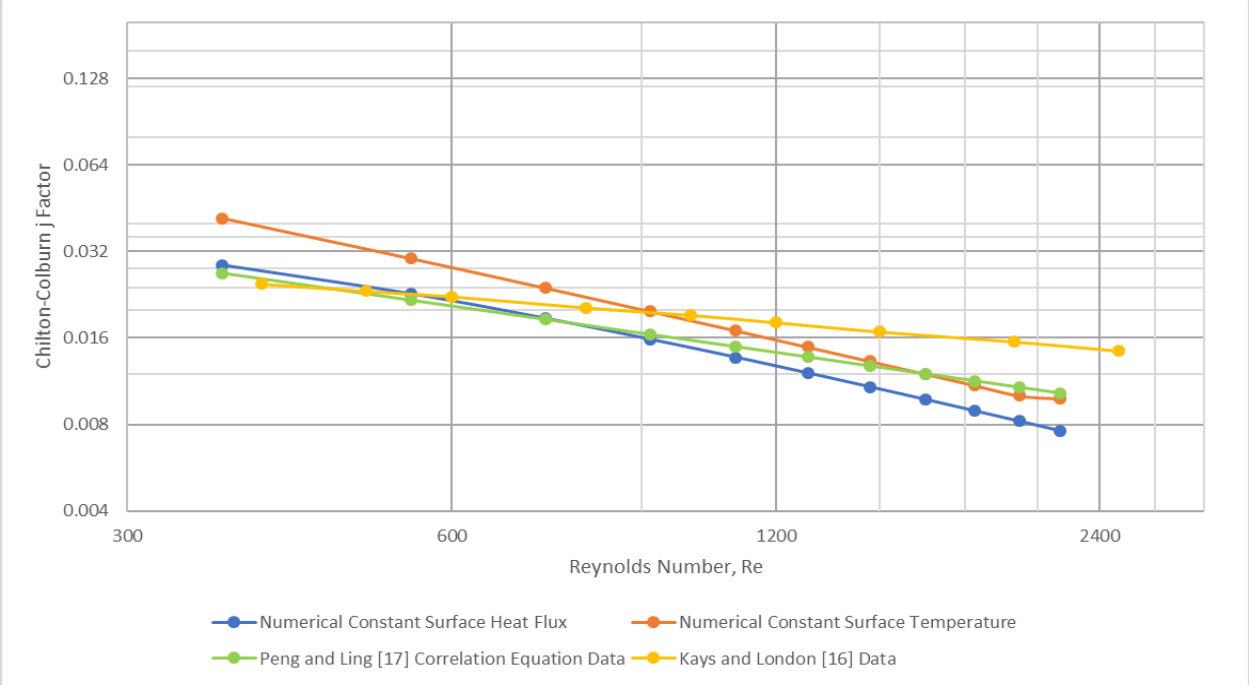

Figure 3.2 Comparison of heat transfer performance of Fin Design 1 [16, 17].

In Figure 3.2, the j factor curve from the numerical results of constant surface temperature shows higher values than the curve of constant surface heat flux for serrated fin Design 1. Both curves are in good agreement with Kays and London [16] and Peng and Ling [17] correlation data. The curves are consistent and show the same pattern of decreased j factor values with increased Reynolds number. Both numerical curves are closer to the Peng and Ling [17] correlation curve than the Kays and London experimental data curve in Figure 3.2. The maximum deviation of constant surface heat flux values with Peng correlation is 24% which occurs at a high Reynolds

number (2000-2300) where the laminar flow region falls into the transition region. On the other hand, the maximum deviation of constant surface temperature values with Peng correlation is 35% which occurs at a low Reynolds number (350-550) where the inlet air velocity is very low. The average difference of Chilton-Colburn j factor values between the two numerical curves is 26%.

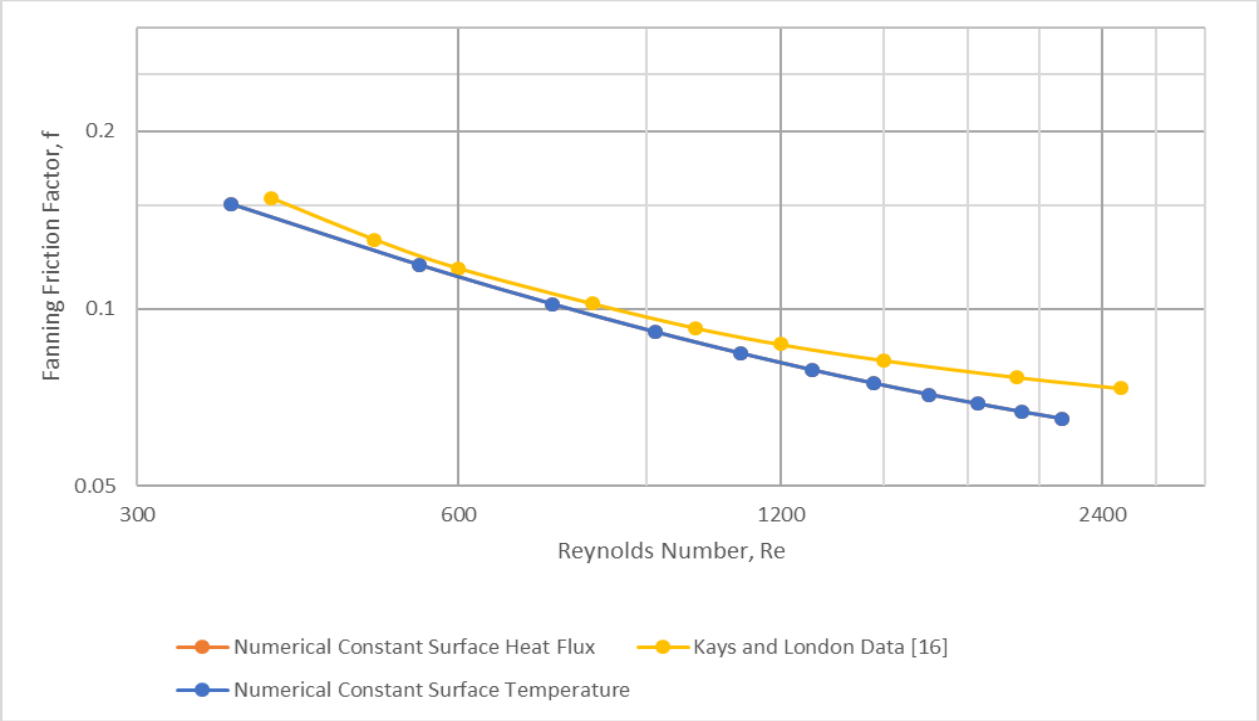

Figure 3.3 Comparison of pressure drop performance of Fin Design 1 [16].

From Figure 3.3, we see that the pressure curves of both numerical results and Kays and London [16] for serrated Fin Design 1 are in good agreement. The numerical results from constant surface heat flux and constant surface temperature cases show the same pressure drop for the same flow rates. Therefore, the Fanning friction factor f values are equal for the two different surface conditions of serrated Fin Design 1. In Figure 3.3, there is just one curve of numerical results instead of two curves. The numerical results show that the friction factor only depends on pressure drop at different velocities rather than the heat transfer surface condition. The maximum deviation of results is 12% for both numerical results with the Kays and London [16] data. From Figure 3.3

we see that the deviation mainly occurs at high Reynolds numbers of 2000-2300 just like Figure 3.2, where the laminar flow region falls into the transition flow region.

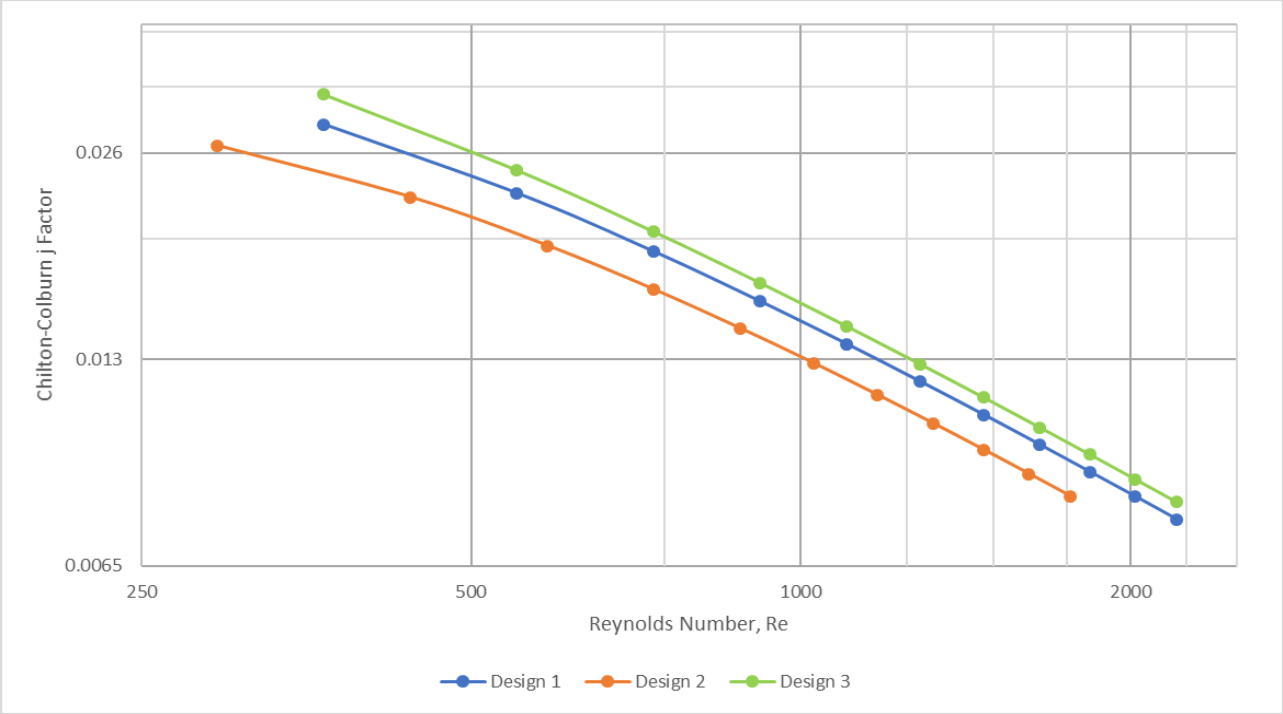

Figure 3.4 Comparison of j factors of different fins.

From the comparison among the three different fin designs in Figure 3.4, the serrated Fin Design 3 has the highest j factor values, while serrated Fin Design 2 shows the lowest values of j factor. Thus, Figure 3.4 indicates that Fin Design 3, the notched serrated fin has the best heat transfer performance because it produces the highest Chilton Colburn j factor values for all flow rates in the laminar flow range. Figure 3.4 shows that the j factor variations are the largest for lower Reynolds numbers. For example, for a Reynolds number of 550, the serrated Fin Design 1 shows approximately 19.5% increase in j factor value than serrated Fin Design 2. For the same Reynolds number, serrated Fin Design 3 Chilton Colburn j values are almost 29% higher than those of serrated Fin Design 2. Again, for the same Reynolds number of 550, Fin Design 3 j factor value is almost 8% higher than Fin Design 1. This indicates that, having a small notch in the fin

design can have an enhanced effect on increasing the thermal performance of the fin, especially when the system is operating in the low Reynolds number range for laminar flow. The small notch design increases the j value a maximum of apparently 8% for a low Reynolds number. Finally, in Figure 3.4 we see that the serrated Fin Design 3 or notched serrated fins has a better thermal performance in comparison to the other two serrated fin designs.

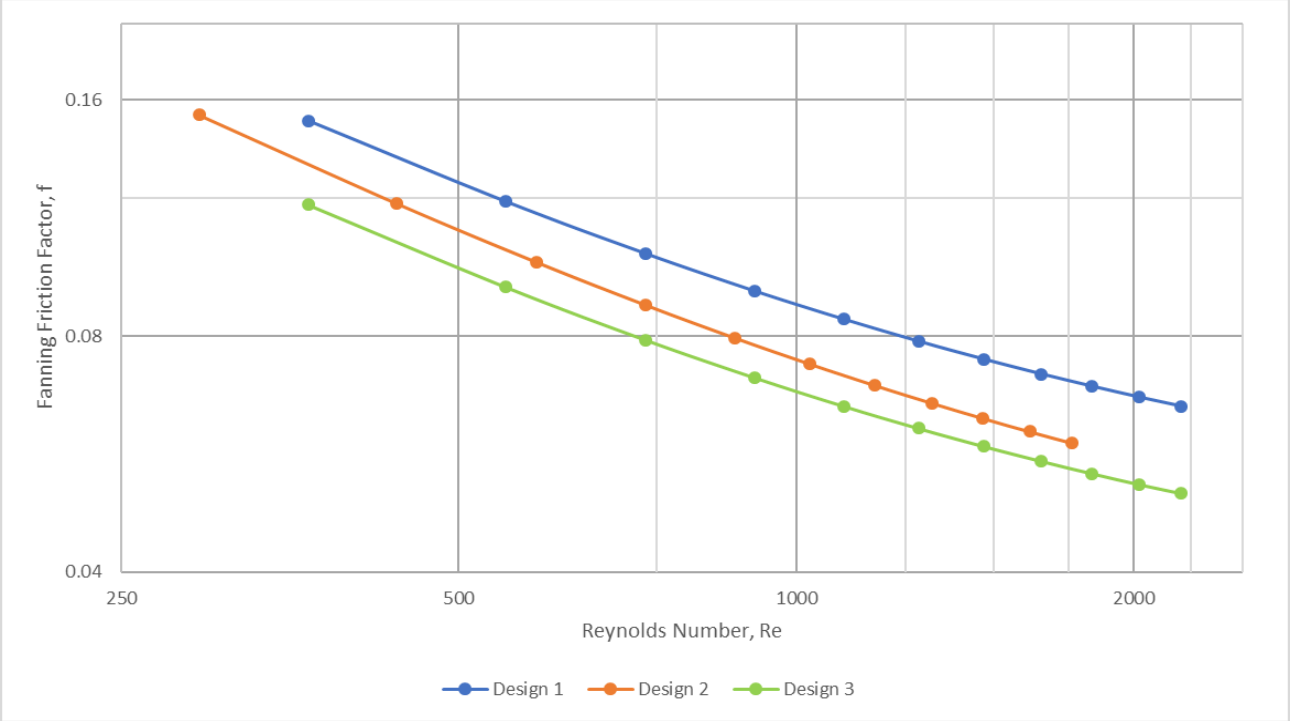

Figure 3.5 Comparison of f factors of different fins.

In Figure 3.5, Fin Design 1 generates the highest values of the Fanning friction factor f. Here we see that serrated Fin Design 3 has the smallest values of Fanning friction factor f of the three fin designs. The Fanning friction factor values of serrated Fin Design 2 is almost 16% less than serrated Fin Design 1 for a Reynolds number of 550. Similarly, the friction factor values of serrated Fin Design 3 are approximately 22% lower than serrated Fin Design 1 for the same Reynolds number of 550. Figure 3.5 shows that a small notch placed in the leading edge of a serrated fin can provide an advantage of increasing the hydraulic performance by lower values of

the friction factor and hence the pressure drop. A small notch can lower the friction factor by as much as 22%. Therefore, Fin Design 3 or the notched serrated fin has the best hydraulic performance among the three serrated fin designs.

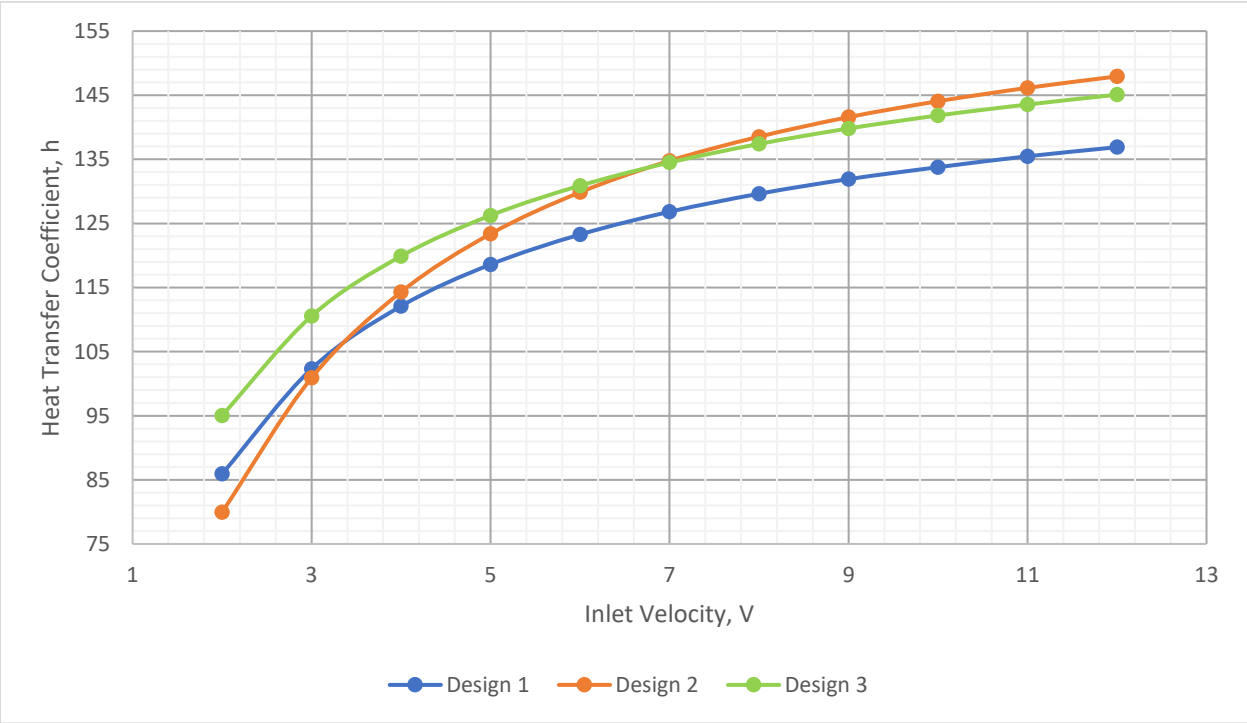

Figure 3.6 Comparison of heat transfer coefficients of different fins.

In Figure 3.6 it is observed that the heat transfer coefficient, h largely depends on the total heat transfer surface area and fluid inlet velocity. Fin Design 2 shows the lowest values of h at lower velocity but the highest values of h at the higher velocity in the laminar flow range. The slope of the curve of Fin Design 2 is much higher than Fin Designs 1 and 3. Just like Figure 3.4, Figure 3.6 also shows that the notched serrated fins have the best thermal performance among the three fin designs since it has the highest values of h for all flow rates. Figure 3.6 also predicts that Fin Design 2 can provide the best thermal performance in comparison to the other two fin designs because it has the maximum amount of heat transfer surface area.

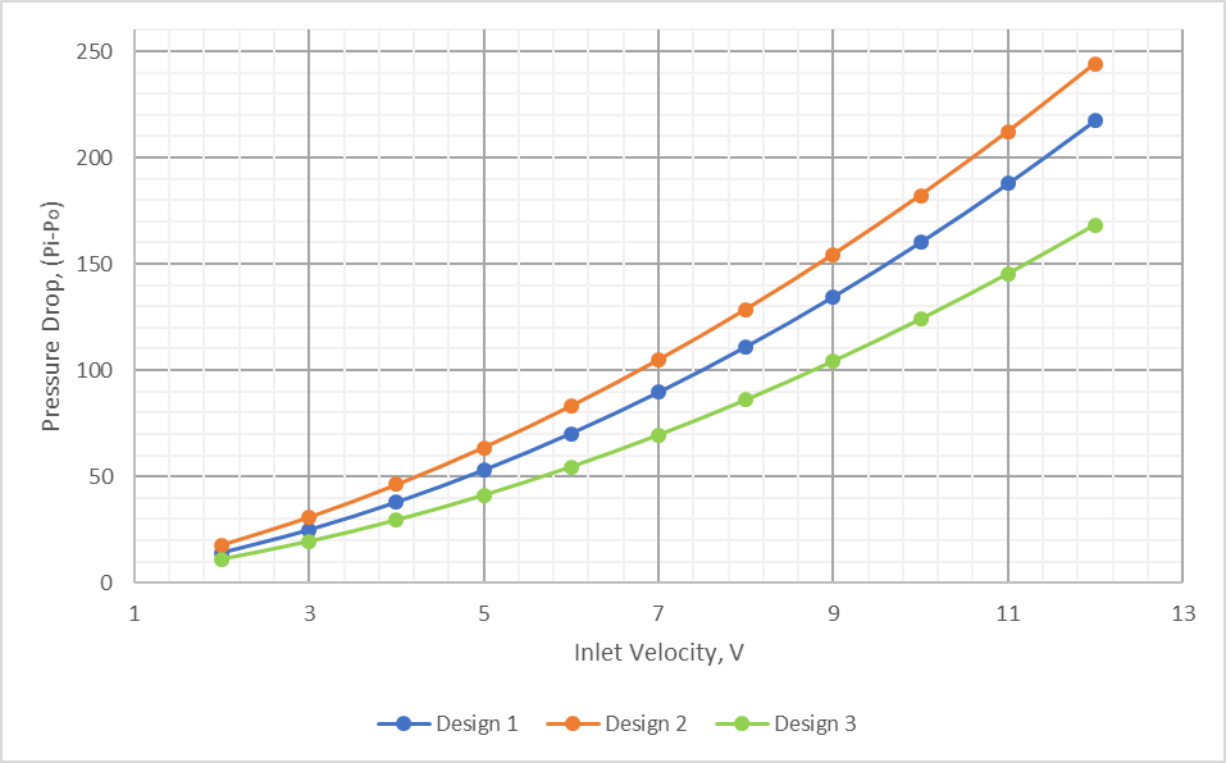

Figure 3.7 Comparison of pressure drop of different fins.

Figure 3.7 shows that Fin Design 2 has the maximum pressure drop as compared to Fin Designs 1 and 3 because it has the greatest number of fins. In Figure 3.7, we see that at lower inlet velocity, the pressure drop is almost same for all the fin designs. As expected, with increasing velocity the pressure drop increases, but is not linear with velocity. The amount of pressure drop is different for the three fin designs. Fin Design 3 has the lowest pressure drop which agrees with the findings of Figure 3.5. Hence, Fin Design 3 or the notched serrated fin has the best hydraulic performance among the three fin designs.

One other part of interest in comparing the results of Figures 3.5 and 3.7 is that, in both graphs the smallest values of friction factor and pressure drop are for Fin Design 3 or the notched serrated fin. Fin Designs 1 and 2 have interchanging results. The friction factor curve is higher for Fin Design 1 in Figure 3.5, but the pressure drop curve is higher for Fin Design 2 in Figure 3.7.

Hydraulic diameter and fluid flow areas have great influence in determining the hydraulic performance. Also, in Figure 3.6, the heat transfer coefficient of Fin Design 2 abruptly increases with increasing Reynolds number and shows very high heat transfer coefficients for higher Reynolds number in the laminar to turbulent transition region. Thus, the heat transfer coefficient curve is much steeper for Fin Design 2 than the curves of Fin Designs 1 and 3 in Figure 3.6.

From the above observations of data, it is concluded that the serrated Fin Design 3 or the notched serrated fins are the most efficient fins as compared to the serrated Fin Designs 1 and 2. The highest Chilton Colburn j factor and the heat transfer coefficient shows that Fin Design 3 has the highest thermal performance in the laminar flow region. Also, the Fanning friction factor f and pressure drop curves are lowest for Fin Design 3, thus provides the highest hydraulic performance as well.

4 PROPOSED EXPERIMENTAL SETUP

In this chapter, an experimental setup is proposed which can be used for future experimental data collection for the three fin designs. These future experimental data will help to further verify the validity of the numerical model and the data analysis. The first challenge is to propose an inlet channel which will allow the fluid to enter the fin assembly in a uniform manner. This inlet channel is made by integrating multiple parts together without any leakage so as to not affect the pressure drop or the air flow rate. In addition, this inlet channel needs to be able to easily detachable from the fin assembly so that multiple fin design assemblies can be tested. Lastly, the proposed experimental design apparatus (sensors, data acquisition devices etc.) is discussed in detail.

4.1 Inlet Channel

The inlet channel shown in Figure 4.1 has been designed into three separate parts:

- Air Knife
- Honeycomb Assembly
- Straight Channel

These three parts have been glued together to reduce complexity of design and use of other fixtures like bolts, nuts, screw, etc. Three parts have been individually 3D printed. Sanding was done to make the surfaces smooth and easier to glue together. A solid bond without having any air leakage was created. The last part, a flange was made by a flat surface having four small holes as shown in Figure 4.1. Using these holes, the inlet channel would attach with the fin assembly by means of screws, washers and flexible rubber sealing in the middle.

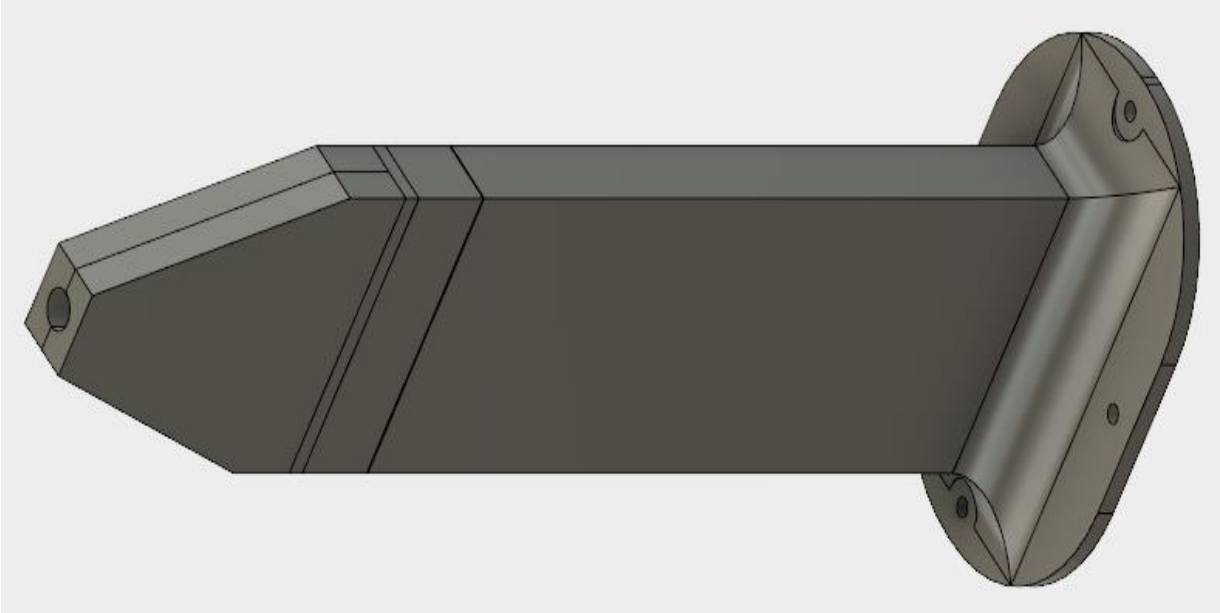

Figure 4.1 Schematic of Inlet Channel.

4.1.1 Separation of Fluid Flow

Fluid flow is prone to separation when the cross-sectional area of the flowing passage increases in the stream-wise direction. This should be an important concern for the design of heat exchanger while installing fittings and valves. Flow separation is a major cause of pressure drop and it also impacts the heat transfer performance.

According to Experimental Heat Transfer, Fluid Mechanics and Thermodynamics [39], for an experiment in fluid flow through a distorted duct having a diverging section of 10-degree angle, the flow visualization showed no separate regions inside the duct. Other sources have stated [26, 27, 28, 40] have stated flow separation for higher than 7-degree divergence angles. Both the 7- and the 10-degree recommendations did not include the possible effect of the Reynolds number, flow rate or flow velocity.

A more recent paper [41] relates flow separation with both the divergence angel and Reynolds number by doing numerical analysis. It was found that flow separation can occur for a diffuser expansion angle of even 5- degree for inlet Reynolds number less than 2000. From 11 to 30-degree divergence angles, simulations showed separation at all Reynolds numbers from the laminar to the turbulent range. The largest stream-wise length of the separation zones occurred at the lowest Reynolds numbers. With increasing Reynolds numbers, the length of the separated region diminishes gradually for small angles like 5-10 degrees. This finding invalidates all previous assertion of the divergence angle [42, 43].

With the proposed experimental design, compressed air with high velocity air flow can be used as the source of the fluid flow inside of the fin assembly. The compressed air pipe followed by a hose pipe has a circular cross section from which the air will flow into the fins at a specific velocity. Two valves have been attached to regulate the air flow rate. The end of the hose pipe has a smaller circular cross section in comparison to the rectangular cross section of the inlet part of the fin assembly. Hence, the necessity of having an inlet channel in-between became essential which will direct the fluid flow thoroughly and uniformly from circular cross-section of the hose pipe towards the rectangular cross section of the fin assembly. Fluid flow separation, laminarization and uniformity without losing much of the flow rate magnitude have been taken into consideration while designing the entrance of the inlet channel [44].

The geometry chosen for this study is an air knife, which is one type of conical diffuser. It receives a fully developed compressed air flow at its inlet from a circular cross-section of hose pipe and mates downstream with a long rectangular channel at its exit. The downstream pipe is long enough to allow full development of the fluid flow. The knife consists of a high-intensity, uniform sheet of laminar airflow section, sometimes known as streamline flow [45]. It is a

pressurized air plenum containing a series of continuous slots through which pressurized air exits in a laminar flow pattern. The exit air velocity then creates a uniform flow in the downstream pipe without altering the developed flow intensity from the upstream flow because no flow separation happens in the small passages of each slot between the solid fins. Here, the air knives are stationary while the fluid passes through it with certain compressed air velocity.

Figure 4.2 is a schematic of the proposed Air Knife. A 3D printer was used to print the air knife vertically in which printing started from the rectangular outlet part facing at the bottom [46]. The printer gradually built the smaller circular cross-section as per Figure 4.2, by reaching at the top and printing narrow threads of plastic one after one. The smaller cross-section entrance part of Figure 4.2 was made of pure solid plastic for a short distance so that it could be tapped later to fit with the screw of the compressed air hose pipe. Each fin thickness in the triangle of the Air Knife of Figure 4.2 has been increased gradually at the outlet end. The narrow fluid flow passages between the fins of Figure 4.2 have been maintained constant in width so that no flow separation can happen. The fins were employed on one side with full height so that ends can be matched easily with the plain non-finned upper plate according to Figure 4.2. The lower plate, upper plate and fins were 3D printed as a single part to minimize the number of joints and complexity of design of the Air Knife.

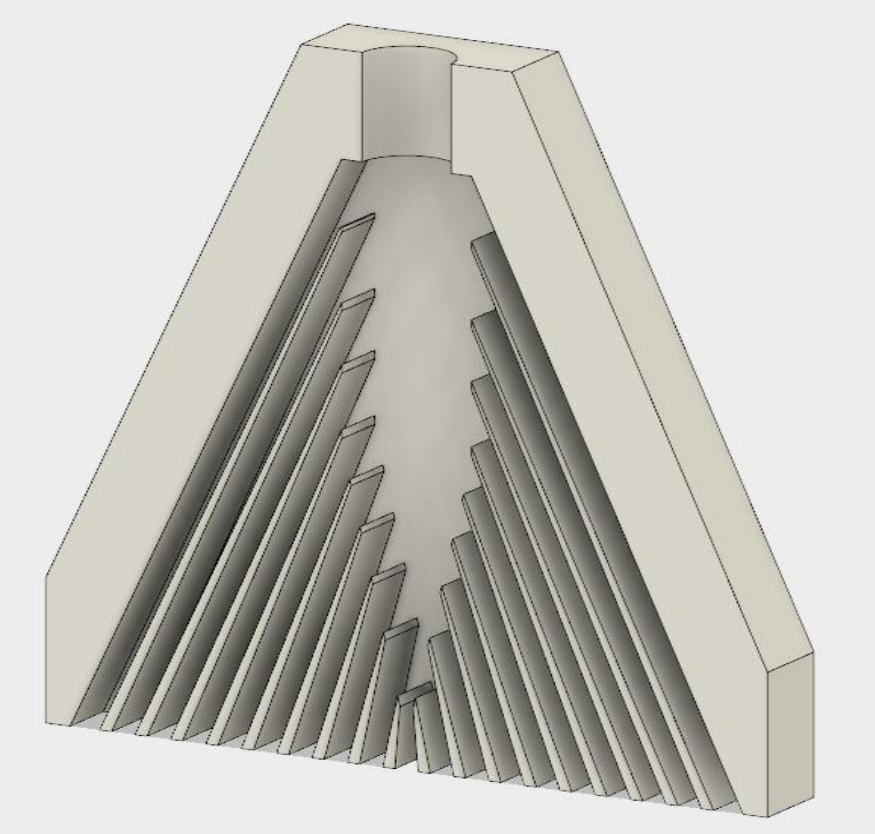

Figure 4.2 Schematic of Air Knife design.

4.1.2 Further Straightening of Fluid Flow

The present numerical study has been done for laminar flow inside of serrated fins. The test samples of the serrated fins have very narrow channels of fluid flow having small hydraulic diameters which contribute to laminar flow. The feed air from the inlet channel to the serrated fins would face much larger hydraulic diameter while flowing inside of the rectangular pipe. This can certainly contribute to turbulent flow inside the pipe because of the high mass flow rate of compressed air. Thus, further straightening of the air flow after passing through the air knife is necessary to reduce turbulence.

Different honeycomb shapes or screens or both are typically used as an operator in the fluid flow system which can suppress the level of incoming turbulence. Honeycomb is a very effective method to reduce lateral turbulence. A considerable amount of theoretical and experimental formulation is available for inspecting the influence of honeycombs on low to high velocity fluid flow fields to reduce the turbulence level in air and water tunnels [43, 44, 47].

One very important study [48] had been done on the effects of honeycomb lengths on free stream turbulence. It also viewed turbulence intensity on downstream distances after passing through honeycombs of different lengths. The study tested a mean velocity of 5 m/s and the results are presented in Figures 4.3-4.6.

Figure 4.3 shows that, for a lower length of honeycomb the pressure drop of fluid passing through it will be lower. Figure 4.4 again shows that the lowest length of honeycomb (2.5 cm) provides the lowest amount of turbulence in the downstream flow. The distance x in the stream-wise direction is measured from the end of the honeycomb to the downstream end of the flow. In any case, the level of turbulence is well below that which existed in absence of the honeycomb. From Figure 4.5 it is conducted that the largest length of honeycomb has the smallest amount of turbulence just after passing through it, but the highest amount of turbulence at a further distance downstream after 3 cm. Figure 4.6 which uses the honeycomb of 2.5 cm, shows that after passing through the 2.5 cm length honeycomb up to 2 cm turbulence is very low. After that part, it starts to reach the peak value of turbulence up to 6 cm. After 6 cm, again the turbulence level starts to decrease and reaches the minimum level at 22 cm and continues to minimize after that. Here, all the honeycombs in this study [48] were made from straws having same circular cross-sectional area.

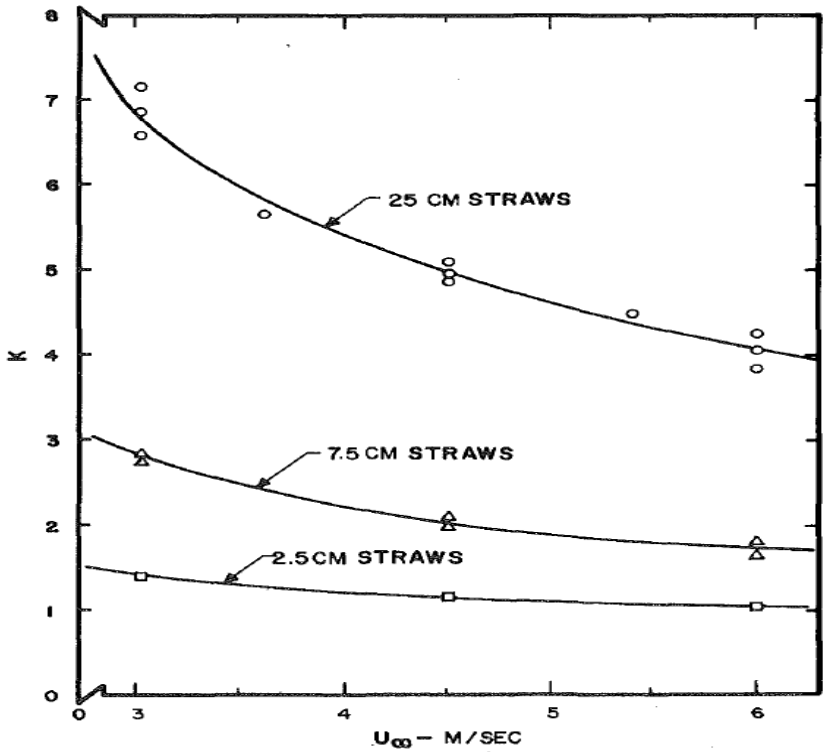

Figure 4.3 Relation of pressure drop of different length honeycombs on free stream velocity [48].

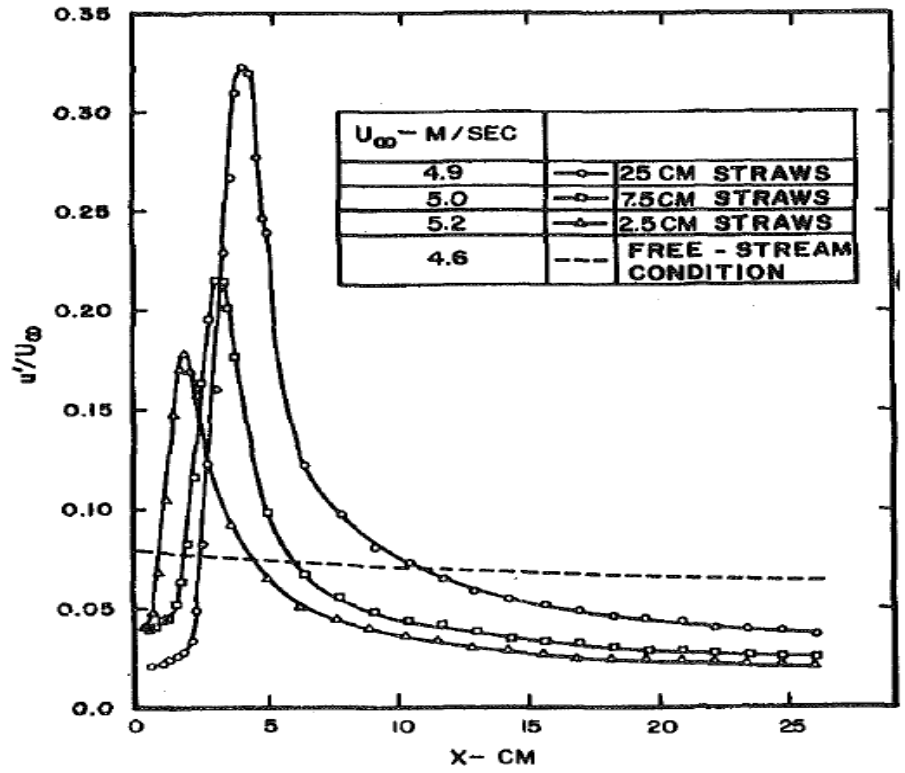

Figure 4.4 Comparison of downstream turbulence for honeycombs of different length [48].

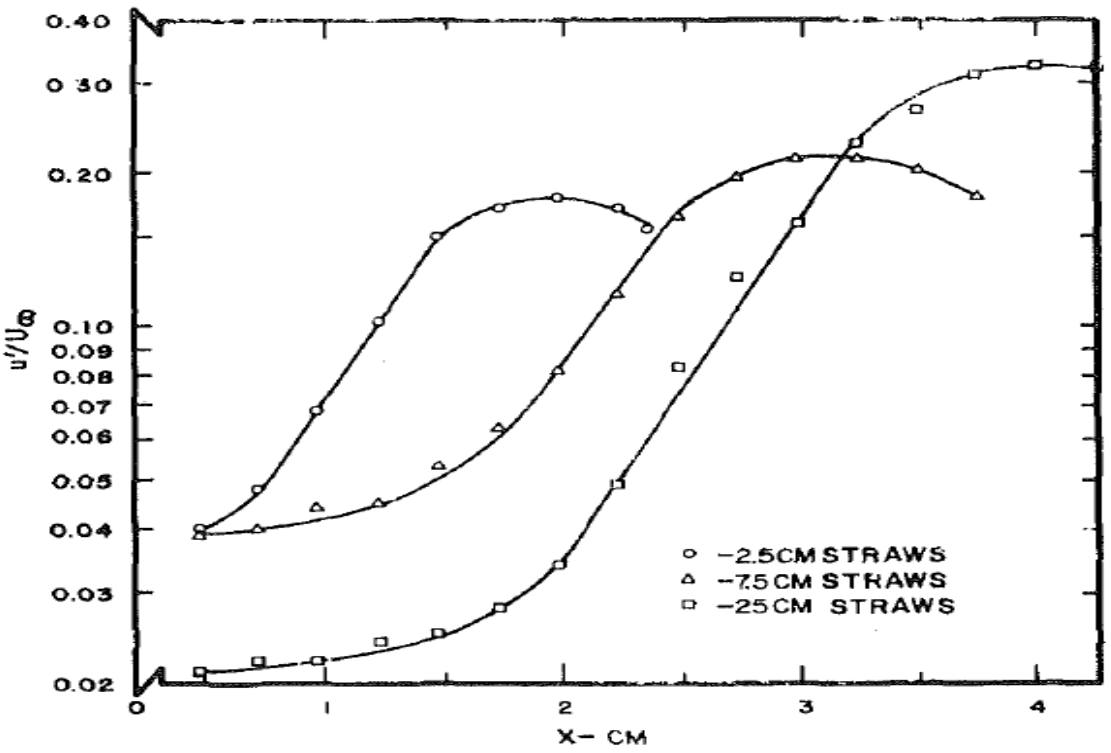

Figure 4.5 Turbulence immediately downstream of honeycombs of different lengths [48].

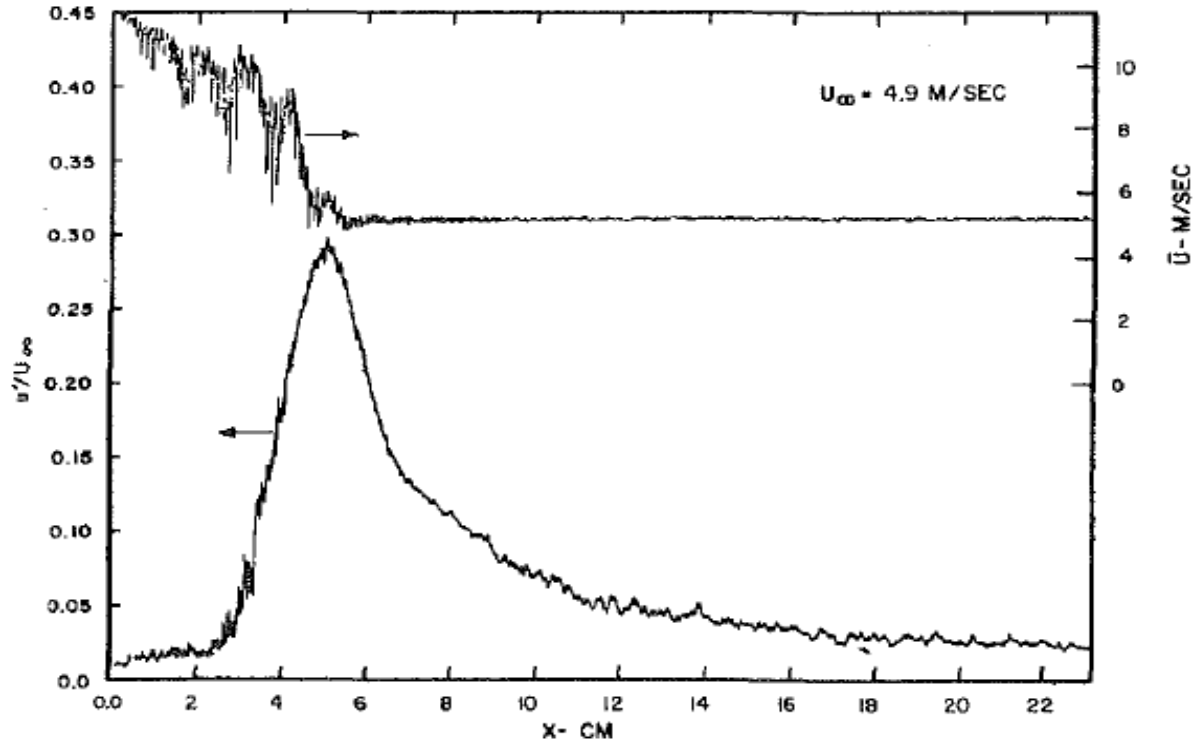

Figure 4.6 Axial profiles of turbulence of a honeycomb made of 2.5 cm straws [48].

Another elaborate study [49] on different shapes of honeycomb investigated the honeycomb diameter, thickness, length and positioning so that minimum level of turbulence and maximum level of fluid flow straightening can be achieved by the setup of the inlet channel. In Figure 4.7, an elaborate relation is shown between the diameter of the honeycomb with the turbulence intensity. From Figure 4.7, we see that for different diameters the distance where turbulence will be maximum after passing through the honeycomb is different. In other words, the maximum turbulence point is not same for honeycombs of different diameters. Figure 4.8 states almost the same thing but instead of the distance after passing through the honeycomb it relates the length of the honeycomb with the turbulence intensity. Once we fix the diameter of the honeycomb is fixed, the honeycomb length and the possible flow length after passing through the honeycomb which would minimize the turbulence most effectively can be determined. Figure 4.9 shows the relation between turbulence level with total distance from where the flow started to that point of the channel where turbulence will be minimum or maximum.

From Figures 4.7-4.9, it has been determined that the least diameter or end-to-end distance of two corners of a honeycomb (d) is most effective in reducing turbulence. Other findings for reducing maximum possible turbulence include-

- $10 < (x/d) < 80$ or above.
- $(l/d) = 8\text{-}12$.
- Minimum possible diameter (d), minimum possible thickness (t) from 3D printer.

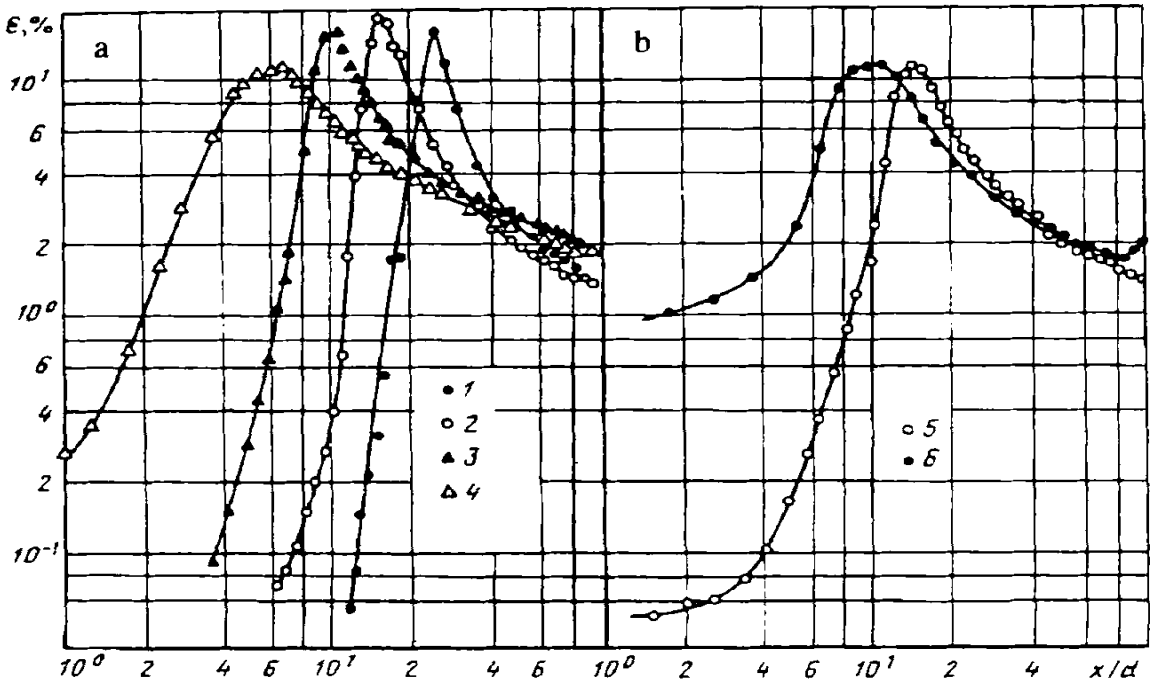

Figure 4.7 Relation between turbulence (Ɛ) with honeycomb diameter (d) and distance after passing through honeycomb (x) [49].

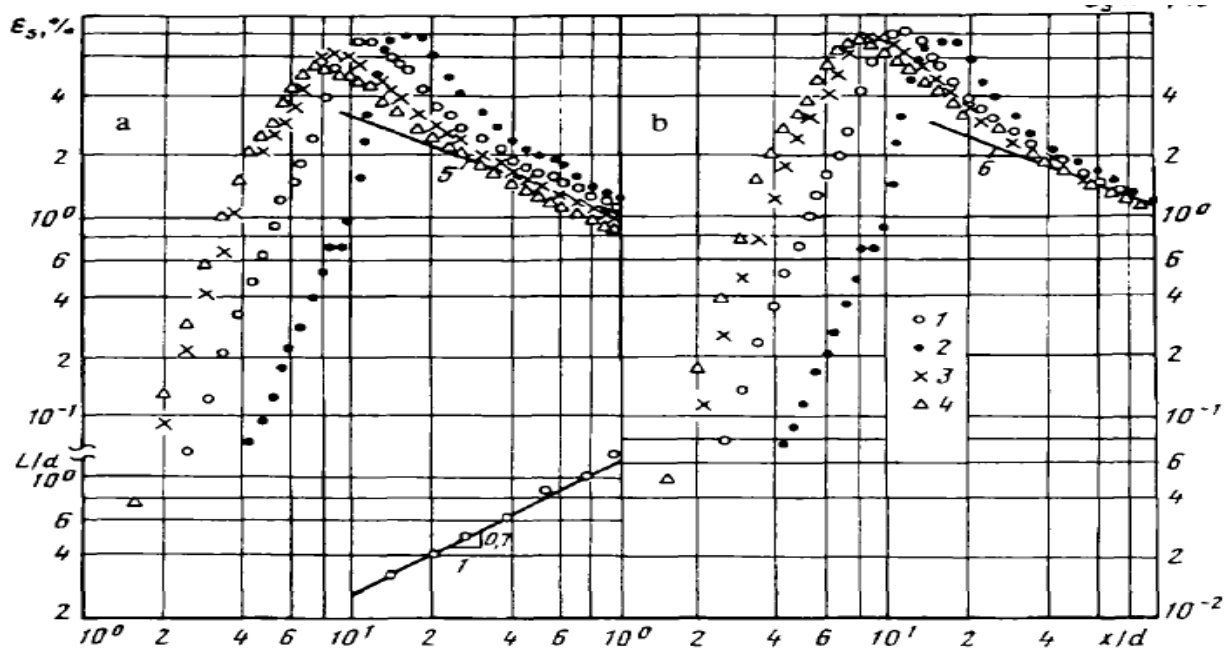

Figure 4.8 Relation among turbulence (Ɛ), honeycomb diameter (d), honeycomb length (l) and distance after passing through honeycomb (x) [49].

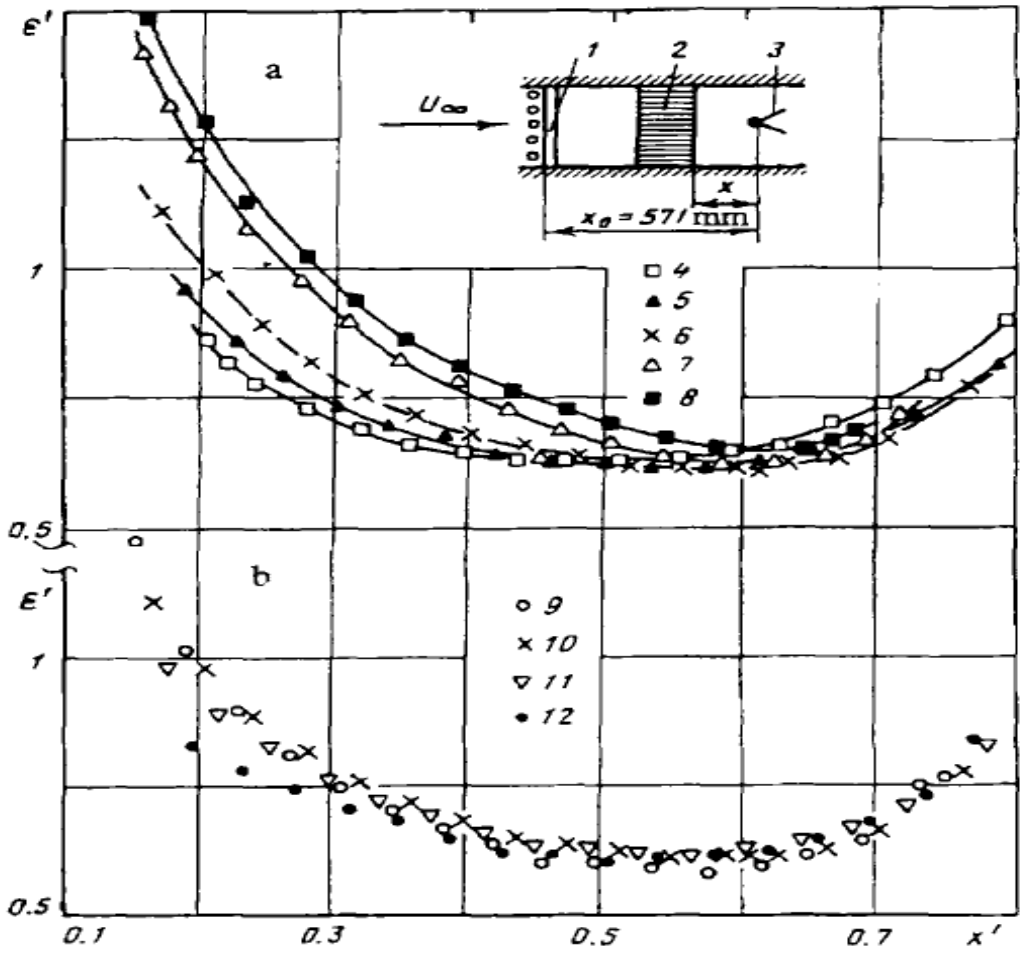

Figure 4.9 Relation of turbulence with total distance from turbulence generator to turbulence measurement point (x_0) and distance after passing through honeycomb (x) ratio ($x^{/}$) [49].

4.1.3 Calculation for 3D Printed Honeycomb and Straight Channel

The minimum diameter and thickness that could be printed from the UWM Prototyping Lab 3D printer is 2.5 mm and 0.4 mm, respectively. Therefore, we used the following:

- Honeycomb corner to corner distance, d = 2.5 mm.
- Honeycomb thickness, t = 0.4 mm.
- l/d = 10.
- Honeycomb assembly length, l = 25 mm.

- x/d = 100.
- Straight channel length after passing through honeycomb, x = 250 mm.
- Total length, x_0 = l + x = 25+ 250 = 270 mm.

Figure 4.10 shows a schematic of the Honeycomb Assembly. At the end of the 3D printing, we could create 28 complete hexagons horizontally in one row and 5 complete hexagons vertically in one column. This honeycomb structure has a depth of 25 mm which would help to further straighten the air flow after passing through the Air knife. The assembly would get attached with the inlet channel directly after the Air Knife. Both the sides of Air Knife and Honeycomb Assembly were sanded to make the surface smooth and then glued together to act like one solid unit.

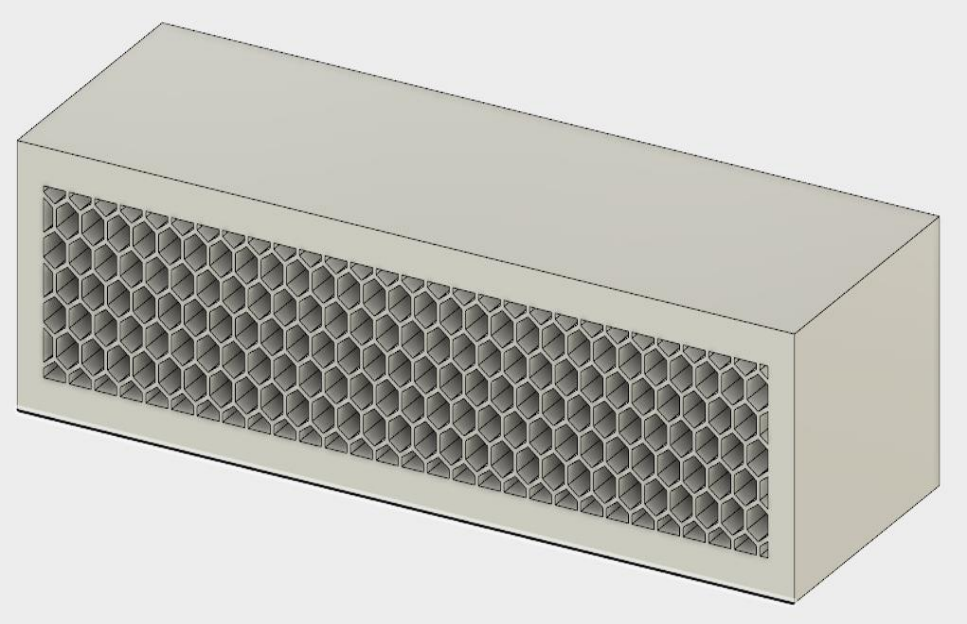

Figure 4.10 Schematic of Honeycomb Assembly.

Figure 4.11 shows the Straight Channel structure which attaches after the honeycomb assembly to form the complete Inlet Channel. As shown, here is neither any fins nor any hexagonal holes inside of this channel of Figure 4.11. It is an empty rectangular duct type structure having a

length of 250 mm which allows the fluid flow to become fully-developed with minimum turbulence after passing through the Air Knife and Honeycomb assembly. At the end of this Straight Channel four holes have been drilled to join the Inlet Channel with the Fin Assembly. In between the two structures, there is placed a thin rubber gasket followed by an insulating plate of acrylic so that the whole assembly can be air tight while preventing the joining plastic part of Inlet Channel to melt from the heat in the plate fin heat exchanger. This gasket also reduces heat loss from the system.

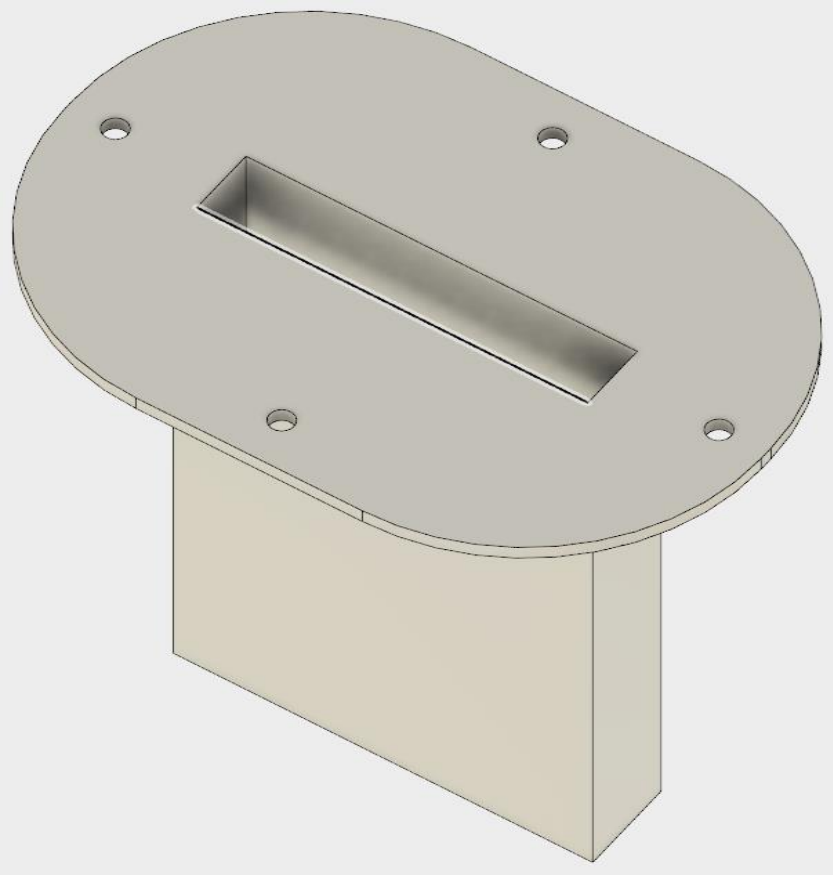

Figure 4.11 Schematic of Straight Channel with screw assembly.

Before printing the honeycomb structure of Figure 4.10, the printer setup was checked because it was needed to operate at the highest possible power to print such a sophisticated design

of a thin layer of 0.4 mm wall thickness. The printing was started from the honeycomb to have the base for creating honeycomb structure where it could lay over the printer surface. The 3D printer gradually built the 25 mm length of honeycomb structure first and ended by creating the free surface of the rectangular duct (a =25 mm) which is shown in Figure 4.11. This rectangular duct has no honeycomb or fins inside the wall.

4.2 Instrumentation and Data Acquisition System

- Figure 4.12 is schematic of the proposed experimental setup. In order to know about the fluid flow intensity, an air mass flow sensor needs to be connected in the compressed air flow pipe to show the air mass flow rate. This connection has been shown in the upper left corner of Figure 4.12.

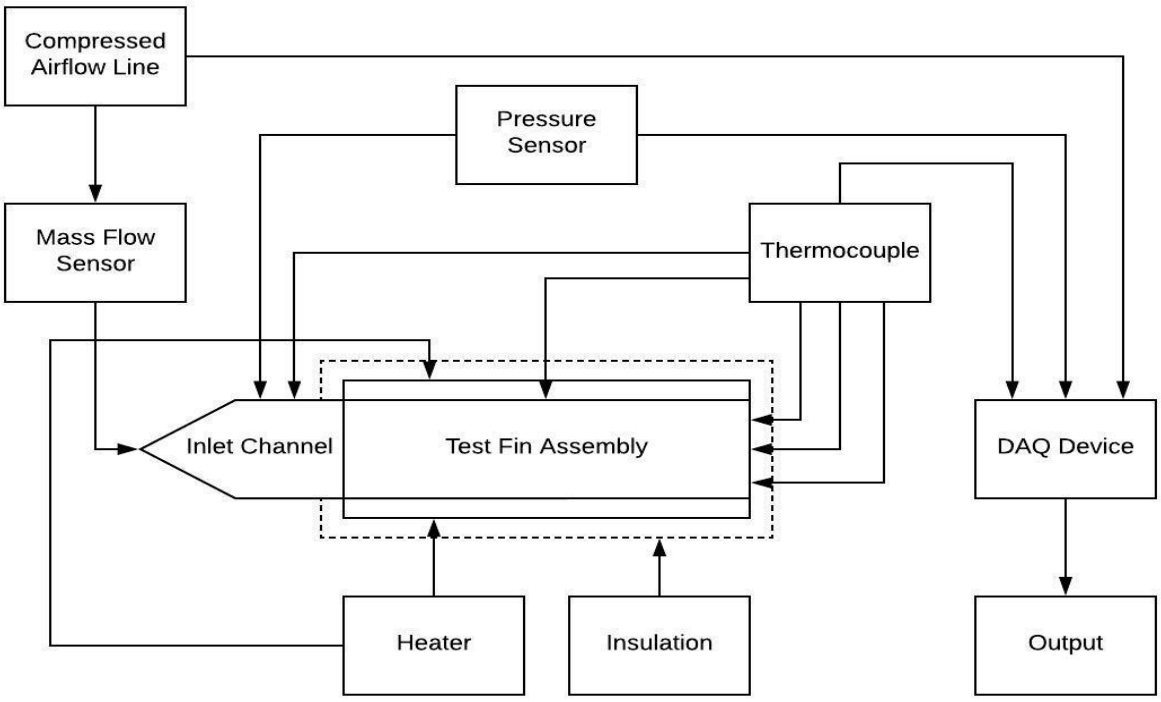

Figure 4.12 Schematic diagram of experimental setup.

- Air pressure Transducer is connected through the small hole at the end part of air inlet channel as shown in Figure 7.19. Figure 7.20 shows the connection of the pressure sensor, while Figure 7.21 shows a manometer that has been connected to gather a rough estimate about the pressure drop. Using this estimation, the range of pressure drop can be determined which will identify the ideal pressure transducer for experimental measurements.
- Two flexible strip heaters need to be installed by adhesive back mounting in the upper and lower plate of the fin assembly. Both heaters should be 3 inches×12 inches in the surface area so that it can be matched exactly with the plate dimension. In Figure 7.22 in the Appendix, a similar type of connection has been shown for the strip heaters. Here, a long strip heater has been wrapped spirally around the whole fin assembly in Figures 7.22 and 7.23.
- Copper-constantan thermocouples can be fabricated by welding. They will be installed to measure inlet air temperature, outside wall temperature and outlet air temperature. A model thermocouple connection and temperature measurement by using data acquisition system are shown in Figure 7.23 of the Appendix.
- The mass flow sensor, the heaters, the pressure sensor and the thermocouples are attached to the data acquisition system (DAQ). The DAQ device will be controlled by the computer software program "Benchlink."
- The mass flow sensor, the heaters, the pressure transducers will power from AC/ DC power supply. The whole fin assembly with the upper and lower plate heaters need to be sealed with some insulating material as shown in Figure 7.24 to minimize the heat loss in the system. In Figure 7.25, fiberglass insulation is used to cover the setup.

5 CONCLUSIONS AND RECOMMENDATIONS

A novel numerical analysis method has been presented in this thesis to find the hydraulic and thermal performances of three serrated plate-fin designs. The focus of the numerical analysis was to provide a simple way of simulation which can later be used for the design of an experimental setup in determining the performance of plate fin heat exchangers. A constant surface heat flux boundary condition was imposed for the different serrated fin designs. In this thesis, the analysis shows that notched serrated or Fin Design 3 provides the best performance. It has been shown that a small notch on the leading edge of a fin can have a huge effect on increasing hydraulic and thermal performance. On an average, Fin Design 3 has almost 6% higher thermal performance and approximately 29% higher hydraulic performance than Fin Design 1. Again, on an average, Fin Design 3 has almost 15% higher thermal performance and approximately 10% higher hydraulic performance than Fin Design 2. An experimental setup has also been proposed for future research needs. The numerical method, calculation strategy and experimental setup can be used for numerous types of plate-fin designs (e.g. herringbone, perforated, straight, etc.). Along with the numerical and experimental performance determination, if an optimization method can be applied for future work, that would assist to determine the most efficient fin for industry-type heat exchangers. The notch pattern in serrated fins can be varied by changing the dimension of the notch and by placing it at different locations. By applying an optimization method and following the same numerical analysis done, one can determine the best location and pattern for notch placement in serrated fins. Thus, it is possible to determine the best performing notched serrated fin having the best combination of hydraulic and thermal efficiencies. Finally, it is recognized that the fin performance varies with varying velocity. It would also be very useful to see how these fins behave in the turbulent flow region. For future study, along with analyzing the laminar flow performance of different fins, it would be beneficial to find their turbulent flow performance as

well. This future research can help us to determine where to use what type of fin for different flow condition. Finally, the work done in this thesis will help to initiate many other research topics which would directly help to know more about industrial heat exchangers and will also create a useful resource to find answers of many unsolved questions.

6 REFERENCES

[1] Alur, S., Experimental Studies on Plate Fin, National Institute of Technology, Rourkela, 2012, pp. 1-5.

[2] Manglik, R. M., Bregles, A. E., Heat Transfer and Pressure Drop Correlations for the Rectangular Offset Strip Fin Compact Heat Exchanger, Experimental Thermal and Fluid Science, Volume 10, Issue 2, 1995, pp. 171-180.

[3] Brogan, R. J., Heat Exchangers, Thermopedia.

Available: http://www.thermopedia.com/content/832/

[4] Kuzmin, D., Introduction to Computational Fluid Dynamics, Institute of Applied Mathematics, University of Dortmund, pp. 1-3.

[5] Aljundi, K., What is A Compact Heat Exchanger, WeBBusterz, 2017.

Available: http://www.webbusterz.org/compact-heat-exchanger/#Usage_in_process_industry.

[6] Shah, R. K., Webb, R. L., Heat Exchangers: Theory & Practice, Washington DC, 1983, pp. 425-468.

[7] Joshi, H. M., Webb, R. L., Heat Transfer and Friction in the Offset Strip- Fin Heat Exchanger, International Journal of Heat and Mass Transfer, Volume 30, Issue 1, 1987, pp. 69-84.

[8] Feng, J., Yu, X., Development of Plate-Pin Fin Heat Sink and Its Performance Comparisons with A Plate Fin Heat Sink, Applied Thermal Engineering, Volume 25, 2004, pp. 173-182.

[9] Peng, H., Ling, X., Analysis of Heat Transfer & Flow Characteristics Over Serrated Fins with Different Flow Directions, Energy Conversion and Management, Volume 9, 2011, pp. 826-835.

[10] Wen, J., Yang, H., Tong, X., Optimization Investigation on Configuration Parameters of Serrated Fin in Plate Fin Heat Exchanger Using Generic Algorithm, International Journal of Thermal Sciences, Volume 101, 2016, pp. 116-125.

[11] Amano, R., Computational Fluid Dynamics & Heat Transfer (ME-723), University of Wisconsin- Milwaukee, 2017, pp. 1-6.

[12] Thulukkanam, K., Heat Exchanger Design Handbook, Second Edition, Taylor & Francis Group, LLC, Ohio, 2013, pp. 10-42.

[13] Shah, R. K., Sekulic, D. P., Fundamentals of Heat Exchanger Design, John Wiley and Sons Inc, 2003, pp. 13-146.

[14] Boehme, R., Parise, J. A., Pitanga, R., Simulation of Multi Stream Plate Fin Heat Exchangers of An Air Separation Unit, Cryogenics, Volume 43, Issue 6, June 2003, pp. 325-334.

[15] Wang, Y. Q., Dong, W. Q., Liu, M. S., Wang, D., Numerical Study on a Plate Fin Heat Exchanger with Plain Fins and Serrated Fins at Low Reynolds Number, Chemical Engineering Technology, Volume 32, Issue 8, August 2009, pp. 1219-1226.

[16] London, A. L., Kays, W. M., Compact Heat Exchangers, Third Edition, McGraw-Hill Book Company, NY, 1984.

[17] Peng, H., Ling, X., Numerical Modeling and Experimental Verification of Flow and Heat Transfer Over Serrated Fins at Low Reynold Number, Experimental Thermal and Fluid Science Volume 32, 2008, pp. 1039-1048.

[18] Dubrovsky, E. V., Highly Effective Plate-Fin Heat Exchanger Surfaces-from Conception to Manufacturing, Aerospace Heat Exchanger Technology, Elsevier, New York, 1993, pp. 501-547.

[19] Patankar, S. V., Prakash, C., An Analysis of the Effect of Plate Thickness on Laminar Flow and Heat Transfer in Interrupted-Plate Passages, International Journal of Heat and Mass Transfer, Volume 24, 1981, pp. 1801-1810.

[20] Suzuki, K., Hirai, E., Miyaki, T., Sato, T., Numerical and Experimental Studies on A Two-Dimensional Model of An Offset Strip-Fin Type Compact Heat Exchanger Used at Low Reynolds Number, International Journal of Heat and Mass Transfer, Volume 28, 1985, pp. 823-836.

[21] Manson, S. V., Correlations of Heat Transfer Data and of Friction Data for Interrupted Plate-Fins Staggered in Successive Rows, NACA Tech, National advisory Committee for Aeronautics, Washington, DC, December 1950.

[22] Wieting, A. R., Empirical correlations for Heat Transfer and Flow Friction Characteristics of Rectangular Offset-Fin Plate-Fin Heat Exchangers, Trans. ASME, Journal of Heat Transfer, Volume 97, 1975, pp. 488-490.

[23] Mullisen, R. S., Loehrke, R. I., A Study of the Flow Mechanisms Responsible for Heat Transfer Enhancement in Interrupted-Plate Heat Exchangers, Trans. ASME, Journal of Heat Transfer, Volume 108, 1986, pp. 377-385.

[24] Foumeny, E. A., Ma, J., Design Correlations for Heat Transfer Systems, in: Heat Exchangers Engineering, Volume 1, Design of Heat Exchangers, 1993, pp. 163-165.

[25] Zhang, L., Wang, J., Heat Transfer Performance of Offset Strip Fins with Variable Staggered Strip Positions, China North Vehicle Research Institute, 1998, pp. 238-243.

[26] Dubrovsky, E. V., Vasilliev, V.Y., Enhancement of Convective Heat transfer in Rectangular Ducts of Interrupted Surfaces, International Journal of Heat and Mass Transfer, Volume 31, 1988, pp. 807-818.

[27] Norris, R.H., Spofford, W. A., High-Performance Fins for Heat Transfer, Trans ASME, Volume 64, 1942, pp. 489-496.

[28] Kelkar, K. M., Patankar, S. V., Numerical Prediction of Heat Transfer and Fluid Flow in Rectangular Offset-Fin Arrays, Augmentation of Heat transfer in Energy Systems, Volume 52, ASME, New York, 1985, pp. 21-28.

[29] Shenone, C., Tanda, G., Forced Convection Heat Transfer from Shrouded Staggered Fin Arrays, International Journal for Heat and Mass Transfer, Volume 17, 1990, pp. 747-758.

[30] Maiti, D. K., Heat Transfer and Flow Friction Characteristics of Plate Fin Heat Exchanger Surfaces- A Numerical Study, Ph.D. Thesis, India, 2002.

[31] Ismail, L. S., Velraj, R., Studies on Fanning Friction and Colburn Factors of Offset and Wavy Fins Compact Plate Fin Heat Exchangers- A CFD Approach, in: Numerical Heat Transfer, Part A: Applications, Volume 56, 2009- Issue 12.

[32] Gerard, C., Szulman, C., Chatel, F., Thonnelier, J. Y., Werlen, E., Corrugated Fin with Partial Offset for Plate Type Heat Exchanger, US Patent US 6415855 B2, July 2002.

[33] Peng, H., Ling, X., Analysis of Heat Transfer and Flow Characteristics Over Serrated Fins with Different Flow Directions, Energy Conversion and Management, Volume 52, Issue 2, February 2011, pp. 826-835.

[34] Chart Industries Website, Applications Served

Available: http://www.chartindustries.com/Industry/Markets-Served

[35] Introduction to ANSYS Workbench, CAE Associates.

Available: https://caeai.com/courses/introduction-ansys-mechanical-workbench

[36] Engineering Simulation platform, ANSYS

Available: https://www.ansys.com/

[37] Qu, W., Mudawar, I., Experimental and Numerical Study of Pressure Drop and Heat Transfer in a Single-Phase Micro Channel Heat Sink, International Journal of Heat and Mass Transfer, Volume 45, Issue 12, June 2002, pp. 2549-2565.

[38] Overview of Flow Solvers, ANSYS Fluent, ANSYS.

Available: http://www.afs.enea.it/project/neptunius/docs/fluent/html/th/node360.htm

[39] Kelleher, M. D., Shah, R. K., Sreenivasan, K. R., Diverging Flow Angles, in: Experimental Heat Transfer, Fluid Mechanics and Thermodynamics, Volume 1, Amsterdam, 1993, pp. 315-324.

[40] Southall, D., Pierres, R. L., Dewson, S. J., Design Considerations for Compact Heat Exchangers, International Congress of Advances in Nuclear Power Plants, California, June 2008, pp. 144-170.

[41] Sparrow, E. M., Abraham, J. P., Minkowycz, W. J., Flow Separation in A Diverging Conical Duct: Effect of Reynolds Number and Divergence Angle, International Journal of Heat and Mass Transfer, March 2009.

[42] Goharkhan, M., Heat Transfer in Channel Flow, in: Convective Heat Transfer, Tabriz, Iran, 2003, pp. 313-320.

[43] Lautrup, B., Channel Entrance Flow, in: Physics of Continuous Matter, January 2013, pp. 64-70.

[44] Cornish, R. J., Flow in A Pipe of Rectangular Cross Section, Ph. D. Thesis, University of Manchester, June 2008.

[45] Air Knife, Wikipedia.

Available: https://en.wikipedia.org/wiki/Air_knife

[46] Air Knife (Compressed Air Diffuser), Thingiverse, February 2015.

Available: https://www.thingiverse.com/thing:664988

[47] Azzouz, H., The Dependence of the Cross-Sectional Shape on the Hydraulic Resistance of Microchannels, Ph. D. Thesis, Technical University of Denmark, July 2004.

[48] Loehrke, R. I., Nagib, H. M., Control of Free Stream Turbulence by Means of Honeycombs: A Balance between Suppression and Generation, Journal of Fluids Engineering, Volume 98, Issue 3, Sep 1976, pp. 342-351.

[49] Mikhailova, N. P., Repik, E. U., Sosedko, Y. P., Optimal Control of Free Stream Turbulence Intensity by Means of Honeycombs, Fluid Dynamics, Volume 29, Issue 3, May 1994, pp. 429-437.

7 APPENDIX

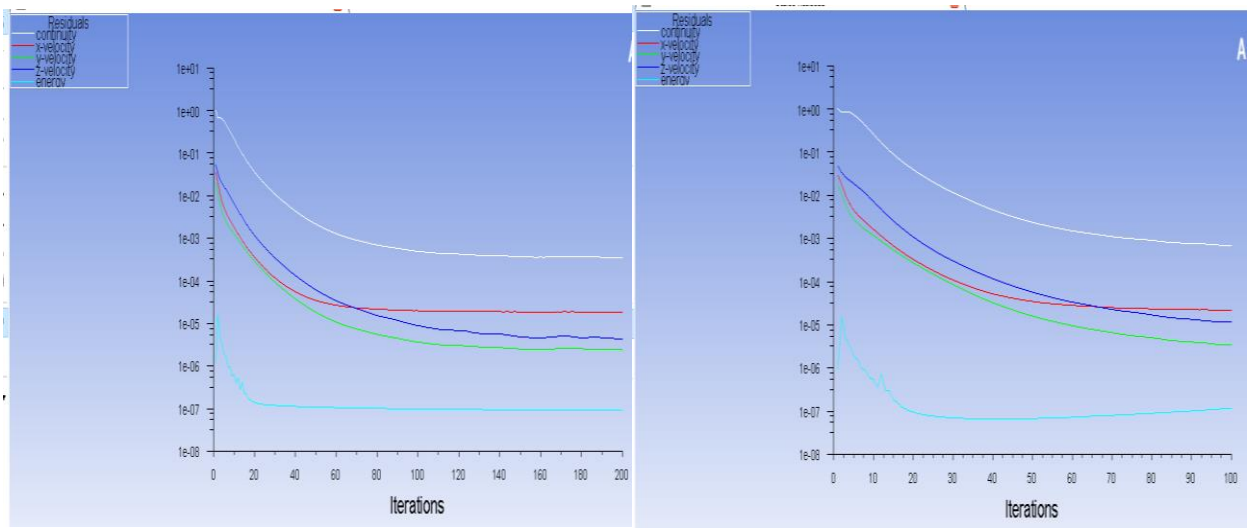

Design 1 Design 2

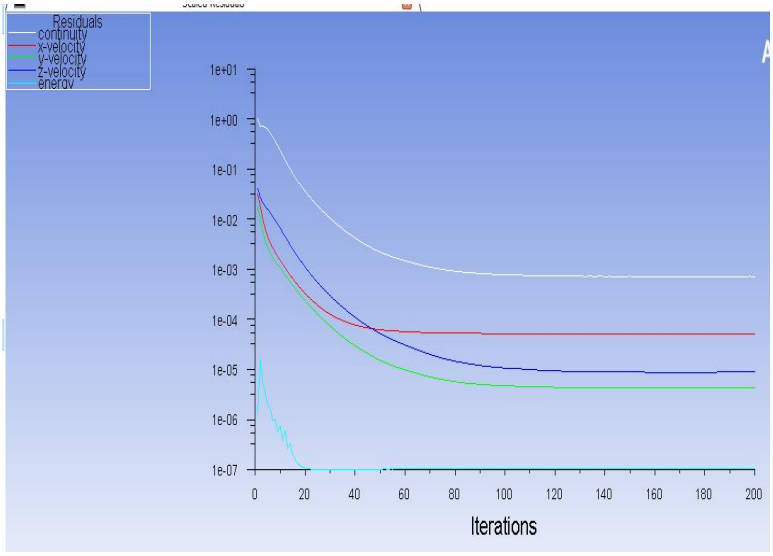

Design 3

Figure 7.1 Convergence graph of serrated fins for 2 m/s velocity.

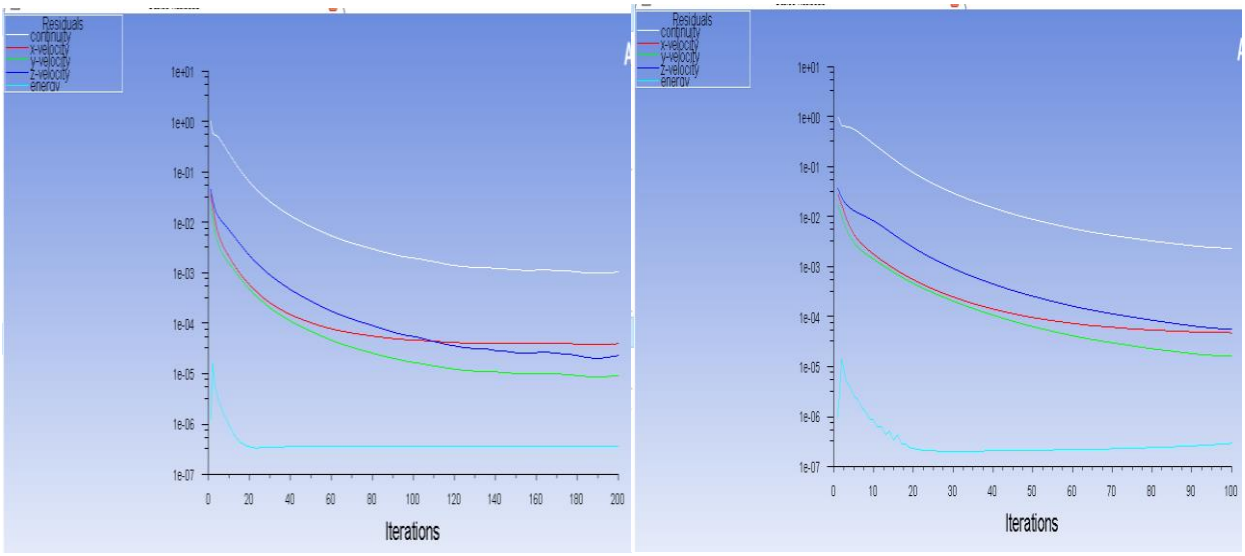

Design 1 Design 2

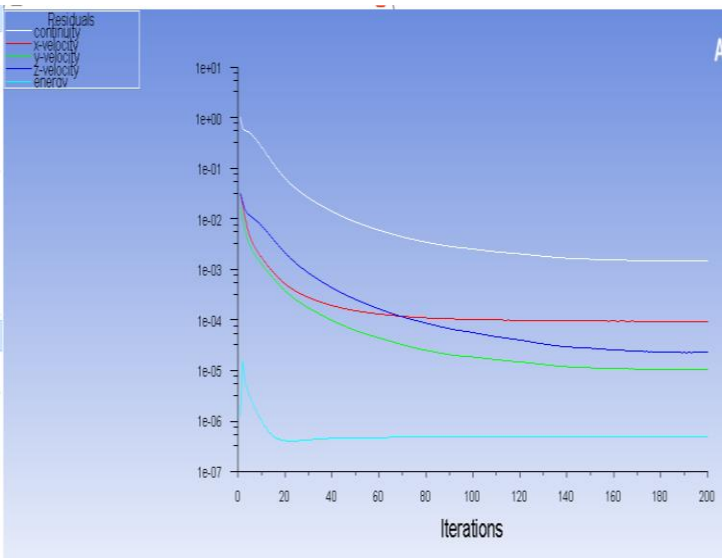

Design 3

Figure 7.2 Convergence graph of serrated fins for 7 m/s velocity.

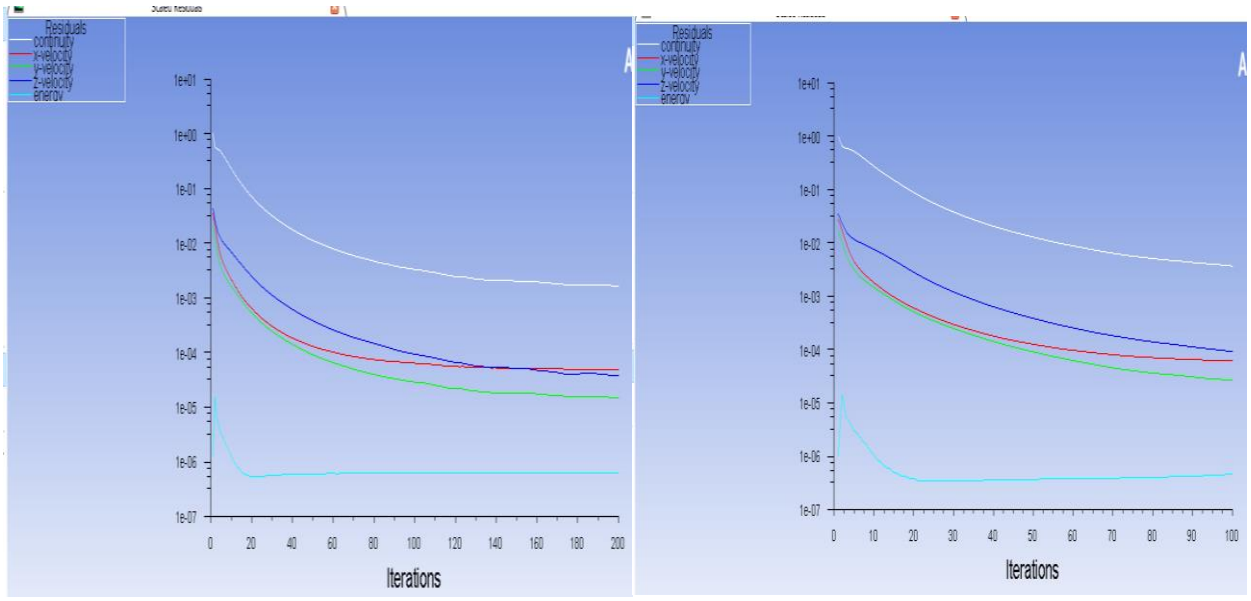

Design 1 Design 2

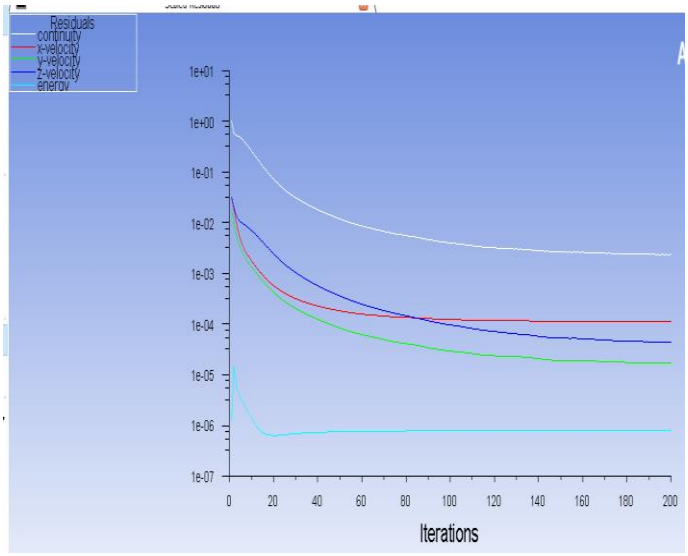

Design 3

Figure 7.3 Convergence graph of serrated fins for 12 m/s velocity.

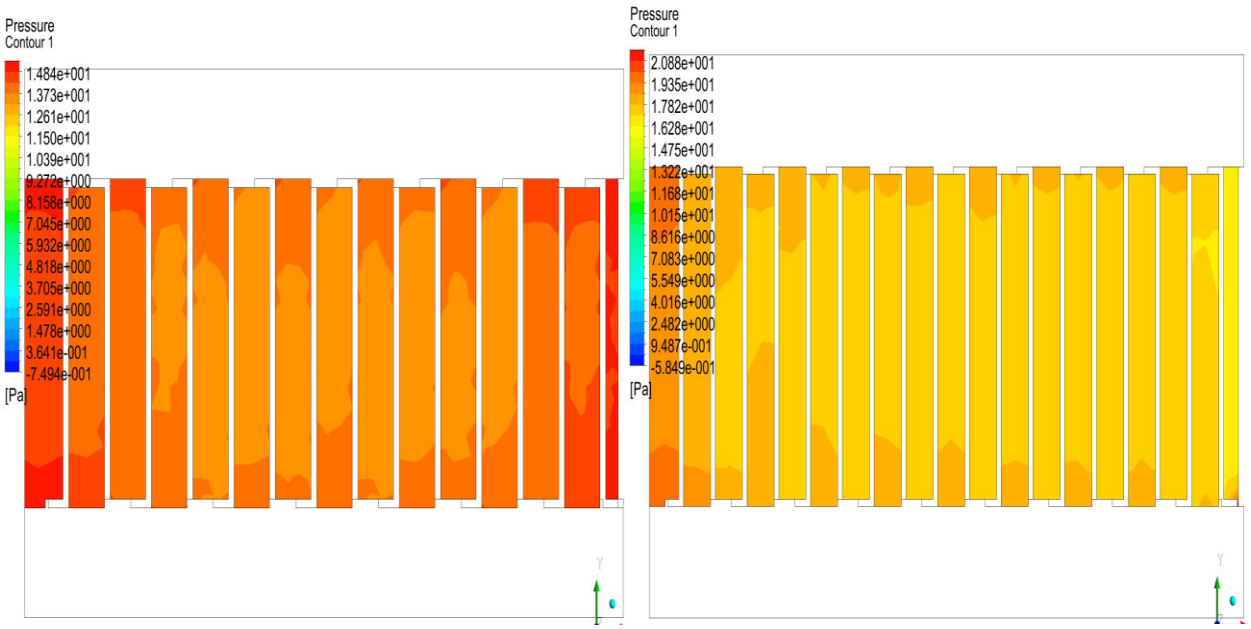

Design 1 Design 2

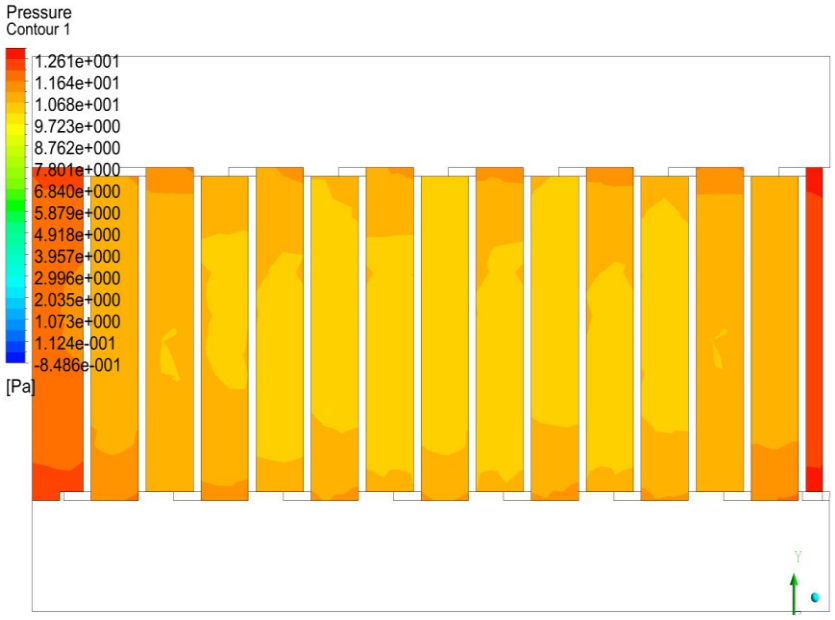

Design 3

Figure 7.4 Inlet pressure contour of serrated fins for 2 m/s velocity.

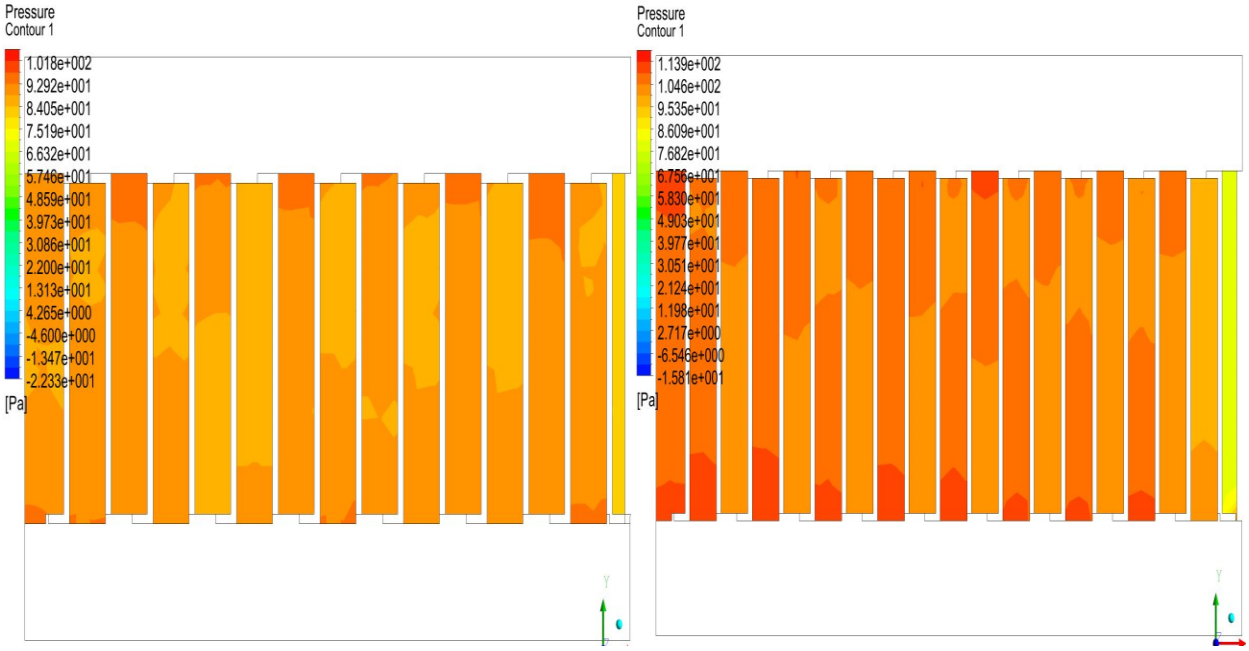

Design 1 Design 2

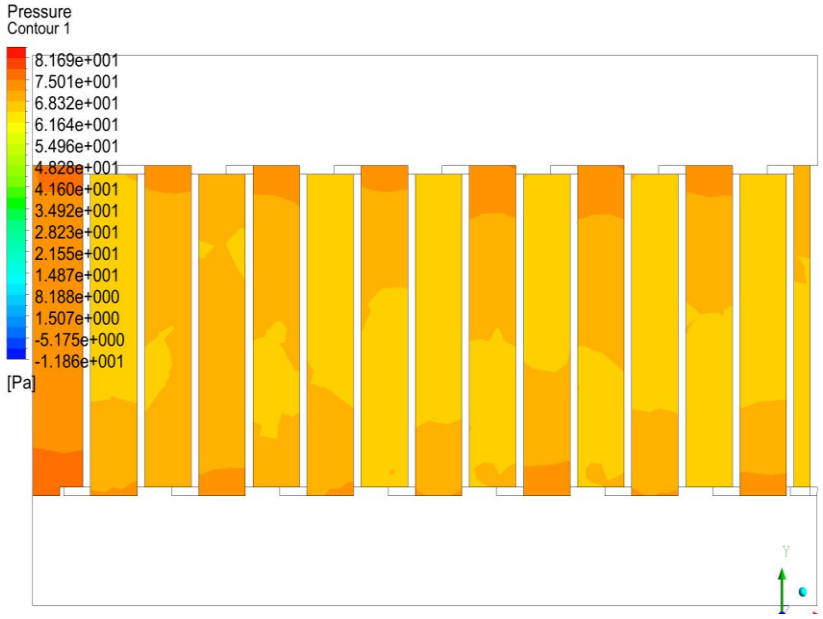

Design 3

Figure 7.5 Inlet pressure contour of serrated fins for 7 m/s velocity.

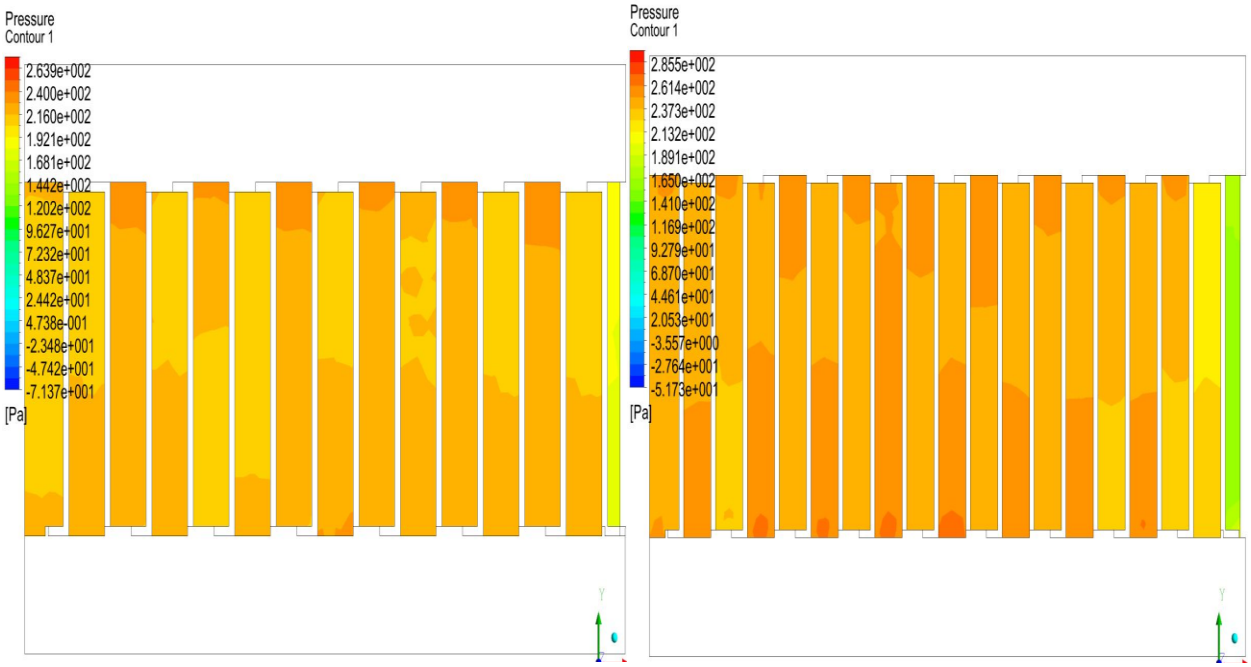

Design 1 Design 2

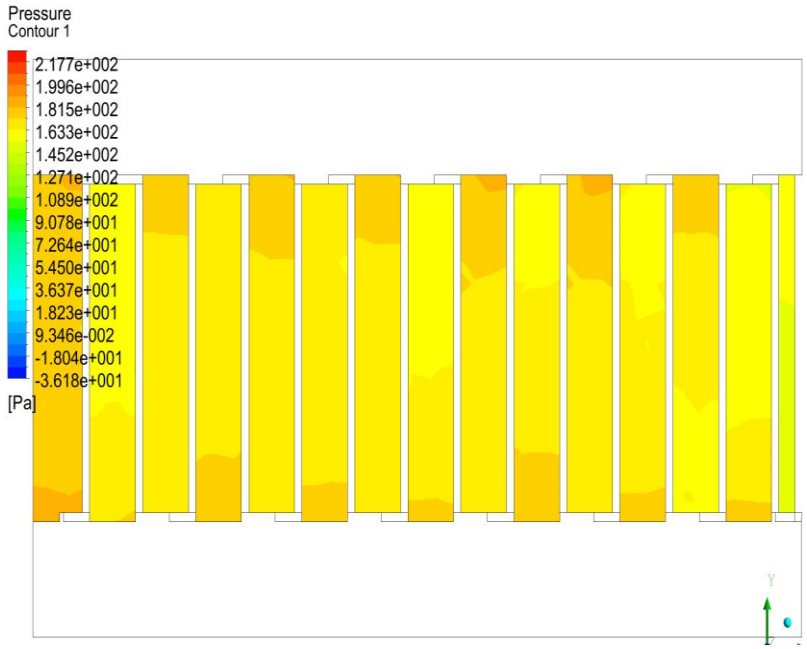

Design 3

Figure 7.6 Inlet pressure contour of serrated fins for 12 m/s velocity.

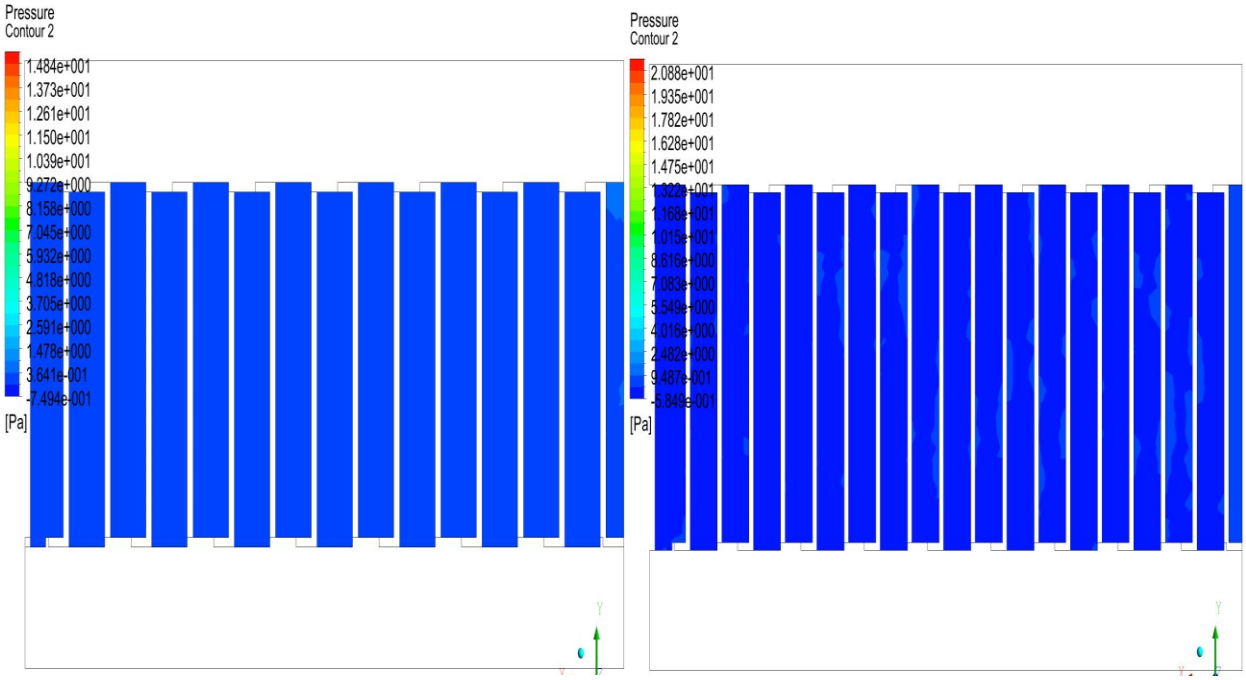

Design 1 Design 2

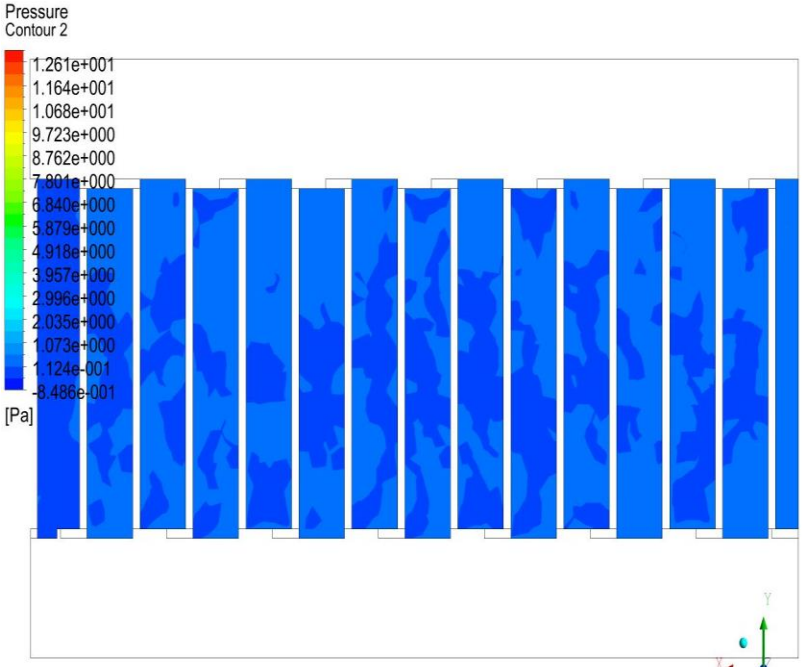

Design 3

Figure 7.7 Outlet pressure contour of serrated fins for 2 m/s velocity.

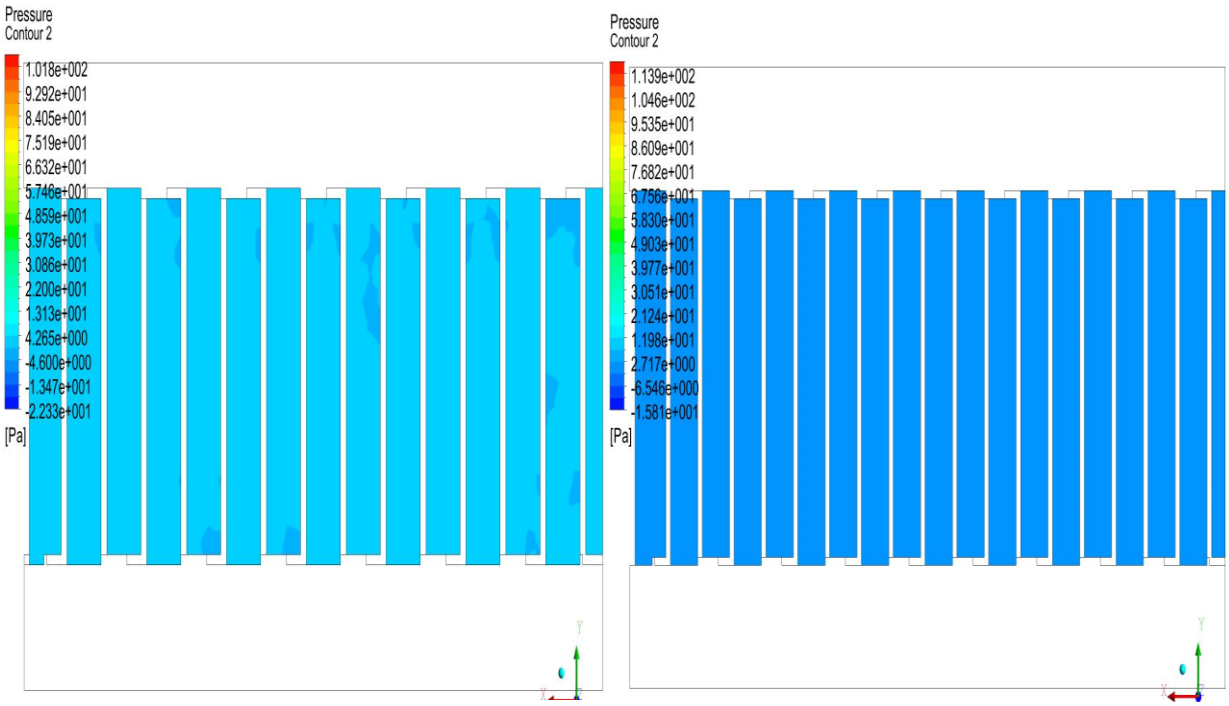

Design 1 Design 2

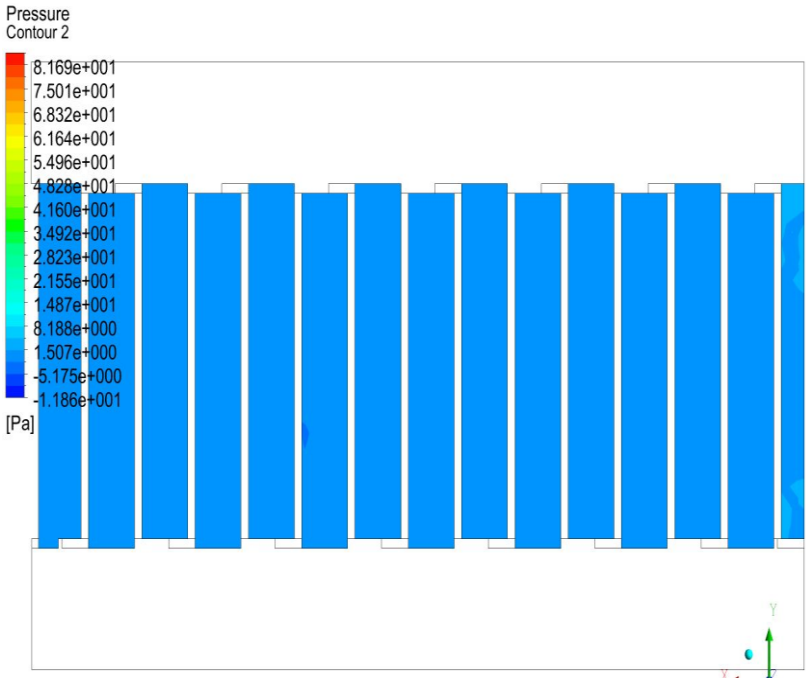

Design 3

Figure 7.8 Outlet pressure contour of serrated fins for 7 m/s velocity.

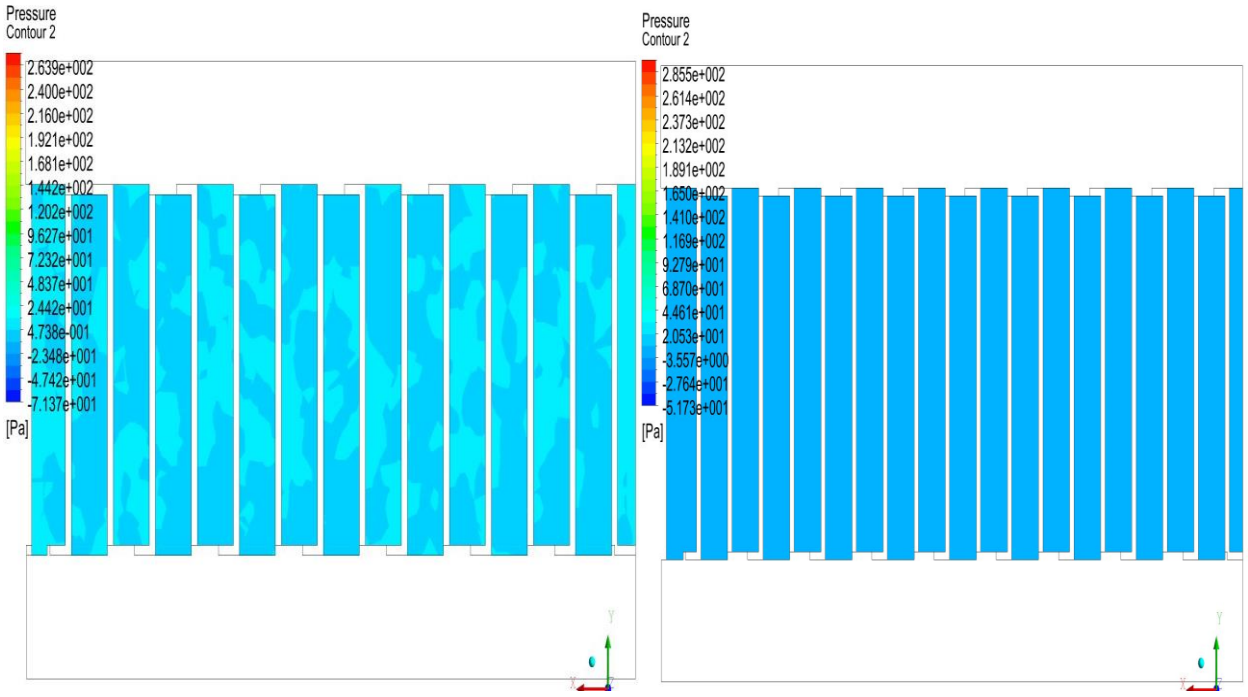

Design 1 Design 2

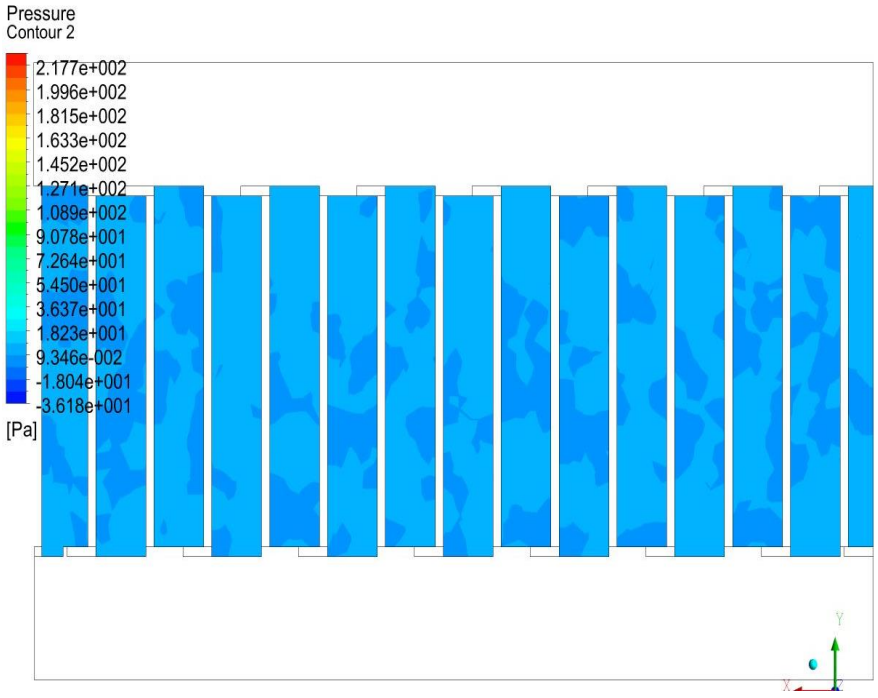

Design 3

Figure 7.9 Outlet pressure contour of serrated fins for 12 m/s velocity.

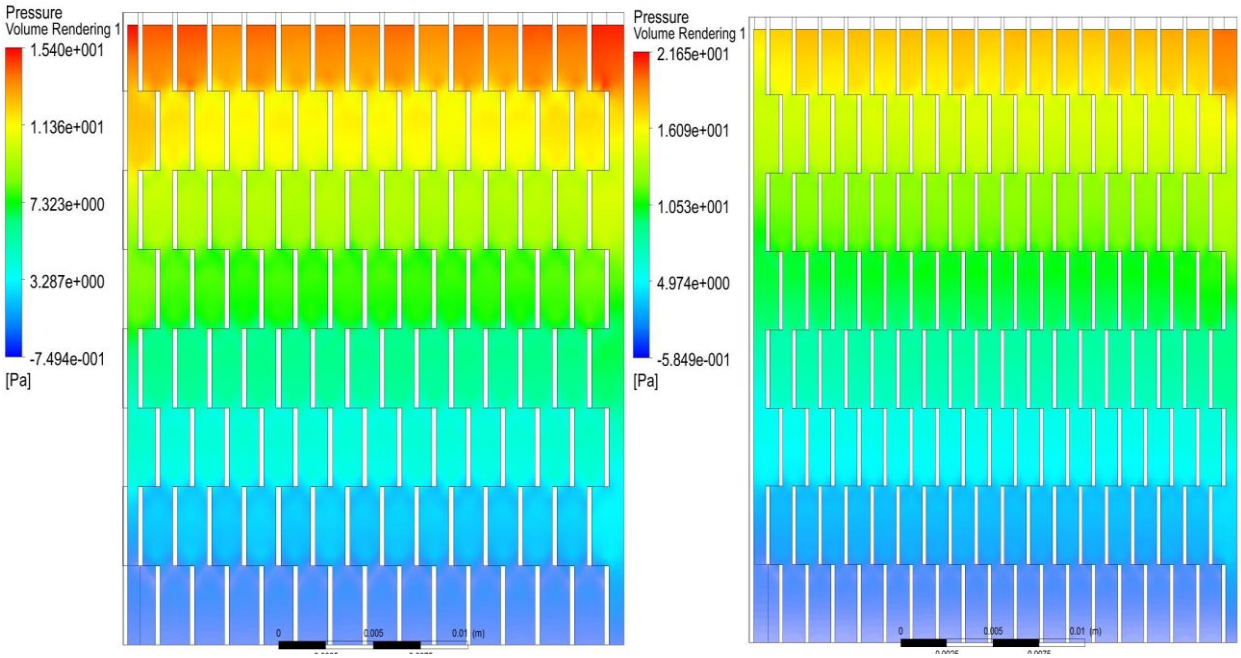

Design 1 Design 2

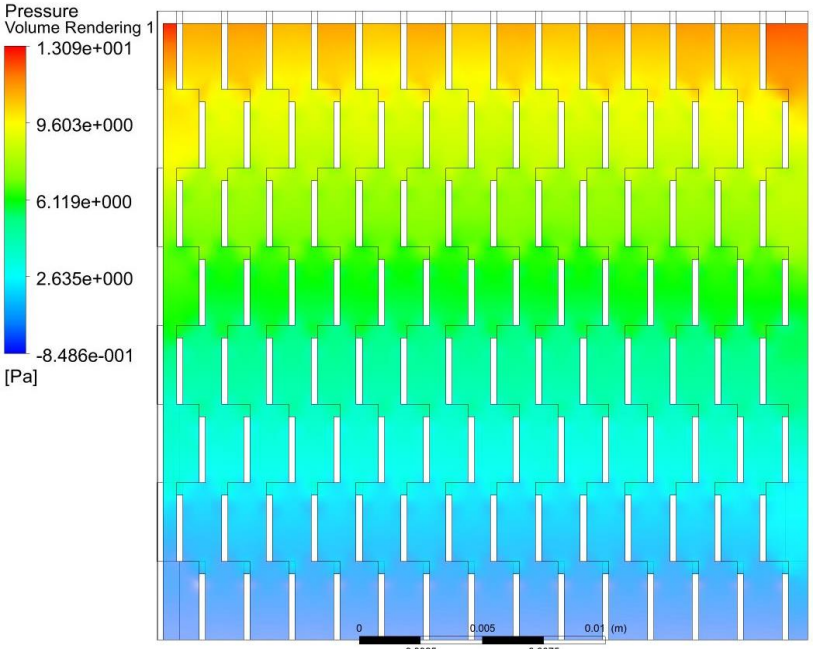

Design 3

Figure 7.10 Pressure drop contour of serrated fins for 2 m/s velocity.

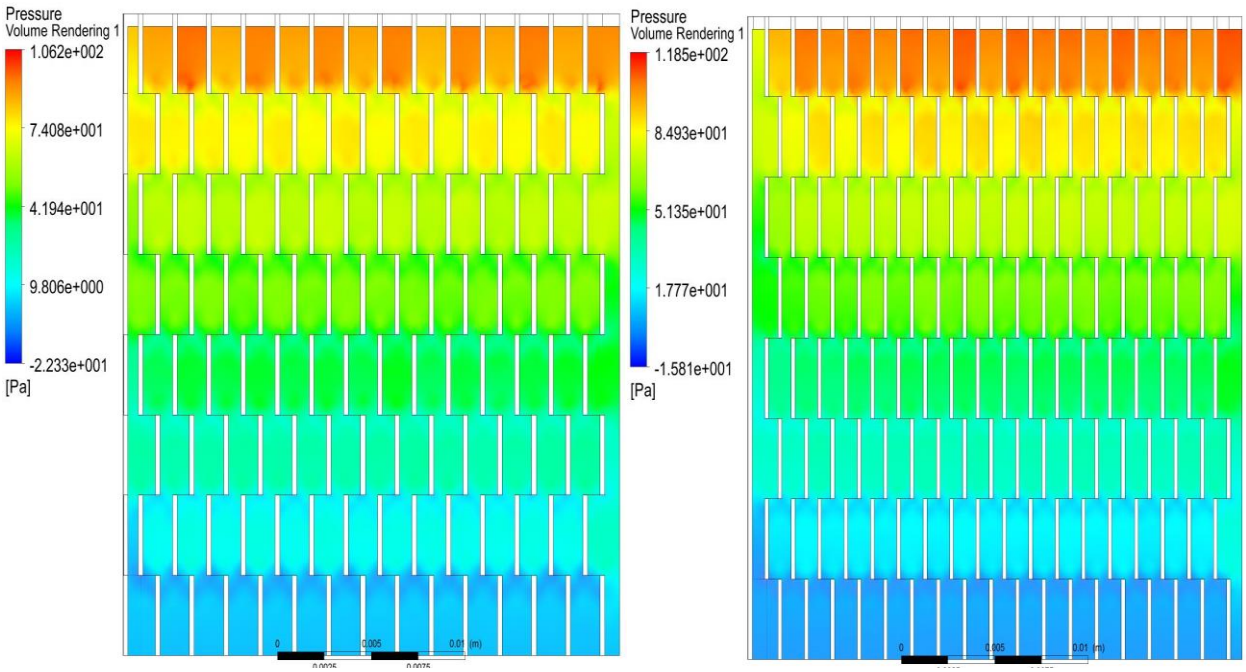

Design 1 Design 2

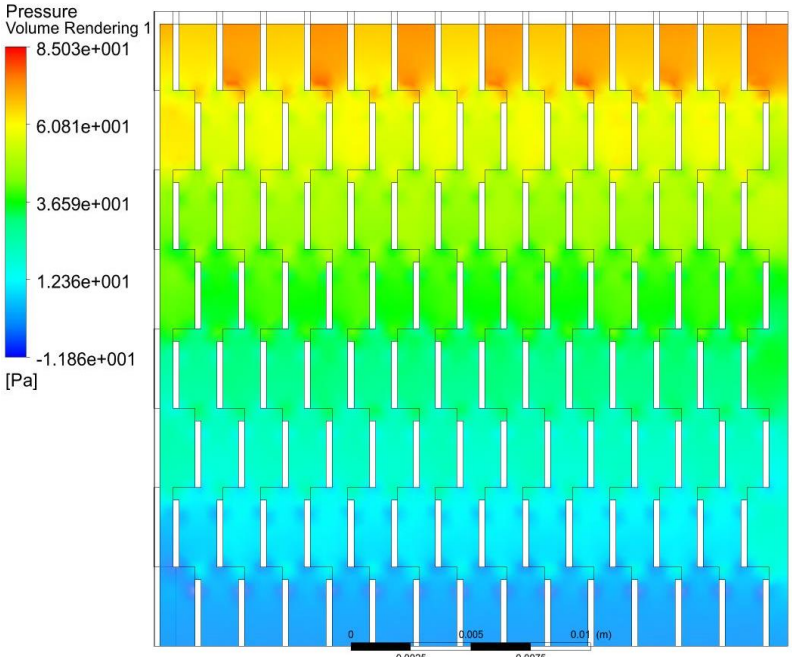

Design 3

Figure 7.11 Pressure drop contour of serrated fins for 7 m/s velocity.

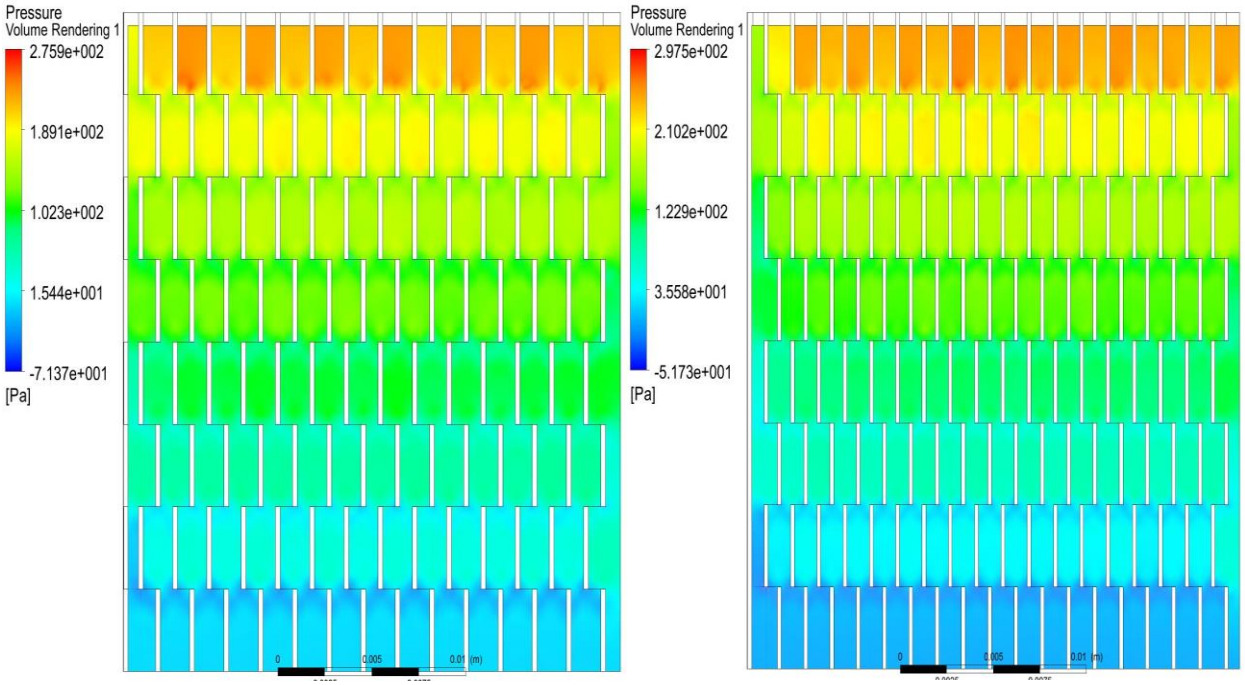

Design 1 Design 2

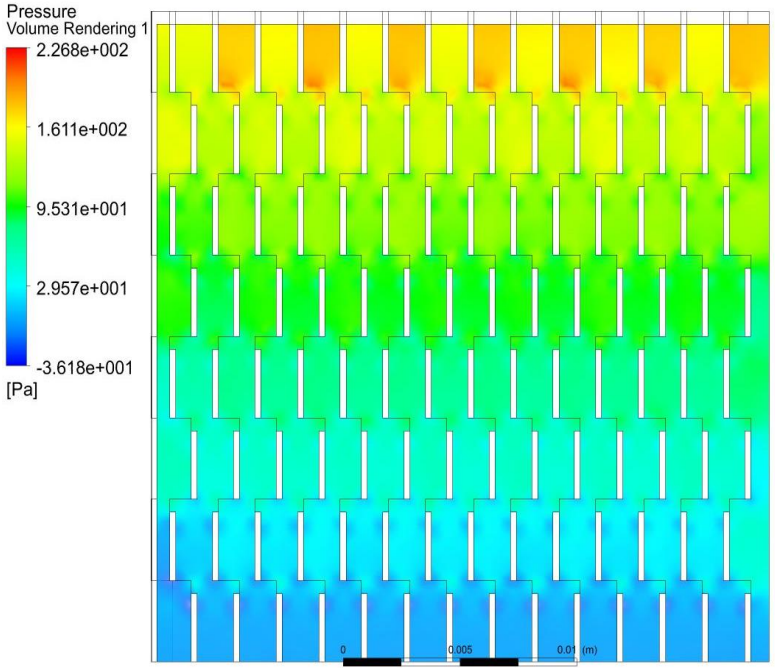

Design 3

Figure 7.12 Pressure drop contour of serrated fins for 12 m/s velocity.

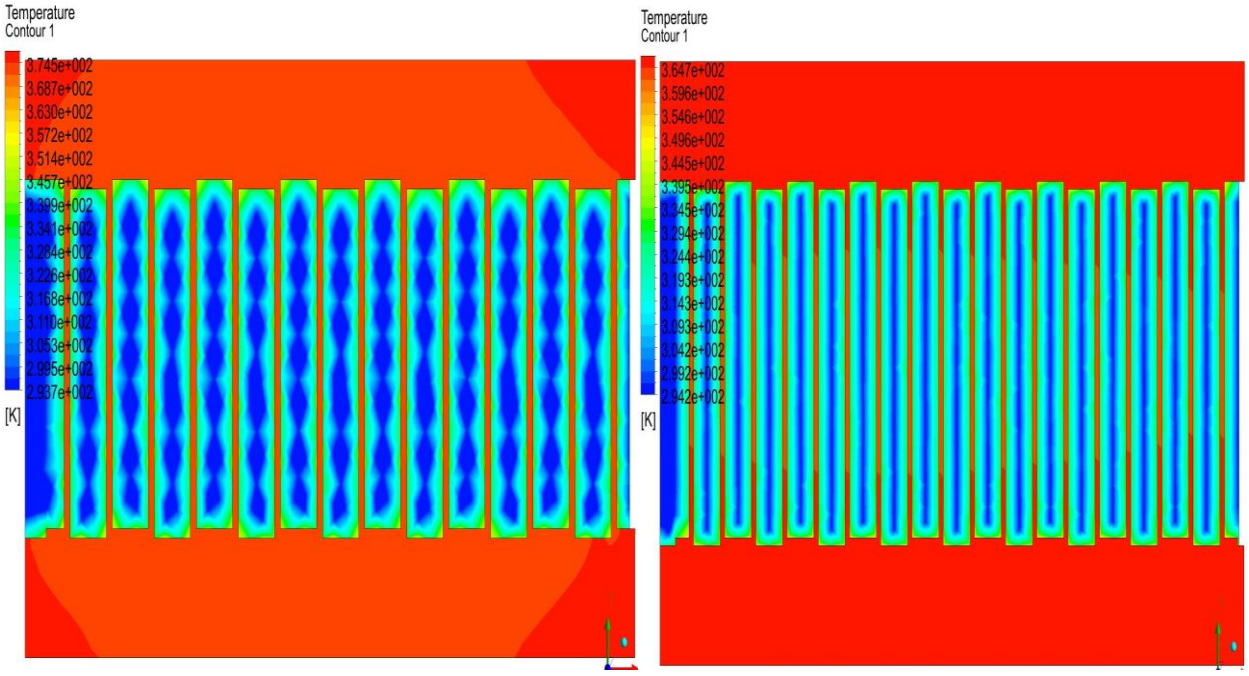

Design 1 Design 2

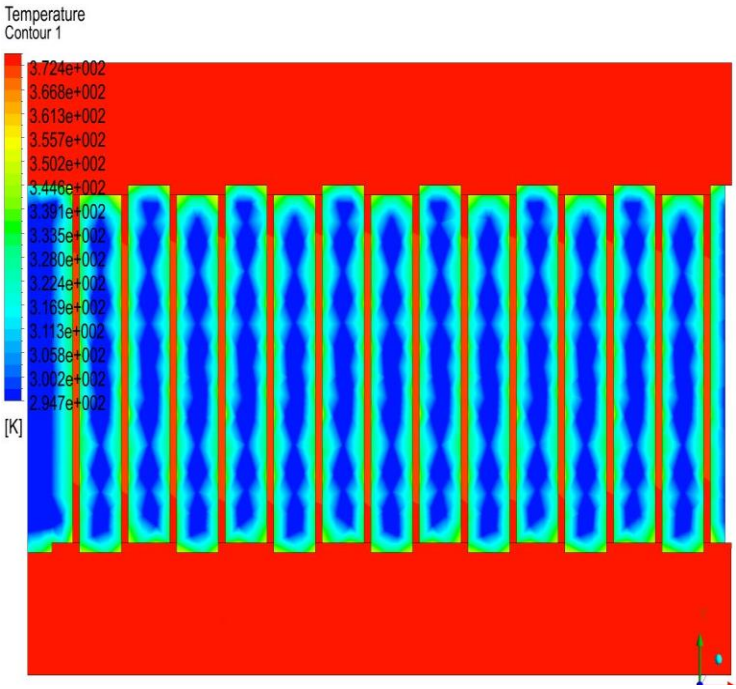

Design 3

Figure 7.13 Inlet temperature contour of serrated fins for 2 m/s velocity.

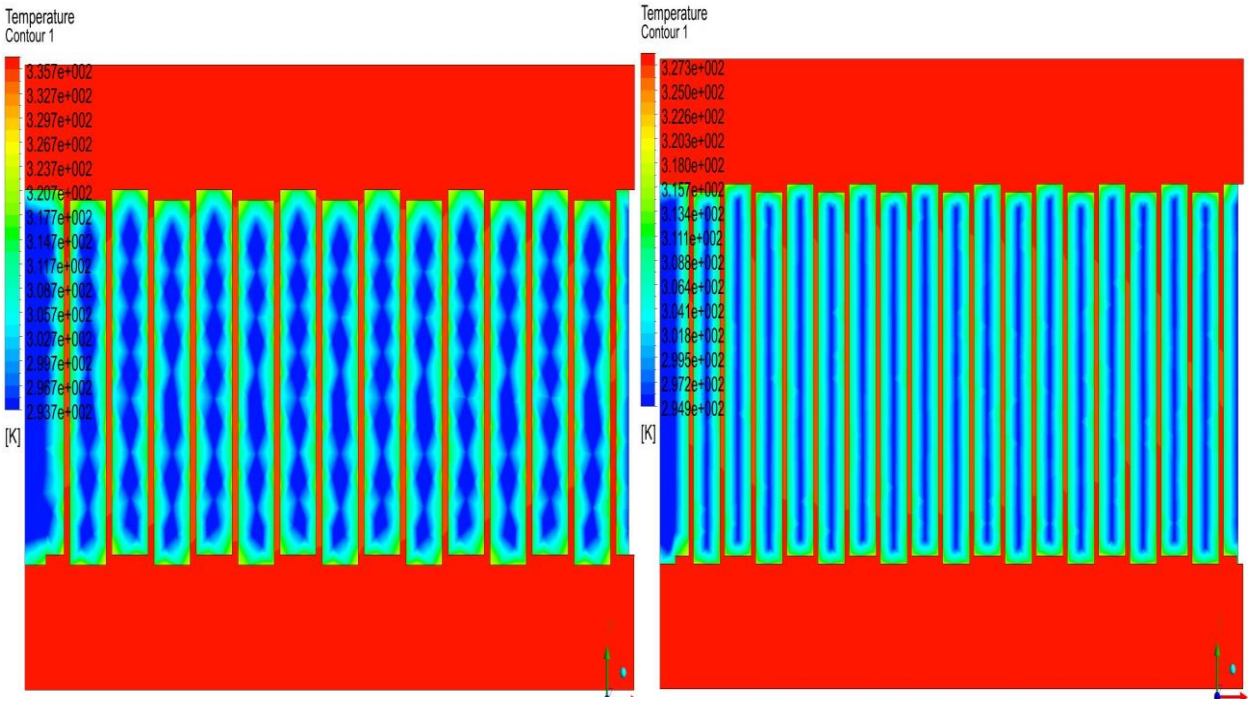

Design 1 Design 2

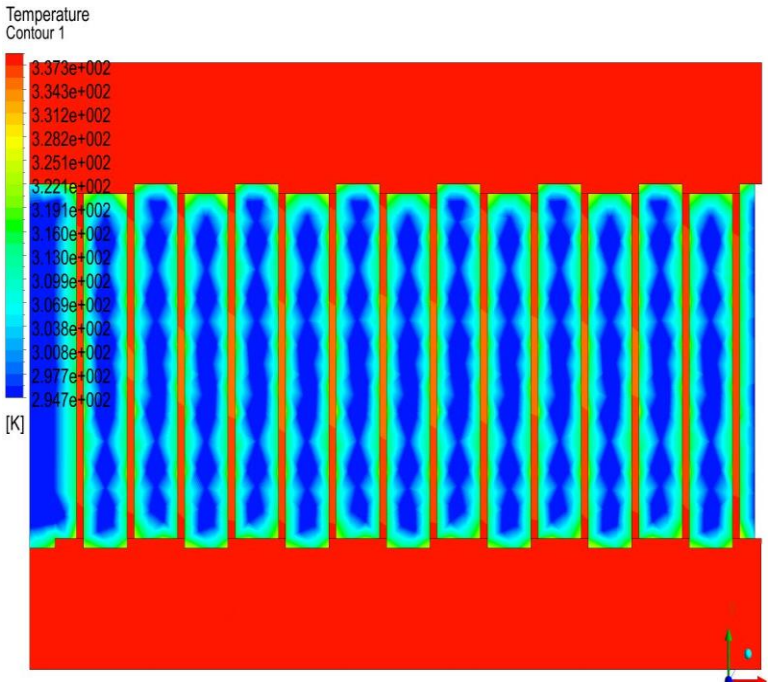

Design 3

Figure 7.14 Inlet temperature contour of serrated fins for 7 m/s velocity.

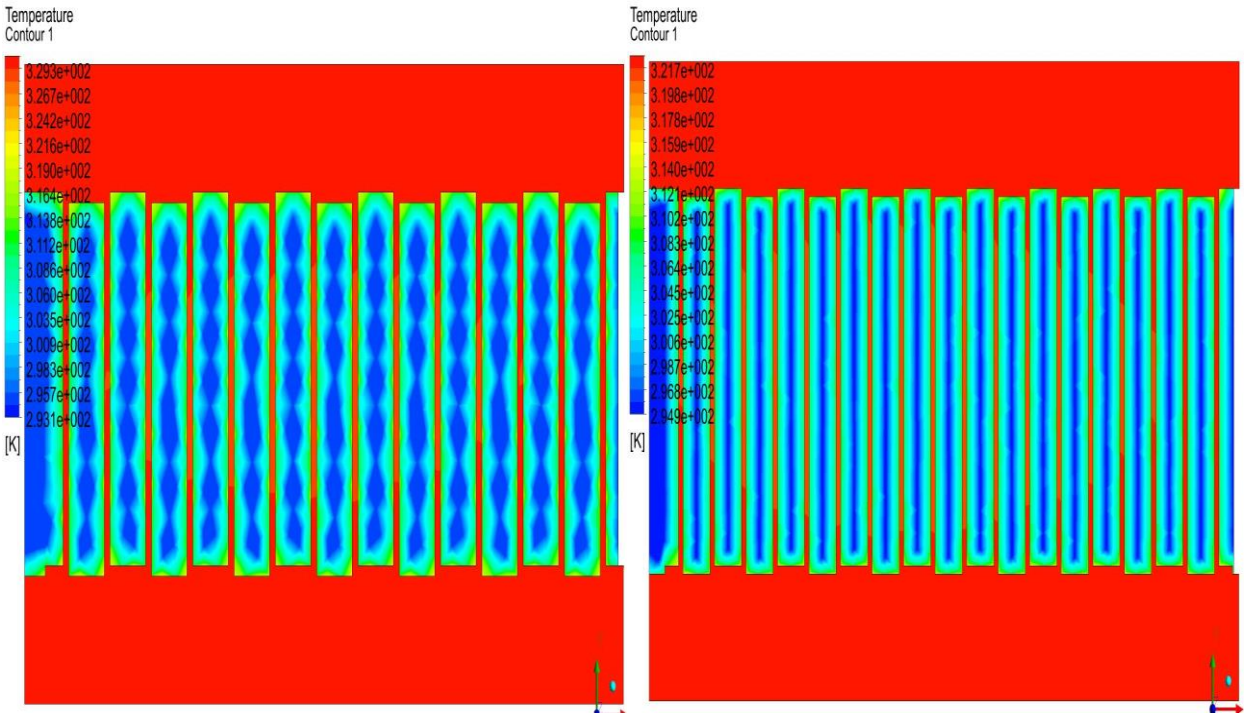

Design 1 Design 2

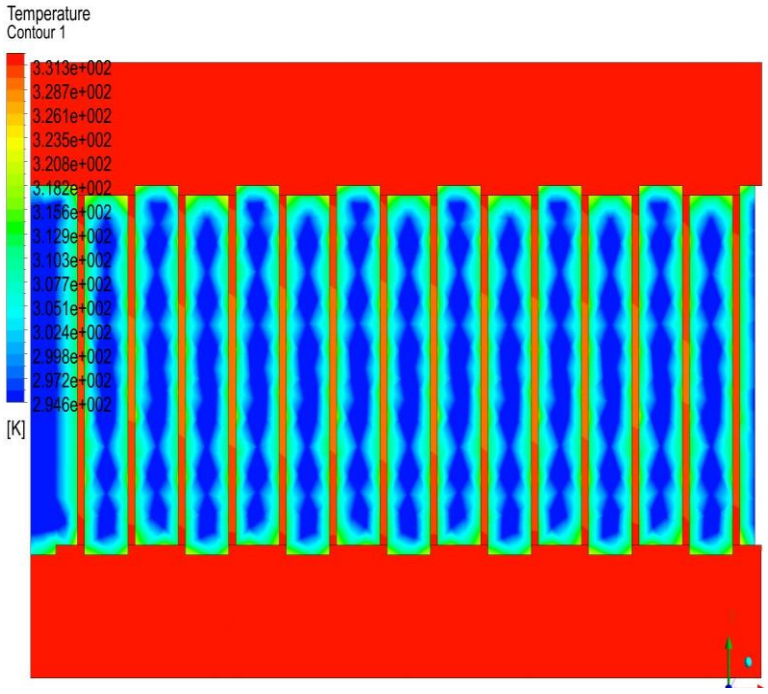

Design 3

Figure 7.15 Inlet temperature contour of serrated fins for 12 m/s velocity.

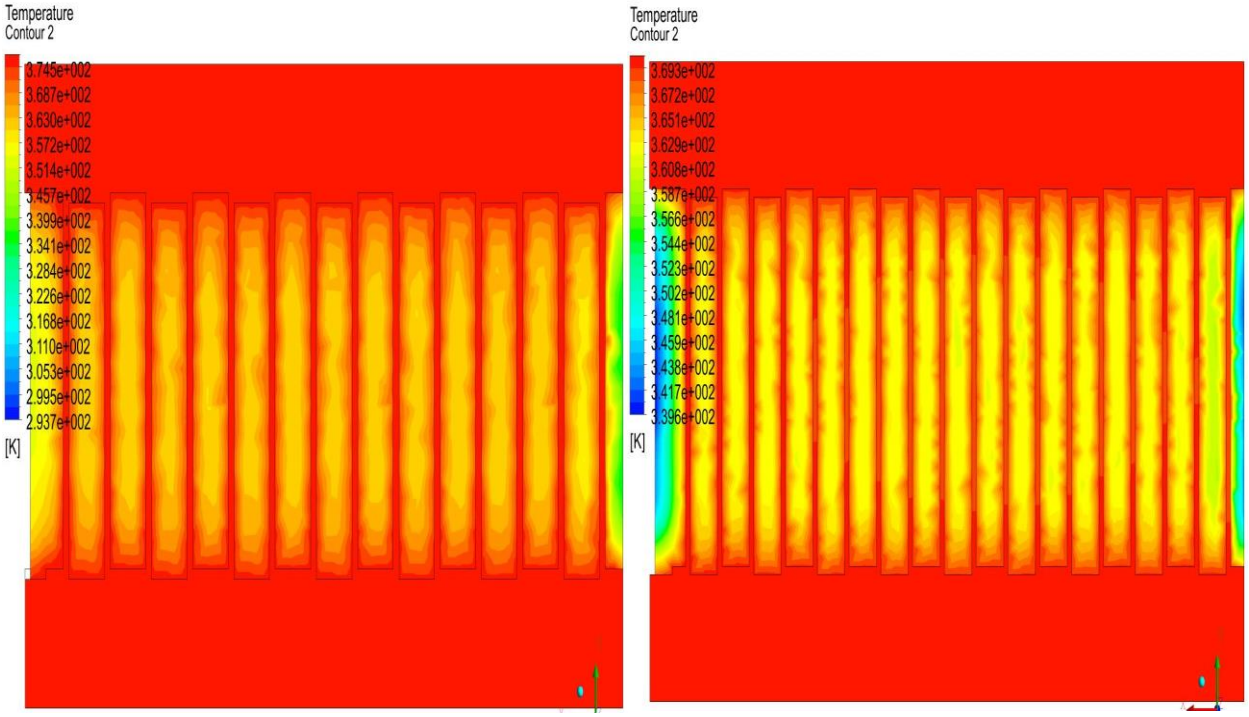

Design 1 Design 2

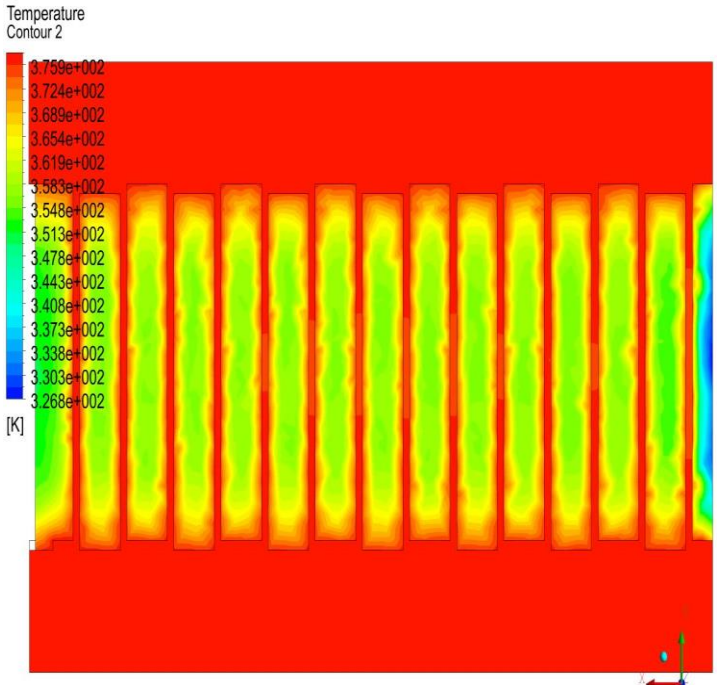

Design 3

Figure 7.16 Outlet temperature contour of serrated fins for 2 m/s velocity.

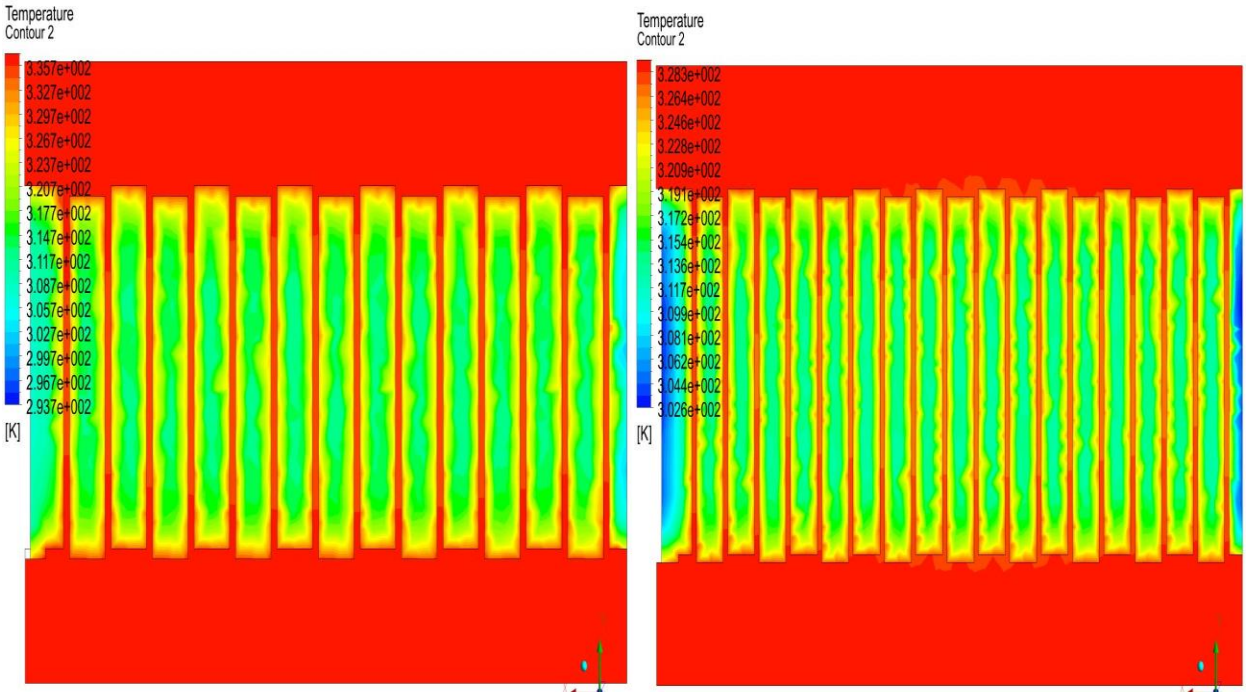

Design 1 Design 2

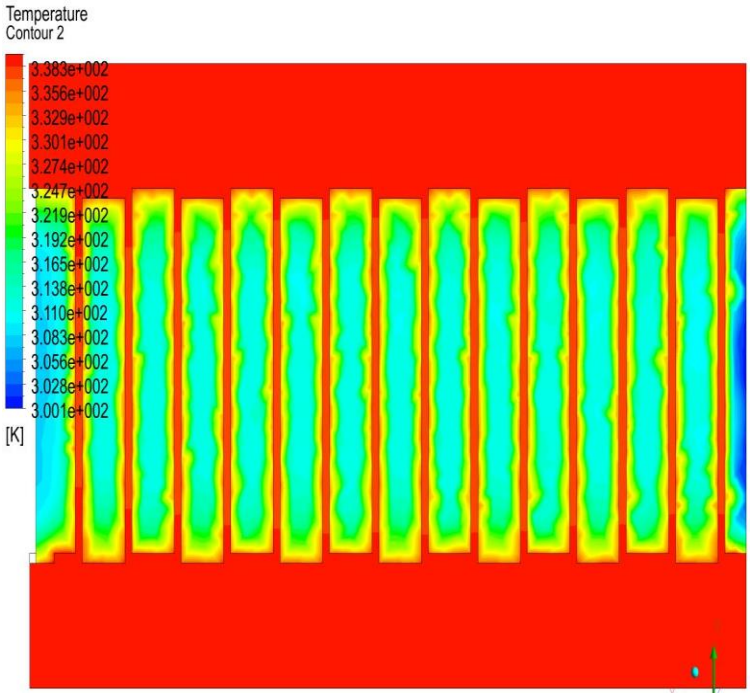

Design 3

Figure 7.17 Outlet temperature contour of serrated fins for 7 m/s velocity.

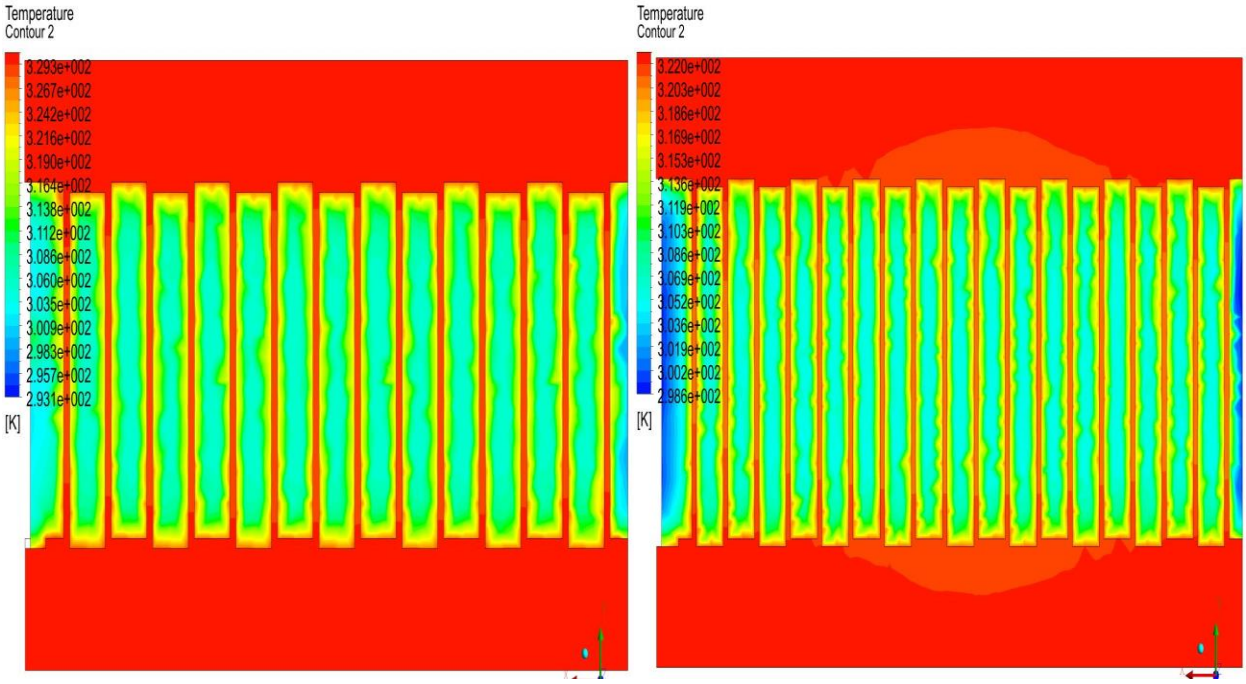

Design 1 Design 2

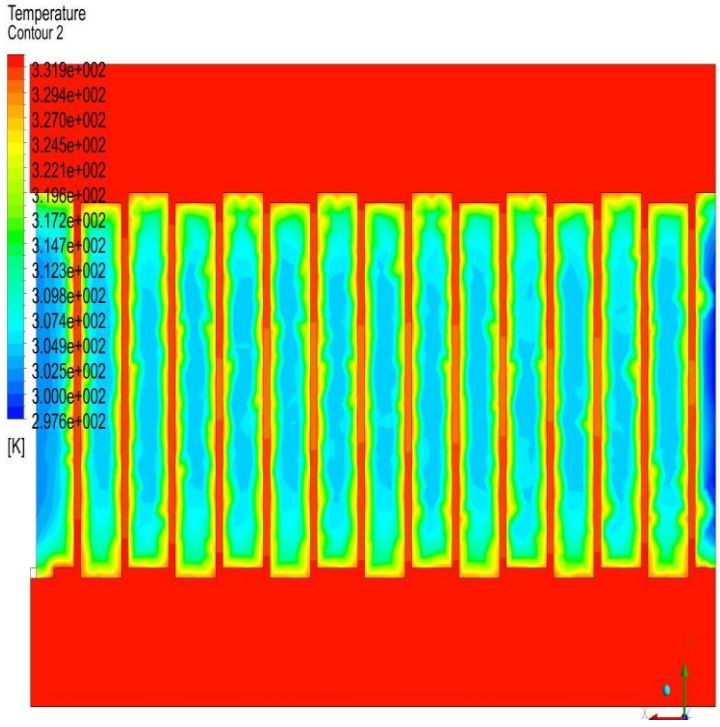

Design 3

Figure 7.18 Outlet temperature contour of serrated fins for 12 m/s velocity.

Figure 7.19 Additional fixtures to attach fin assembly and pressure gauge with the inlet channel.

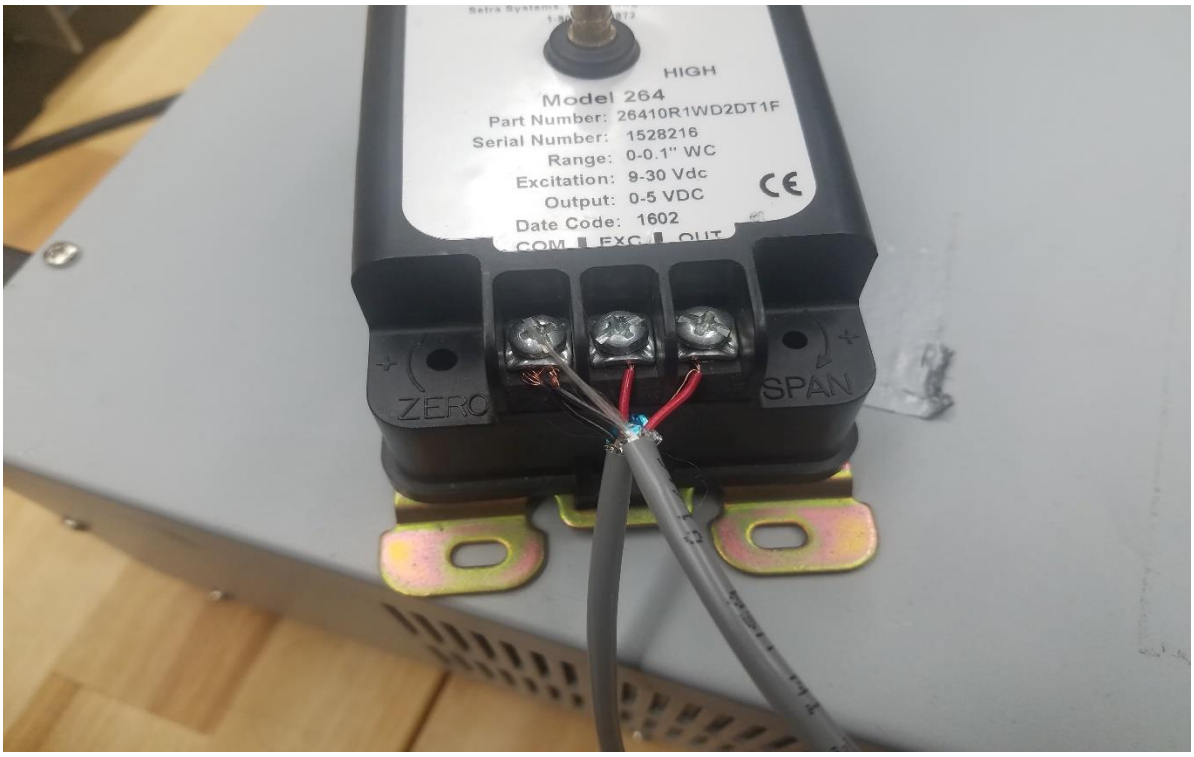

Figure 7.20 Pressure transducer connection.

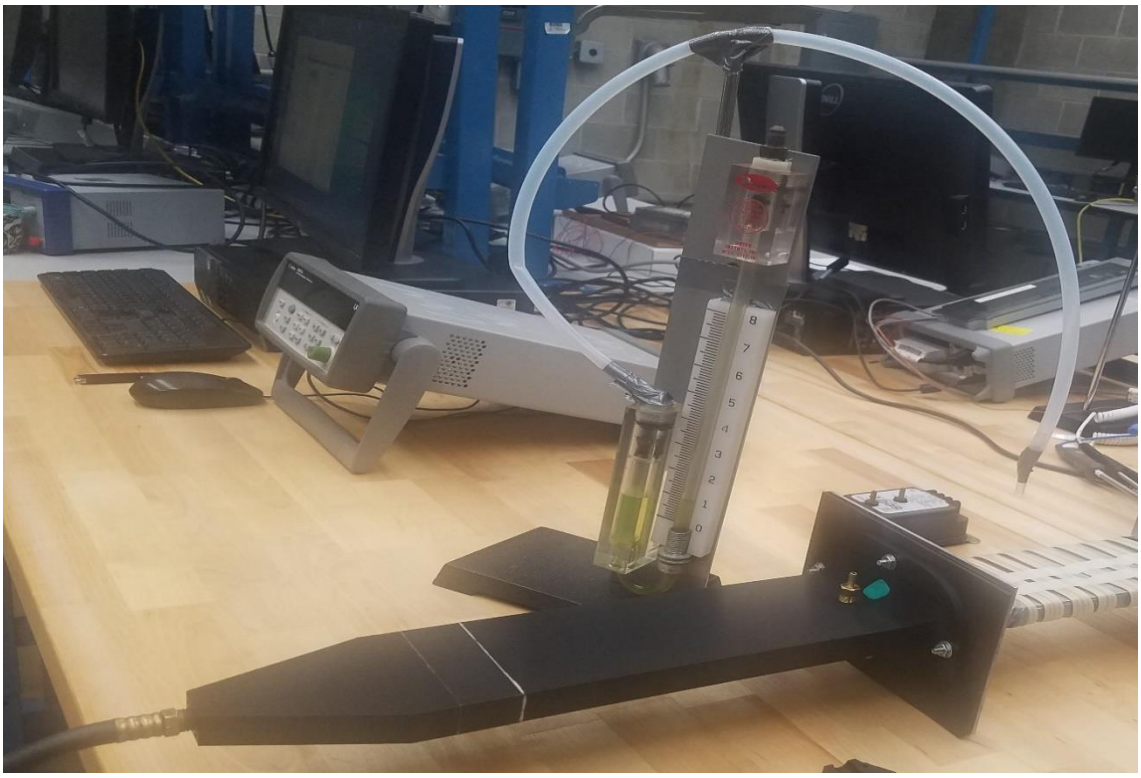

Figure 7.21 Manometer connection for calibration of pressure transducer.

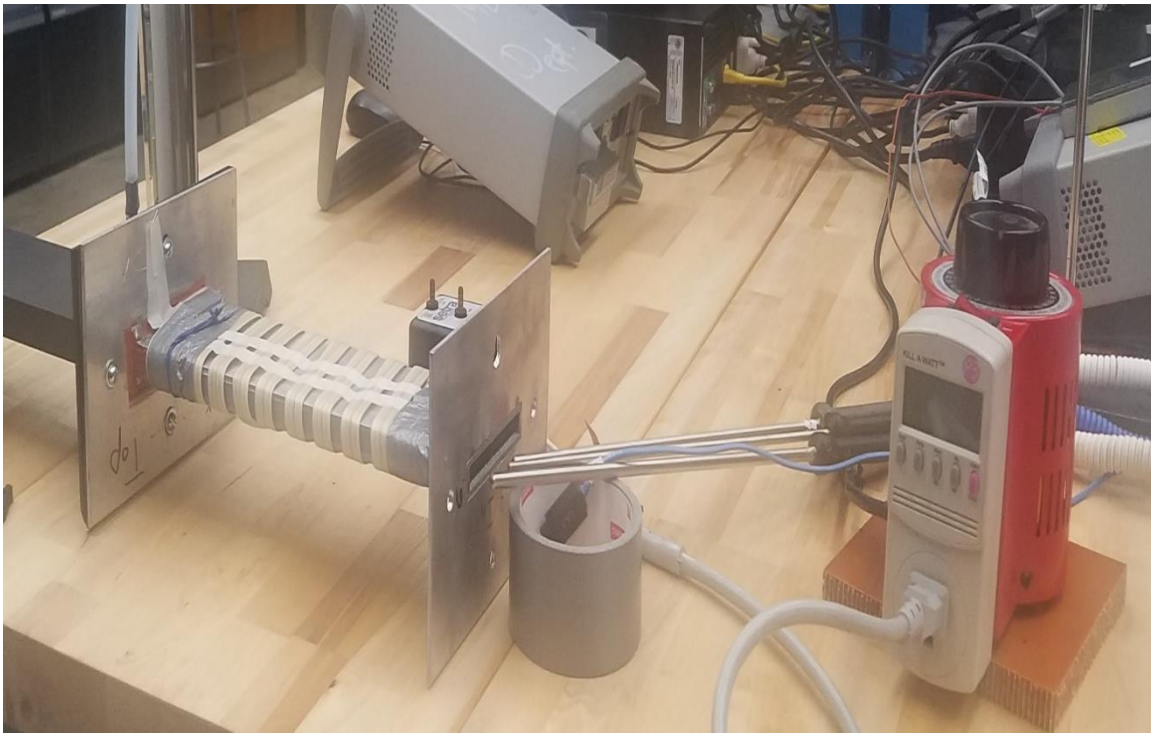

Figure 7.22 Thermocouples and strip heater connection.

Figure 7.23 Previous setup using acrylic box for insulation.

Figure 7.24 Final setup using fiberglass wool insulation.

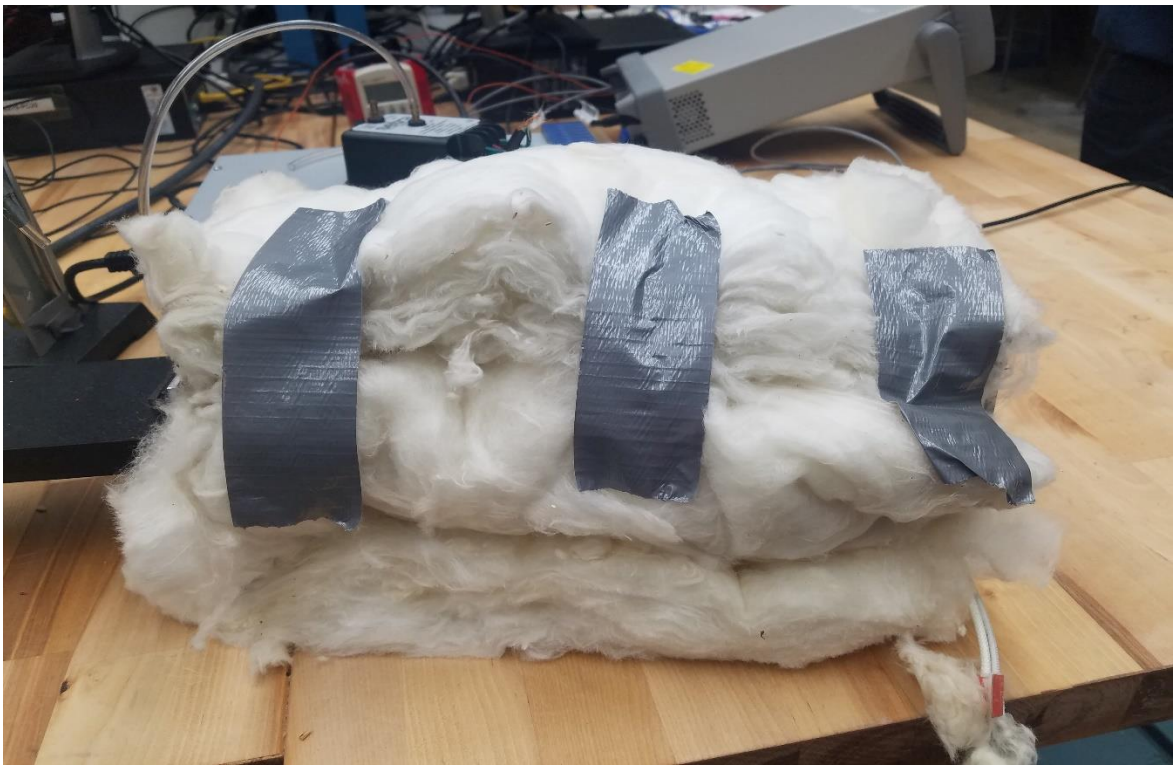

Figure 7.25 Fiberglass insulation around the fin assembly.